Generalised Linear Diversity Receivers for Wireless TDMA Systems

Matthew G. Hebley, BE (1st Class Hons)

A thesis presented for the degree of
Doctor of Philosophy
in
Electrical and Electronic Engineering
at the
University of Canterbury,
Christchurch, New Zealand.

August 1997

ABSTRACT

The continual demand for increased mobile radio capacity prompts continued development of new technology to increase system performance. This thesis presents an investigation of the performance of a generalised linear diversity receiver, as an implementable approximation to the optimum diversity receiver. The receiver utilises space, or antenna, diversity combining to combat the effects of multipath fading experienced in the mobile channel. The receiver is intended for coherent reception of linearly modulated wideband time division multiple access (TDMA) digital transmissions. The receiver structure is also restricted to the linear case.

Two major analyses are undertaken in this thesis: the performance of the diversity receiver with finite-length fractionally-spaced branch equalisers, assuming ideal channel-state-information and synchronisation; and the performance of a carrier frequency offset recovery algorithm, assuming only knowledge of the channel autocorrelation function, and burst synchronisation.

This thesis presents a general time-varying frequency-selective multipath Rayleigh fading model.

The system model includes non-white, non-Gaussian co-channel interferers as well as non-white, but Gaussian co-channel interferers. However, adjacent channel interference is not modelled.

Simulation results are presented for the best possible performance (with ideal channel-state-information) of the diversity receiver, showing the effects of diversity and finite equaliser length, and are compared to results for the optimum linear receiver. The results show that increased diversity is very powerful in improving the performance of the receiver, and that the equaliser lengths can be quite short (e. g., 10 taps) and the receiver will still perform close to the optimum. The receiver is shown to be more capable of combating non-Gaussian co-channel interference than Gaussian (or noise-like) interference.

The performance of the carrier frequency offset estimator is also determined by simulation. It is found that in most cases, doubling the diversity reduces the error standard deviation by a factor of two or more. The estimator is found to be relatively insensitive to symbol timing, channel delay spread, frequency offset and signal-to-noise ratio, especially with high diversity.

PREFACE

This thesis presents a study of a diversity receiver structure operating in the frequency-selective multipath fading environment. Two distinct areas are focussed on: bounds on the performance of a linear receiver with finite-length fractionally-spaced diversity branch equalisers assuming ideal channel state information and synchronisation, and the performance of a maximum-likelihood carrier frequency offset algorithm.

Chapter 1 introduces the field of digital mobile radio. It introduces the goal of providing universal voice and data communication, outlines the conceptual task performed by a digital communication system, presents the limitations encountered in the mobile environment, includes some relevant literature summaries, and presents the aims of the thesis.

Chapter 2 sets out the system model assumed throughout the thesis. It discusses the general cellular model, and the parts of the general model that are modelled in the analysis. It presents the generalised time-varying frequency-selective channel model assumed, based on the Karhunen-Loéve expansion. The form of the transmitted signals and interference modelling are given. The time-varying channel model is an original extension of the pseudo-static model presented by Clark [1992].

Chapter 3 details the generalised linear diversity receiver structure. It gives the motivation for the structure being a finite-length equaliser synthesis of the optimum linear receiver structure. Practical considerations are discussed, such as equaliser training, synchronisation, and implementation on one or more digital signal processors.

Chapter 4 presents the study of the effect of finite-length equalisers on the performance of the diversity receiver optimised for minimum-mean-square-error. The study is an original extension to the work of Clark [1992]. The global optimisation of the diversity equalisers is presented assuming ideal channel state information and synchronisation. Results are presented showing the effect of diversity and finite-length of the equalisers, which are compared to results for the optimum (i. e., infinite-length) linear receiver [Clark 1992].

Chapter 5 presents the study of a maximum likelihood carrier frequency offset estimate for the diversity receiver. The estimator is an original extension to the work of Luise and Reggiannini [1995], which applies to a single branch receiver (no diversity)

and requires channel state information. Results are presented showing the effect of diversity on the expected value, and error standard deviation of the estimator.

Finally, Chap. 6 presents concluding remarks and topics for future research.

The top right corner of each even page shows a link frequency response generated by the time-varying frequency-selective channel model, (2.27), where the real and imaginary parts of the complex response are plotted against frequency (on the axis with the arrows). The time-varying nature of the channel can be seen by flipping the pages.

List of Papers

The following papers have been written as a result of the research presented here.

Hebley, M., Kennedy, W. and Taylor, D., "The Performance of a Space Diversity Receiver with Finite-Length Fractionally-Spaced Equalisers with Frequency Selective Rayleigh Fading and Co-Channel Interference," *IEEE Global Commun. Mini-Conference*, November, 1994, pp. 90-94.

Hebley, M., Taylor, D., "The Effect of Diversity on a Burst-Mode Carrier Frequency Estimator in the Frequency-Selective Multipath Channel," Accepted for publication in *IEEE Trans. Commun.*, Dec, 1997

ACKNOWLEDGEMENTS

I am gratefully indebted to my two supervisors William K. Kennedy, and Desmond P. Taylor. Throughout my studies they have both contributed in discussions, provided guidance, and edited many draft manuscripts.

I would like to acknowledge financial support from the following sources: the NZ Vice-Chancellors Committee Postgraduate Scholarship, the IEEE student travel grant, and financial support from the Electrical and Electronic Engineering Department.

I thank my gym buddies, Dave Hawkins, Elwyn Smith, and Dinh Quang who made working out at the gym more enjoyable. Also, many thanks to Elwyn for introducing me to climbing and caving and sharing his gear on many an occasion. I would like to thank my friends and flatmates, especially Tasha Northcott and Derek Ward, who have supported me in my studies. I will remember "The Comms Lab" and the guys in R9. Also, thanks go to Derek Ward and Ben Benison for their help with proof-reading.

Finally, I would like to thank my parents for their unending support, without which I would not have made it.

GLOSSARY

Mathematical Notation

$\sum$	Summation Operator
δ	Dirac or Kronecker Delta Function
$\mathcal{Re}\{\cdot\}, \mathcal{Im}\{\cdot\}$	Real Part and Imaginary Part
$e^{\cdot}, \exp(\cdot)$	Base e Exponential Operator
$\jmath$	Imaginary Quantity $\sqrt{-1}$
$E[\cdot]$	Expectation Operator
$\{\cdot\}$	Sequence
$[a, b)$	Range from a to, but not including, b
$\mathcal{F}\{\cdot\}, \mathcal{F}^{-1}\{\cdot\}$	Fourier and Inverse Fourier Transform
$\cdot^T, \cdot^H$	Matrix Transpose and Hermitian (Conjugate) Transpose
$\cdot^*$	Complex Conjugate
$\lfloor \cdot \rfloor$	Round to the Nearest Integer Towards $-\infty$
∇	Gradient Operator
$\lvert \cdot \rvert$	Absolute Value Operator
$\arg\{\cdot\}$	Argument (or Angle) Operator
$\in$	Is Contained In

Symbols

N_d	Number of Dominant Sources
N	Number of Dominant Co-channel Interferers
N_s	Number of Co-channel Sources
f_s	Fractionally-Spaced Sampling Frequency
$\bar{f}_s$	Synchronously-Spaced Sampling Frequency
W	Signal Bandwidth
β	Excess Bandwidth Factor
T_s	Fractionally-Spaced Sampling Period
T	Synchronously-Spaced Sampling Period
t_s	Sampling Instant
t_n	Symbol Offset Relative to Desired Source
$P(\tau)$	Channel Impulse Response Correlation Function

$R(f)$	Channel Frequency Response Correlation Function
$\Xi(f_1, f_2; t_1, t_2)$	Channel Pulse Frequency Response Correlation Function
$\bar{\psi}_{l-k,l'-k';l,l'}$	Synchronously-Spaced Link Impulse Response Correlation
λ_{ni}	Karhunen-Loéve Eigenvalues
$c_{nmi}(t)$	Karhunen-Loéve Weight Random Processes
$\phi_{ni}(f)$	Karhunen-Loéve Eigenvectors
J_n	Number of Karhunen-Loéve terms
Δf	Carrier Frequency Offset
$\widehat{\Delta f}$	Carrier Frequency Offset Estimate
ϕ	Carrier Phase Offset
f_n	Transmitter Oscillator Frequency
f_r	Local Oscillator Frequency
$\Phi_m(l)$	Weighted Received Sample Correlation
$\eta_m(t)$	Received Noise Sample
$\tilde{\eta}_m(t)$	Passband Received Noise Sample
σ^2	Received Noise Sample Variance
σ_e^2	Equalised Noise Sample Variance
ε	Carrier Frequency Offset Estimate Error
μ	Offset Estimate Expected Value
μ_ε	Offset Estimate Error Expected Value
σ_ε	Offset Estimate Error Standard Deviation
u_{ml}	Hypothesized Noiseless Received Samples
$\widetilde{\Delta f}$	Hypothesized Carrier Frequency Offset
$\widetilde{\phi}$	Hypothesized Carrier Phase Offset
$\tilde{x}_k$	Hypothesized Data
$\tilde{\bar{q}}_{mkl}$	Hypothesized Symbol Spaced Link Sample
$c_n(t)$	Pulse Shaping Filter Impulse Response
$C_n(f)$	Pulse Shaping Filter Frequency Response
$\tilde{h}_{nm}(\tau, t)$	Passband Channel Impulse Response
$\tilde{H}_{nm}(f, t)$	Passband Channel Frequency Response
$h_{nm}(\tau, t)$	Complex Baseband Channel Impulse Response
$H_{nm}(f, t)$	Complex Baseband Channel Frequency Response
τ_{nm}	Total Transmission Delay
S_n	Average Transmitter Gain
ϕ_n	Transmit Oscillator Phase Relative To Desired Source
α_{nm}	Total Transmission Delay Including Symbol Offset
ϕ_{nm}	Total Phase Offset
$q_{nm}(\tau, t)$	Complex Baseband Link Impulse Response
$Q_{nm}(f, t)$	Complex Baseband Link Frequency Response
$z_{nm}(\tau, t)$	Complex Baseband Link Impulse Response Without Delay

$Z_{nm}(f,t)$	Complex Baseband Link Frequency Response Without Delay
$\hat{r}_{ml}$	Fractionally Spaced Received Sample
$\bar{r}_{ml}$	Synchronously Spaced Received Sample
r_{ml}	Fractionally Spaced Received Sample Without Carrier Offset
q_{mkl}	Fractionally Spaced Link Sample
$\bar{q}_{mkl}$	Synchronously Spaced Link Sample
y_l	Fractionally Spaced Output Sample
$\bar{y}_k$	Synchronously Spaced Linear Estimate
$\hat{x}_k$	Synchronously Spaced Data Estimate
σ_x^2	Variance Of Data Symbols
$p_{n,m}(t)$	Matched Filter Impulse Response
$\tilde{v}_{mkl}$	Infinite Length Equaliser Impulse Response
v_{mkl}	Fractionally Spaced Equaliser Impulse Response
ϵ	Mean Square Error
g_{nki}	Intersymbol Interference Term
p_k	Real Part Of Intersymbol Interference Term
ρ_i	Filtered Noise Term
z_K	Intersymbol Interference Random Variable
N_{mc}	Number Of Monte Carlo Trials
$N_{\bar{\psi}}$	Number Of Link Correlation Terms
L_{TS}	Length Of Training Sequence
L	Observation Interval
J	Equaliser Length

CONTENTS

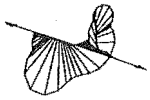

Chapter 1

INTRODUCTION

The use of radio has allowed people to communicate with each other by means of a wireless portable hand-held device. The first radio systems only allowed communication between users on the same system, and only over short distances. Cellular technology has allowed the connection of portable devices to the fixed wire telephone network enabling people to communicate with other people all over the world. Unfortunately, existing cellular systems are fast reaching capacity in dense urban environments [Lee 1991] prompting research into how to increase the density of mobile devices in a given area. In order to increase the density of users and make cellular technology available to more people, efforts must be made to make more efficient use of available bandwidth, yet retain or improve the quality of reception, whilst decreasing the unit-cost of the mobile devices.

The requirements are that users may initiate or receive calls using a hand-held radio transceiver. They should be able to move to different parts of the city, country, or ideally, anywhere in the world and be able to use their transceiver in the same manner independent of where they are. This implies that each transceiver would have a unique phone number to identify it anywhere within the system. A user should be callable from any other fixed or mobile phone anywhere using this single identifying number. The system should be able to trace the location of the transceiver whenever it is turned on, and must allow the user to move throughout the cellular system during a call.

A simplistic solution is to allocate each user a unique frequency band. Then the system merely has to track the position of the transceivers, and maintain radio links between the transceivers. However, there is only a very limited number of useful and available frequency bands (also called available bandwidth), so this solution would only support a very small number of users.

To increase the number of users in the system for a given bandwidth, the area to be covered is divided into *cells*, and frequency bands are reused in distant cells [Goodman 1991].

1.1 GENERAL CELLULAR CONCEPTS

It is not feasible to have large numbers of radio transmissions from portable transceivers to other fixed or portable phones anywhere in the world. The solution is to have base stations, situated throughout the coverage areas, which are connected to the public switched telephone network (PSTN) via fixed wire or fibre-optic links. Radio links between the transceivers and the base stations can be switched through the PSTN to any fixed phone, or to any other base station which will set up another radio link to another transceiver.

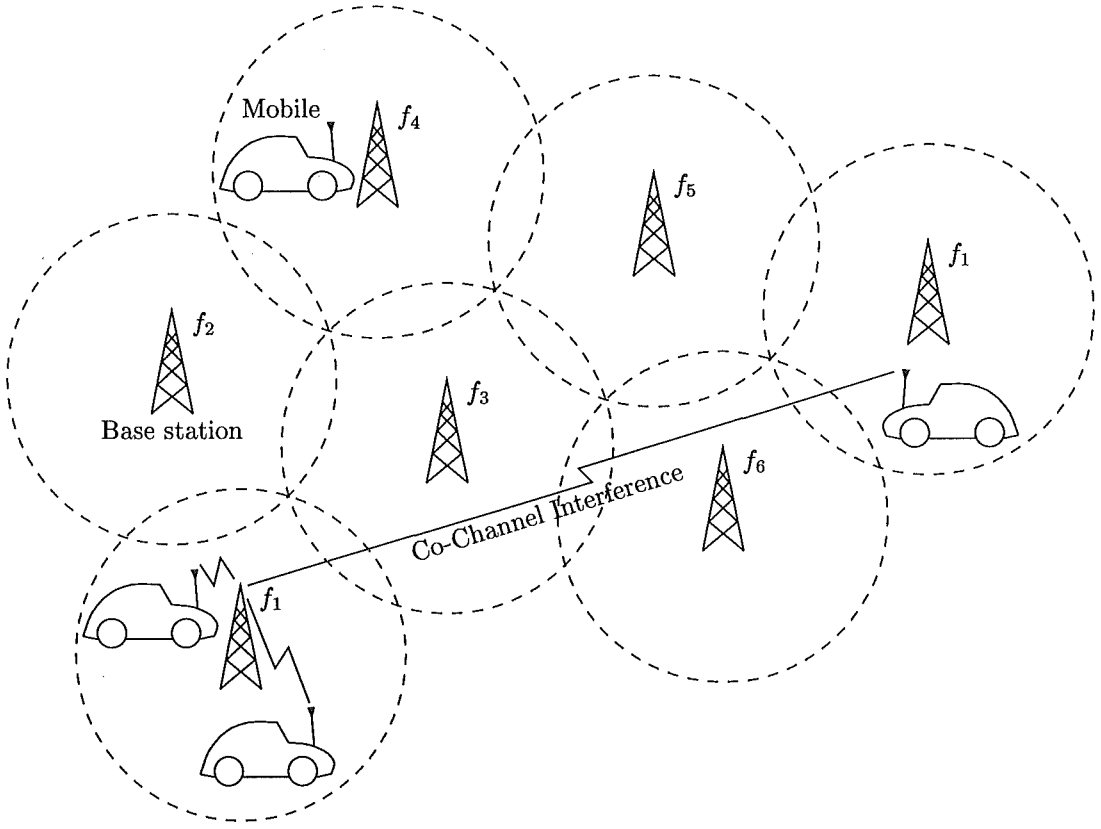

Figure 1.1 Cellular system showing co-channel interference

In any given cell there may be many mobile transceivers (or users) whose radio links (or *channels*) are separated from each other by some form of multiplexing, e. g., frequency division multiple access (FDMA), time division multiple access (TDMA), or code division multiple access (CDMA) [Kucar 1991]. Figure 1.1 shows an idealised part of a cellular system. It depicts several cells with their base stations, mobile users. Each cell is assigned a *set of frequencies* labelled f_1 to f_6. (This notation is used merely to indicated that the same frequency bands are reused in distant cells.) Note that Figure 1.1 shows circular cell boundaries arranged on a "hexagonal" basis, however, in a real system the cell boundaries are irregular due to the physical contours of the

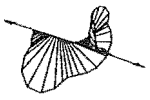

environment. As well as not being regular, the boundaries are indistinct, and move as the radio links fluctuate. Because of the limited bandwidth resource, the density of the mobile users in the system is increased by reuse of the cell frequency bands in distant cells. However, this introduces co-channel interference. A user in a particular cell assigned to a particular frequency band considers users in a distant cell which are assigned the same frequency band as *co-channel interferers*, and would experience *co-channel interference* (CCI) from the radio transmission of the distant mobile and the distant base station [Lee 1991]. In Fig. 1.1 two co-channel users are shown operating on one of the channels in the set of channels called f_1. The number of sets of frequencies and the cell size, or in other words, the amount of frequency reuse, determines the level of CCI experienced by the users.

As a result of the cellular arrangement, the concept of *handoff* arises [Weissman *et al.* 1993]. Handoff occurs when a user moves from one cell to another during a call. The system must decide when to perform a handoff, and terminate the radio link between the transceiver and the original base station and initiate another link to the new base station. When a handoff occurs, there is a chance that there will be no available channels to establish a radio link to the new base station, and the call gets *dropped.* This problem is somewhat circumvented by CDMA systems which merely become more noisy as more users join a cell. There is a whole discipline devoted to the analysis of cellular control systems [Beck and Panzer 1989, Frech and Mesquida 1989, Falciasecca *et al.* 1989, Tekinay and Jabbari 1991].

This thesis, however, is restricted to the analysis of the physical radio link itself, and does not contend with problems of handoff or tracking the position of the mobiles. In other words, it is assumed that the call is initiated, the mobile is moving through a cell, the data transmission is affected by channel distortion and interference, and the performance of the transceiver is analysed.

1.2 FUNDAMENTALS OF COHERENT DIGITAL TRANSMISSION

The aim of digital radio is to reliably transfer information or message bits from one location to another using radio wave propagation. Several fundamental concepts must be understood in order to analyse and discuss the process of transmitting and receiving digital data. Note, that these concepts are not necessarily performed in an actual system exactly as described here, but they do describe the system theoretically, and are useful for understanding the problems associated with coherent digital transmission.

The message bits are converted into an analog message wave. First the message bits may be grouped into symbols, then the analog wave is created by summing pulse shape functions, one per symbol interval, where the symbol determines the magnitude of the pulse shape for that symbol interval. The pulse shape is chosen to have a Nyquist

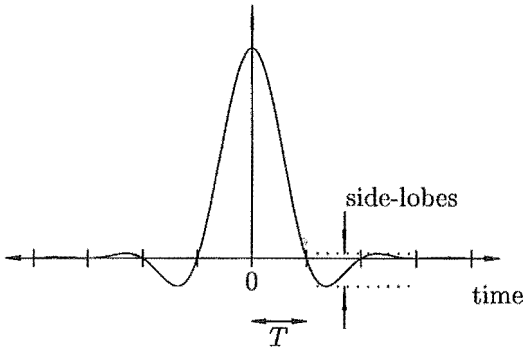

(a) Impulse response of pulse shape

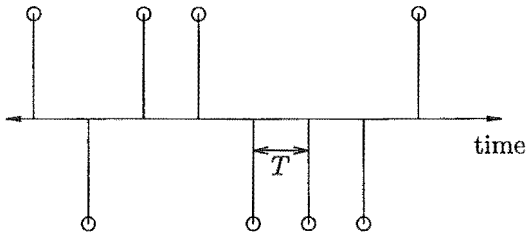

(b) Binary message sequence

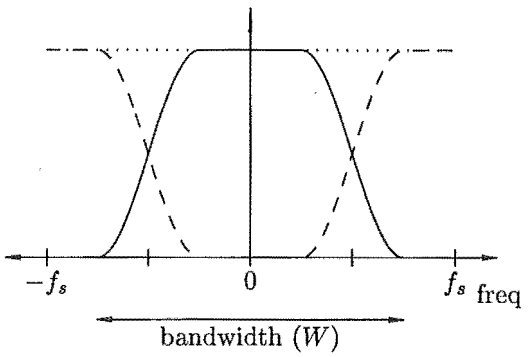

(c) Frequency response of pulse shape

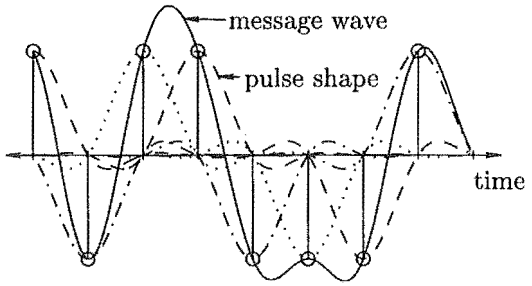

(d) Corresponding message wave

Figure 1.2 The construction of a message wave

response [Gitlin *et al.* 1992, p. 254] (i.e., have a value of zero at all but one sampling instant, or equivalently, have constant sampled frequency response), and have as small a side-lobe size as possible, while having as small a bandwidth as possible. Figure 1.2(a) shows an example of the time domain response of a pulse shape. Notice the response goes through zero at multiples of the symbol period, T, and the side-lobes die away quickly. Figure 1.2(c) shows the frequency domain response of the same pulse with excess bandwidth factor given by

$$\beta = \frac{W}{f_s} - 1 \tag{1.1}$$

It shows the frequency response of the continuous time domain pulse in solid. When the time domain pulse is sampled, the frequency response is repeated at multiples of the sampling frequency, $f_s = \frac{1}{T}$, (shown dashed). The sum of the repeated spectra is a constant, shown dotted, indicating a Nyquist response. Figure 1.2(b) shows eight message bits displayed with the two states, ± 1, and Fig. 1.2(d) shows how the appropriately shifted pulse shapes (dashed and dotted) are combined to make the message

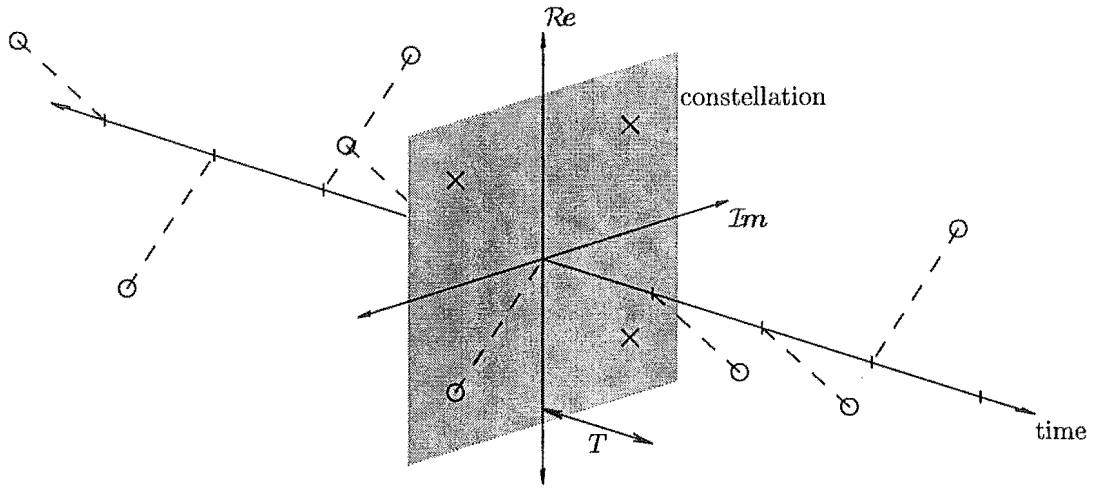

Figure 1.3 A sequence of symbols from a four point constellation

wave (solid). In this case the symbols consist of only one bit. Notice how the message wave goes through the ± 1 symbol values at the sampling instants indicating that the wave is only a function of one symbol at the sampling instants.

The analog message wave modulates a carrier sinusoid, which has a frequency much greater than the bandwidth of the message wave, to produce a high frequency passband signal [Haykin 1983, p. 543]. This has four effects. First, the passband signal has much better propagation properties than the baseband message signal. Second, the physical size of the antennae that are efficient at transmitting and receiving is reduced to practical sizes. Third, the size of the antennae is matched to the signal across the whole bandwidth. And fourth, the carrier frequency can be chosen to avoid other transmissions. The passband signal is amplified and emitted by the transmitter.

The receiver's local oscillator, oscillating at the carrier frequency, is used to demodulate the received passband signal. This recovers the baseband analog message wave at the receiver. Excluding the effects of additive noise and if everything is ideal (i. e., the receiver's local oscillator frequency and phase is exactly the same as the carrier frequency and phase, and there is no distortion introduced between the transmitter and the receiver) then the message wave will be recovered exactly. However, if there is a phase offset between the two carrier waves, then the amplitude of the recovered message wave will diminish. If the phase offset is exactly $\frac{\pi}{2}$, then the amplitude of the recovered wave will be zero. This phenomenon enables the transmission of two message waves on carrier waves that are $\frac{\pi}{2}$ out of phase (in quadrature). At the receiver, each message wave can be recovered independently by demodulating with a local oscillator that is in phase with one of the carrier waves.

This process of transmitting two message waves by quadrature carrier waves can be elegantly represented mathematically by using complex notation, $e^{j2\pi f_c t} = \cos(2\pi f_c t) +$

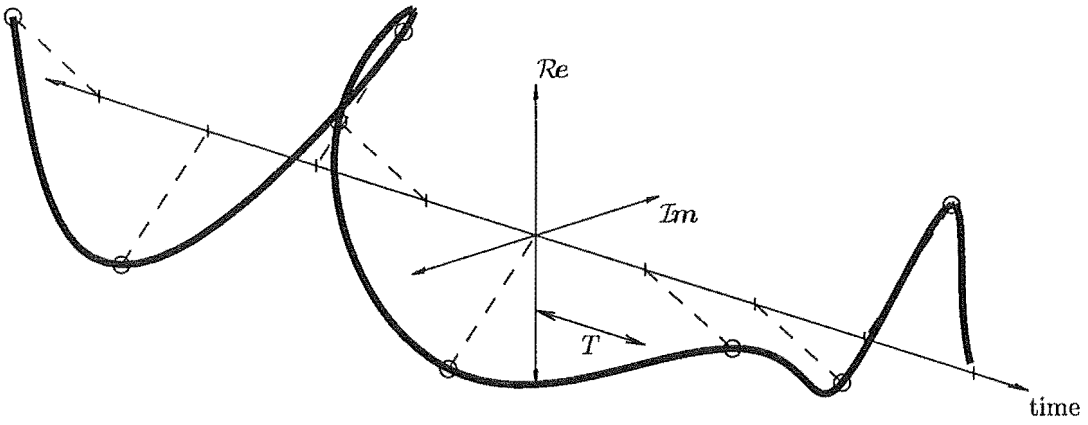

Figure 1.4 Message wave for symbols from a four point constellation

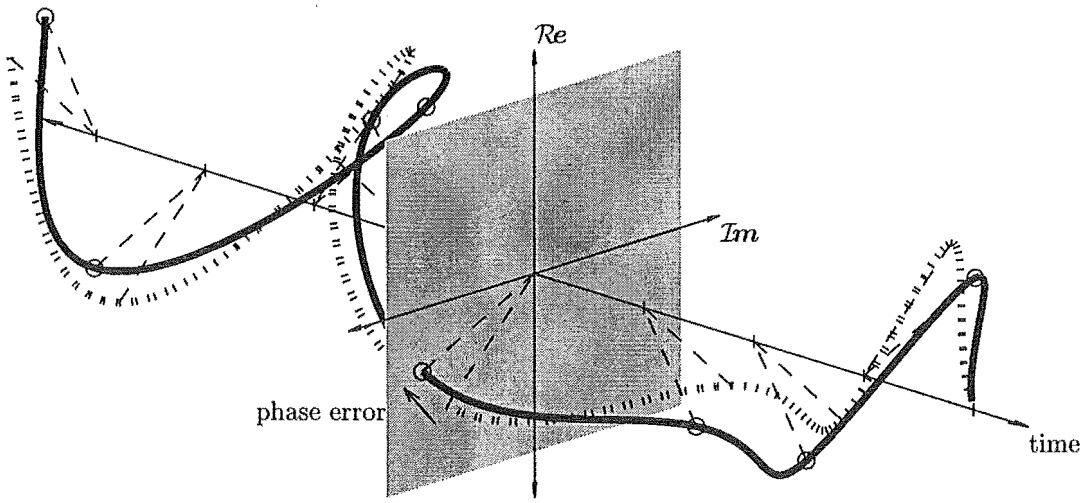

Figure 1.5 Illustration of a phase mismatch between transmitter oscillator and receiver oscillator

$j\sin(2\pi f_c t)$. Complex message symbols can be constructed from two real data symbols, $x_k = a_k + jb_k$. The message symbols can be thought of as points in a constellation, which is a plot of all the possible symbol points on the complex plane. Figure 1.3 shows a plot of a sequence of complex data symbols. The real and imaginary parts are plotted against time. In this case, there are two bits per symbol giving four possible symbol values, as shown by the three crosses and one circle in the real-imaginary plane at $t = 0$. The other symbols take one of these values and are shifted in time by multiples of the symbol period. Figure 1.4 shows the complex baseband message wave for the data sequence shown in Fig. 1.3, constructed in exactly the same way as the single bit-per-symbol wave of Fig. 1.2(d). Although it is difficult to perceive three dimensional figures rendered onto two dimensions, it is instructive to consider the complex wave in three dimensions rather than as a magnitude and phase.

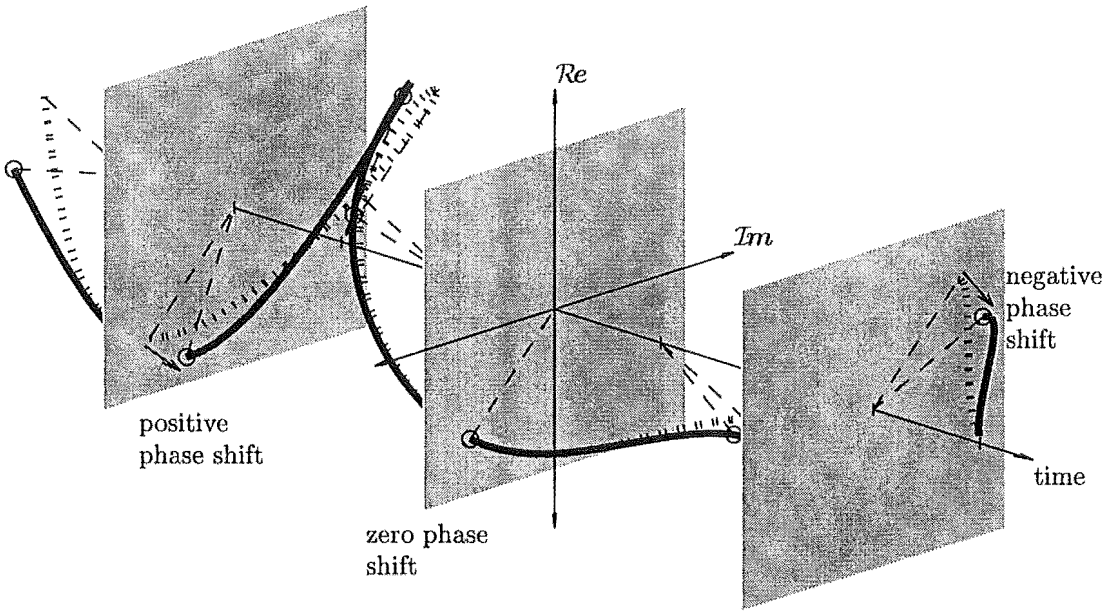

Figure 1.6 Illustration of a frequency mismatch between transmitter oscillator and receiver oscillator

The recovered baseband wave can also be considered as a complex waveform, and the phase error between the complex transmitted carrier wave and the complex receiver local carrier now can be viewed as rotating the complex transmitted baseband wave around the origin in the complex plane. Figure 1.5 shows how a phase error can be interpreted as a rotation around the time axis from the transmitted wave (dotted) to the recovered wave (solid). A *frequency* error manifests itself as a linear phase trend, which can be thought of as twisting the recovered baseband wave along the time axis. Figure 1.6 shows the effect of a frequency error. It shows no phase error at $t = 0$, but an increasing phase error for $t < 0$ and an opposing phase error for $t > 0$.

The complex symbols are recovered by sampling the recovered baseband wave at appropriate sampling intervals and the complex samples are mapped to symbol estimates by the receiver. This mapping is done by defining decision regions. In the case of the example, the decision regions are the four quadrants of the real-imaginary plane. If a sample falls outside of the correct decision region, the symbol estimate will not be the same as the original message symbol, and an error occurs. If the receiver samples the wave at instants other than the correct sampling instants (i. e., when the adjacent pulses have do not zero value) then intersymbol interference occurs. This means that the current sample depends on all other symbols rather than just the desired symbol.

Additive noise, which is present in any system, affects the reception of the digital message data. The received sample is influenced by noise and can appear in the wrong decision region and be mapped to the wrong constellation point. The receiver must

make accurate estimates of the carrier frequency, phase and sampling instants in order to maximise the chance of making a correct decision even though the samples are corrupted by noise. In other words, if the carrier mismatches and intersymbol interference are considered separately from the noise then the receiver must try to make the noise-free sample as close to the transmitted symbol value so there is the smallest possibility that the noisy sample will be in error.

A further impediment to detecting the transmitted symbols occurs when the channel distorts the transmitted wave. This is discussed in Sec. 1.4.

1.3 OVERVIEW OF SOME EXISTING SYSTEMS

The ultimate goal is to provide a seamless service for voice and data transmission from a single portable device anywhere in the world. Currently, subsets of this goal are realised by different systems: cellular radio, cordless telephone, and wireless data networks [Padgett *et al.* 1995].

Cellular and cordless radio systems are categorised as first generation (analog) and second generation (digital). First generation cellular systems allowed a connection to the global wired telephone network, via cellular base stations, and allowed seamless movement from cell to cell at vehicle speeds. First generation cordless phones replaced standard wired phones to allow a wireless equivalent, and allow movement of up to 50-100 m from the user's base station. They are commonly referred to as indoor channel systems [Goodman 1991]. Second generation digital cellular and cordless phones have essentially the same properties (i. e., provide the same basic service) as the first generation phones, but were developed to overcome some of the limitations of the first generation phones, such as inefficient bandwidth usage, inflexibility, and poor security.

The distinction between digital cellular and digital cordless systems is that digital cellular technologies are optimised for bandwidth efficiency and frequency reuse in a macrocellular, high-speed fading environment, whereas digital cordless technologies are optimised for low complexity equipment and high-quality speech in quasi-static environments [Padgett *et al.* 1995]. Nevertheless, the speed of the channel fading is measured relative to the data rate, so the channel fading can be considered slow if the data rate is high enough.

1.3.1 Analog Cellular Radio

First generation systems use analog frequency modulated (FM) voice channels, and digital frequency shift keying control channels. Different systems use bandwidths up to 30 kHz [Kucar 1991]. FM is inherently robust against channel fading, and the message signalling rate of the control channel is low, up to 10 kb/s, and does not suffer significantly from the effects of channel fading.

The technology has been successful, with several incompatible systems covering many different countries. The Americas, Canada, and Australasia have employed Advanced Mobile Phone Service (AMPS), using 30 kHz channels. Different European countries use Total Access Communication System (TACS), Radio Telephone Mobile System (RTMS), and Nordic Mobile Telephone (NMT) which use 25 kHz channels, C-450 using 20 kHz, and Radiocom 2000 using 12.5 kHz channels. In Japan, two systems are available, Nippon Telephone and Telegraph (NTT) and a system based on the European TACS system, using 25 kHz channels [Padgett *et al.* 1995].

1.3.2 Digital Cellular Radio

Second generation mobile systems are digital because the voice signals are converted to digital streams and transmitted by a digital modulation technique. Like the analog systems, several different protocols have been developed, but the digital systems are only just starting to be commissioned in different countries. Digital systems have several advantages:

- They are compatible with data transfer. Therefore any signal (such as facsimile, email, and possibly even video, as well as speech) can be digitised and transmitted using well known data transfer protocols.
- The choice of channel bandwidth is more flexible, unlike analog systems where the bandwidth is determined by the speech signal.
- Although the process of sampling and digitising an analog signal usually results in a digital signal with a bandwidth that is wider than the original analog signal, efficient speech coding [Spanias 1994] can be used to reduce the amount of digital information required to be transmitted for "adequate" voice quality. Thus between three and ten digital channels can be transmitted in the same bandwidth used by one analog channel.
- Encryption algorithms can be easily implemented allowing for safer, more secure, transmissions.

Europe has developed the Groupe Spéciale Mobile (GSM) system and the Digital Cellular System 1800 (DCS1800) [Potter 1992], which are essentially the same system operating at different carrier frequencies. They use a combination of TDMA and FDMA multiplexing, with eight time slots per 200 kHz channel. The speech coder rate is 13kb/s [D'Aria *et al.* 1992], and the digital transmission is Gaussian Minimum Shift Keying (GMSK) [Murota and Hirade 1981]. The wideband channel requires equalisation, and the standard specifies a 26 symbol training sequence mid-amble to be used to acquire the channel response. In North America, the digital system IS-54 has been developed. It is sometimes called Digital AMPS, because it has a 30 kHz channel and can be used

in the frequency slots of the analog AMPS system. The standard allows for dual mode terminals which is convenient for the user as coverage evolves from analog to digital. Each channel can carry three users, making the digital system three times as efficient, as the original analog one.

Japan has a similar system called Personal Digital Cellular (PDC) with a 25 kHz channel allowing for the transition from analog to digital. PDC uses $\pi/4$ Differential Quadrature Phase Shift Keying (DQPSK), and requires a minimum of antenna selection diversity at the base station to overcome the effects of the fading channel [Petersson and Svensson 1994].

1.3.3 Analog Cordless Telephones

In a similar manner to the analog cellular systems, analog cordless telephones transmit the speech channel using frequency modulation (FM). They are designed to communicate with one base station, and do not perform hand-offs [Goodman 1991].

1.3.4 Digital Cordless Telephones

Like the digital cellular systems, there are several incompatible digital cordless systems. These include CT2/Common Air Interface in the United Kingdom, Digital European Cordless Telecommunications (DECT) in Europe, Personal Handyphone System in Japan, Personal Access Communications Systems (PACS) in the United States [Padgett *et al.* 1995]. These systems use time-division duplex (TDD) meaning the transmit and receive channels are multiplexed in time on the same frequency. This has the advantage of eliminating the need for a duplex filter, allowing transmit and receive diversity, and relieving requirements on bandwidth allocation.

DECT has a large bandwidth and requires equalisation or antenna diversity or both. Personal Handyphone System specifies transmission diversity on the forward link, and reception diversity on the reverse link, so that all diversity is at the base stations, thus reducing handset complexity. PACS specifies two-branch polarisation diversity at both the handset and the base [Padgett *et al.* 1995].

1.4 LIMITATIONS ENCOUNTERED IN DIGITAL SYSTEMS

As mentioned in Sec. 1.2, the transmission of digital signals in a mobile environment results in distortion of the received signal. The distortion is caused by multipath fading, which may result in intersymbol interference. Also, shadowing and co-channel interference limit the performance of digital systems. These problems must be overcome to increase capacity and quality without increasing the required bandwidth [Jakes, Jr. 1974].

Multipath fading is caused when the transmitted signal is scattered by the terrain, buildings, vehicles and other obstacles in the environment, and arrives at the receiver via many paths, each path having a different attenuation and delay. When a transmitter is operating in a multipath channel, the reflections result in several similar versions of the same signal arriving at the receiver. If these versions of the signal happen to add destructively the signal will be cancelled at the receiver. This cancellation is called a *fade*, and can be very deep, as much as -40dB relative to the average signal power [Sousa *et al.* 1992]. The multipath fading can cause the response of the radio channel to be frequency dependent because two independent paths with different time delays will cause a phase shift that depends on the frequency of the wave. So waves of one frequency may have relative phase shifts that cause signals to add destructively while others may have phase shifts that cause signals to add constructively. This frequency dependence is significant if the transmission is wideband, i. e., the delays caused by the multipath channel are relatively long compared to the bit or symbol period. In this case, the fading is said to be *frequency-selective.* On the other hand, if the transmission is narrowband, and therefore, all the frequencies (and also the phase shifts) are approximately the same, the fading is called *flat fading.* The response of the channel also changes as the obstacles (such as neighbouring mobiles) move. So the response from the transmitter to the receiver changes temporally (as the standing wave changes) and spatially (as the mobile moves around). Another way of considering the changing channel response is to consider the motion of the mobile relative to the base station. This causes a Doppler shift, Δf, on the frequency of each of the scattered signals, according to $\Delta f = \frac{v}{\lambda} \cos \alpha$, where v is the mobile's velocity, λ is the wavelength of the radio-frequency signal, and α is the angle of incidence of the wave [Parsons 1992]. In a dense urban environment, the combination of many incident waves with different arrival angles, and therefore, different Doppler shifts, results in Doppler spreading [Proakis 1989, Chap. 7]. Doppler spreading describes the way the channel evolves.

Shadowing is the attenuation that occurs when a mobile moves so that there is an obstruction, such as a hill, between the mobile and the base station. It is not frequency-selective, but causes a decrease in signal-to-noise ratio [Loo and Secord 1991].

Frequency-selective fading causes distortion called intersymbol interference (ISI). In order for a digital system to have no ISI, the combined response of the transmit filter, channel, and receive filter must obey the *Nyquist criterion.* In the time domain, this can be achieved when the combined impulse response is zero at all sampling instants except one. In the frequency domain, this is equivalent to the combined sampled frequency response being constant for all frequencies within the bandwidth of interest. (Due to the sampling process at the receiver, the combined frequency response will be repeated in frequency at integer multiples of the sampling rate.) The ISI introduced by multipath fading can be visualised in the time domain by considering a pulse received from a path with a long delay that will overlap a pulse received from a path with a short

delay, and result in non-zero contributions at a number of sampling instants instead of just one. In the frequency domain, ISI is visualised as altering the amplitude and phase of the frequency response components from their desired Nyquist constant.

Co-channel interference (CCI) is the interference caused by other users operating on the same channel in a distant cell. The effects of CCI are made worse by fading, because the desired signal can be suppressed to a level lower than that of the CCI.

Fading, ISI and CCI limit performance in the following ways:

- Symbol detection is more difficult during a fade because the ratio of signal power to additive noise and CCI powers is reduced
- Transmission data-rates are limited by ISI because as the data-rate increases, the symbol period decreases so, for a given amount of multipath delay spread, a more significant amount of a delayed symbol distorts adjacent symbols.
- The number of users per area is limited by the allowable level of CCI because as more mobiles use the cellular network, more CCI is contributed by other mobiles.

A high signal-to-noise ratio is desirable especially in a fading environment. The usual way to increase the signal-to-noise ratio is to increase the transmitted power, because the *additive* noise (present in any communications system) will remain constant. However, increasing the transmitted power in a cellular system will not increase signal-to-noise ratio because the power level of ISI (and usually CCI) will increase by the same amount as the signal power. As it is desirable to have high data-rates and dense cell usage, ways of combating fading, ISI and CCI in the mobile environment must be found.

1.5 INCREASING PERFORMANCE IN THE DIGITAL CELLULAR ENVIRONMENT

1.5.1 Diversity

Diversity is an effective method of increasing performance in a mobile environment [Van Etten 1976, Balaban and Salz 1991] and can combat fading by simultaneously utilising several near-independent channels. There are three types of diversity: time, frequency and space.

1.5.1.1 Time diversity

Time diversity means that the same message is transmitted at different times. For *wideband* transmission with frequency-selective fading, the symbol periods are short compared with the multipath delay (a measure of the spread in delays of the multiple

paths), so severe ISI results on all the diversity transmissions. Consequently, time diversity does not offer much improvement. However, for *narrowband* transmission, the flat fading will cause drop-outs that will be different for each diversity transmission, so time diversity may help to increase the probability of receiving the symbols correctly. An example of time diversity is repetition coding.

1.5.1.2 Frequency diversity

In *narrowband* transmission, frequency diversity means that several carriers are used to transmit the same information, as there is a higher probability that at least one frequency channel will not be faded.

In *wideband* transmission, the information is transmitted on a single carrier, but an intrinsic frequency diversity is encountered [Clark 1992] because only a portion of the total bandwidth is faded and the distortion can be corrected by suitable equalisation, (see Sec. 3.1).

1.5.1.3 Space diversity

When compared to a system with no diversity, time diversity systems utilise the same bandwidth for a longer time, while frequency diversity systems utilise more bandwidth over the same time. Consequently, this inefficient use of time and bandwidth means that neither time nor frequency diversity is used in mobile cellular systems. In contrast, a receiver utilising space diversity has several antennae deployed to receive *independently faded versions* of a *single transmitted signal.* A space diversity receiver uses the same time and bandwidth as a receiver with no diversity, but is less likely to have all its independent signals faded over the same frequency band at the same time, and so can obtain a much better estimate of what was sent. There are two types of space diversity: selection diversity and combining diversity. Selection diversity means that the receiver chooses one signal from the diversity branches using some criteria, e. g., highest received power. Combining diversity means that the receiver combines the contributions from the diversity branches in some way. Combining results in a better performance because all the branches contribute to the receiver's linear estimate even if they are faded, thus the linear estimate is better than if only one branch was used.

Space diversity can combat CCI in the following way. The signals from the desired source and the co-channel sources arrive at each antenna with different phases, so if the desired signal's phase in each of the diversity branches can be aligned, and all the signals summed, the co-channel interference will tend to cancel.

The receiver to be analysed in this thesis is a space combining diversity receiver.

1.5.2 Equalisation

Equalisation is employed to reduce the effects of ISI [Qureshi 1985]. Equalisation is the term given to filtering of a received signal in order to compensate for the undesirable effects of the channel. The ideal channel has unity gain and zero phase across the frequency band of interest. Real channels do not have ideal characteristics, so equalisation is used to make the combined response of the channel and equaliser closer to ideal.

The simplest type of equaliser is the transversal filter or *tapped delay line* (TDL) [Qureshi 1985]. In the transversal filter, past and present samples are weighted by equaliser coefficients and summed to produce the output. There are a number of criteria used in the calculation of the equaliser coefficients:

- A zero-forcing TDL forces zeroes in the combined *impulse* response at the sampling instants. It approximates the inverse of the channel *frequency* response, so the *combined* frequency response of the channel and equaliser is almost ideal. However, if the channel has high attenuation at any frequencies, which is likely in the frequency-selective mobile channel, the equaliser will have to have very high gain at those frequencies and thus will result in noise enhancement.
- Another criterion for the equaliser is to chose the weights to minimise the mean-square-error (MSE) of the signal at the output of the equaliser. This criterion maximises the signal-to-distortion-plus-noise ratio at the output of the equaliser within the constraint of the finite equaliser length.

The channel response must be known in order to calculate the equaliser coefficients using either of the above criteria. However, in a practical implementation the channel response is not known, so the tap coefficients must be calculated using training sequences and adaptive techniques.

1.6 CLASSIFICATIONS OF THE MOBILE ENVIRONMENT

The rate of the fading is determined by the relative speeds of the transmitters and receivers, and by the movement of any scatterers in the environment. The signal bandwidth is determined by the data rate, and the pulse shaping. The amount of frequency-selectivity across the signal band is determined by the signal bandwidth, and the delay spread of the channel.

The fading is either called fast or slow, depending on the fade rate relative to the data rate, and frequency-selective or frequency-non-selective depending on the symbol period relative to the delay spread. E. g., if the fade rate (determined by the Doppler spread bandwidth) is small compared to the data rate (the reciprocal of the symbol period), then the fading is called slow, and if the delay spread (difference in delays between different multipath components) is small compared to the symbol period, then

the fading is called frequency-non-selective. See Proakis [1989, Chap. 7] for a detailed discussion of channel characterisation. Usually, systems with low data rates encounter fast, frequency-non-selective (or flat) fading, while wideband systems with high data rates encounter slow, frequency-selective fading.

The most difficult aspect of slow, flat fading to overcome is the fact that during a fade, the signal strength diminishes for many symbol intervals causing loss of data and loss of synchronisation. When the fading is fast and flat, the problem changes because during a fade the signal experiences rapid phase changes which are difficult to track, and these cause difficulties in frequency and phase synchronisation.

Wideband, frequency-selective, fading exhibits intrinsic frequency diversity because it is unlikely that the signal will be faded over the entire signal bandwidth, hence enabling signal information to be received (albeit somewhat distorted). Synchronisation is made more difficult, in this case, and the received signal must be equalised to minimise the effects of distortion.

A system designer has to choose a suitable data rate, and therefore bandwidth, for the particular fading characteristics that will be encountered. Bandwidth efficiency and high data rates are desired. Systems that can cope with frequency-selective fading allow increases in data rates, and therefore reduce the relative fade rate.

Differential detection schemes have been used to avoid carrier frequency synchronisation, however, these usually suffer a performance degradation from the performance of coherent schemes, (3 dB or more in the white noise channel). The degradation of a differential system from a coherent system depends in some sense on the ability of the coherent system to accurately acquire the carrier frequency, and the performance loss of any carrier frequency mis-match. Differential detection also suffers in fast fading due to rapid phase shifts (or phase jumps) during fades. It has been shown that coherent detection is better than differential detection in quasi-static fading even when space diversity is employed [Chuang 1990].

1.7 RELATED STUDIES OF DIVERSITY AND EQUALISATION

There have been numerous studies on the ability of equalisation and space diversity to reduce the limitations encountered in cellular radio. Three studies are particularly relevant to this research because they provide groundwork that can be extended.

Amitay and Greenstein [1984] studied the ability of adaptive equalisers with a finite number of taps to combat fading in a two path channel. The multipath fading model used was a Rummler model [Rummler 1979, Rummler 1981] derived using measurements of existing microwave links. Although the fading experienced on a microwave link differs from that on a mobile link, this study is still relevant because it shows the ability of adaptive equalisers to decrease outage probability on one type of fading

channel. Amitay and Greenstein considered both symbol spaced and fractionally spaced transversal equalisers and derived expressions for the signal-to-noise ratio (SNR). They derived equations for the minimum mean-square-error (MMSE) for equalisers with an infinite number of taps and with a finite number of fractionally spaced taps. Simulation was used to find outage probability versus SNR for a range of the following parameters: symbol rate, roll-off factor, number of taps. Their finding was that an equaliser with five taps gave approximately the same results as one with an infinite number of taps. The channel model used had one ISI path at a delay of 6.3 ns, so for the chosen range of symbol rates (15 Mbaud to 30 Mbaud), the filter tap spacings (66.7 ns to 33.3 ns) would be much larger than the ISI path delay.

Balaban and Salz [1991] studied a dual-diversity system (two antennae). The channel was modelled as a two path independent Rayleigh (complex Gaussian) fading channel with additive Gaussian noise. They derived expressions for the least-mean-square (LMS) error for a linear receiver consisting of two diversity branches, each branch containing a filter matched to the corresponding diversity channel, followed by a combiner (sum of the two branches), and an infinite length TDL. They then derived a similar expression for a non-linear receiver which is the same as the linear receiver, but followed by a non-linear decision-feedback equaliser (DFE). They also calculated an upper bound on the probability of error for both the linear and non-linear receivers under a zero-forcing equaliser criterion. The final part of their study was to perform Monte Carlo simulations to graph:

- the probability of error versus SNR, relative delay spread and filter roll-off,
- the outage probability versus relative delay spread, and filter roll-off,
- the error rate distributions,

for quadrature phase shift keying (QPSK), all both with and without space diversity. Their major finding was that dual diversity can significantly reduce the average probability of error, in some cases, by up to two orders of magnitude.

Clark [1992] considered an M-branch diversity receiver operating in a more general multipath fading channel than that considered by Balaban and Salz. He considered one mobile to be the *desired* source, a number of other mobiles to contribute coloured non-Gaussian CCI, and the remaining (large number) of mobiles as contributing coloured Gaussian (*noise-like*) CCI. The channel introduced ISI, and additive Gaussian noise (which was lumped with the noise-like CCI).

The channel was modelled using the Karhunen-Loéve expansion of the frequency coherence function, $R_H(\alpha) = E[H^*(f)H(f+\alpha)]$, where $H(f)$ is the channel frequency response. The expansion of the coherence function results in a set of orthonormal functions that can be weighted by independent random variables to obtain a sample channel response.

Clark studied three receiver structures. They were the maximum likelihood receiver, the optimum linear receiver, and the memoryless linear receiver. In each case, the receivers were analysed using a complex baseband model. However, if the receivers were to be implemented, they would have a *receiver front end* that would perform band-pass filtering and demodulation. Also, the complex baseband signal would be processed as real and imaginary parts.

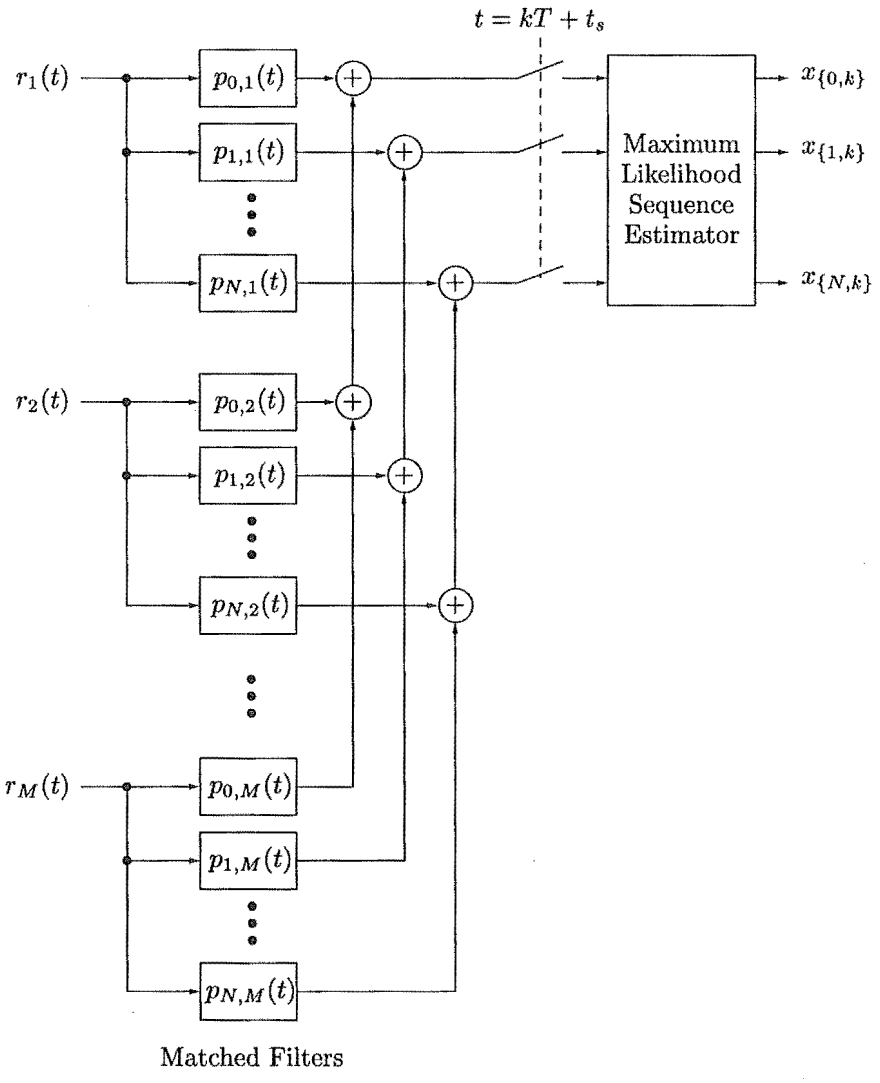

Figure 1.7 Maximum likelihood receiver

The following describes the three receiver structures studied by Clark.

(1) The maximum likelihood receiver shown in Fig. 1.7 is the best possible receiver [Van Etten 1976]. It minimises the bit-error-rate (BER) for a given set of system parameters, such as diversity order, channel characteristics and interference levels. The receiver front end is assumed ideal. The receiver has one *matched filter* matched to each channel between the N sources and the M branches, i. e., MN matched filters.

The matched filter outputs corresponding to each *source* are summed, and the N sums are fed to a *maximum likelihood sequence estimator* (MLSE). The maximum likelihood receiver is difficult to analyse, but Clark determined a bound on the its performance (the *matched filter bound*) by assuming that a single symbol was transmitted in isolation and that all of the co-channel interference was modelled as Gaussian coloured noise. The analysis of the MLSE then reduces to analysing a simple (linear) memoryless threshold detector. Expressions for the outage probability and average bit-error-rate were derived.

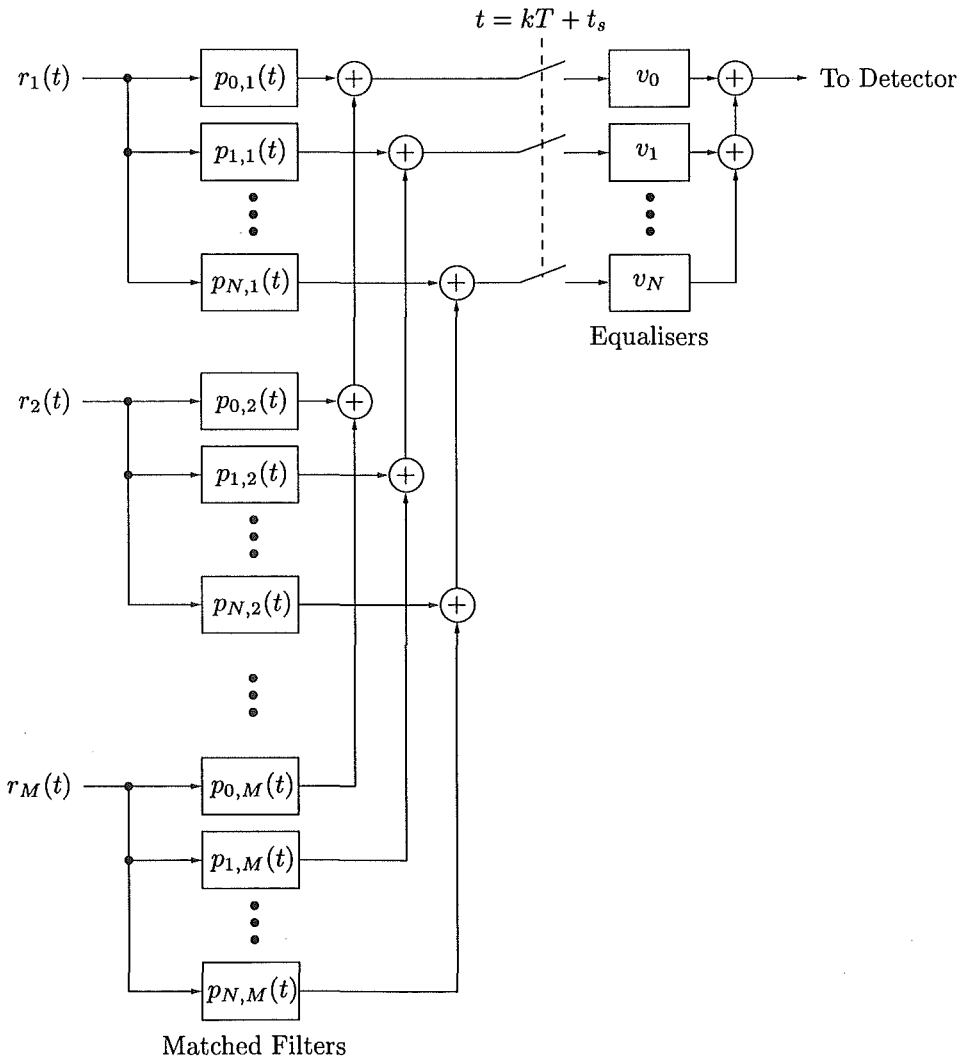

Figure 1.8 Optimum linear receiver

(2) The optimum linear receiver is shown in Fig. 1.8. It has MN matched filters, and N tapped delay lines (TDL), the outputs of which are summed to obtain the receiver output. The receiver is linear and computes the most likely input for a single desired source on a symbol-by-symbol basis. Expressions were derived for the *equaliser responses* under the criterion of minimum mean-square-error. Also, an expression was

given for the mean-square-error and the error performance was estimated.

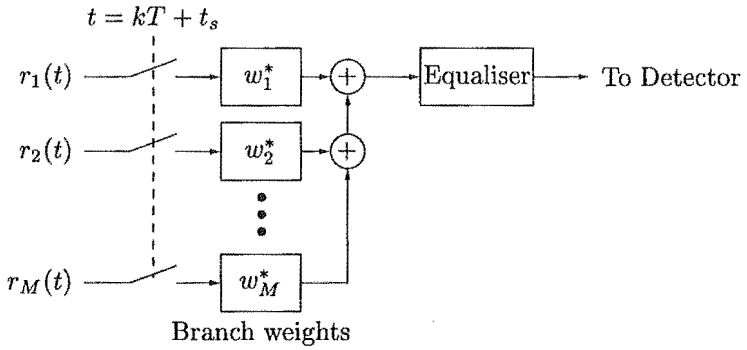

Figure 1.9 M-branch diversity receiver with memoryless branch filters and post-combiner equalisation

(3) Figure 1.9 shows an M-branch receiver consisting of M branch filters whose outputs are summed and fed through a postcombiner equaliser, (the front ends are for demodulation as mentioned above). A receiver with *memoryless* linear combining has branch filters consisting of a *single complex tap weight.* Clark studied five variations of *memoryless* receivers with slightly different filters and performance criteria. The five different criteria were:

- maximal ratio combining without post-combiner equalisation
- minimum mean-square-error (MMSE) combining without post-combiner equalisation
- maximal power combining with ideal post-combiner equalisation
- maximal power combining with linear post-combiner equalisation
- MMSE combining with ideal post-combiner ISI cancellation

Clark computed, via simulation, the following relationships:

- outage probability versus BER threshold given a fixed level of interference
- outage probability versus signal-to-interference ratio (SIR) given a fixed BER threshold (SIR includes dominant CCI in the cases where more than one source is used)
- average BER versus SIR

Each of these relationships were evaluated for various combinations of delay spread and diversity order. The use of the Karhunen-Loéve orthogonal expansion provided for fast convenient channel modelling on a computer as well as an analytical tool to aid in the various derivations.

1.8 RELATED STUDIES IN CARRIER FREQUENCY RECOVERY

There are many frequency recovery schemes for the frequency-selective fading channel, however, most appear to use Orthogonal Frequency Division Multiplexing (OFDM) to overcome the effects of frequency-selective fading [Tuisel and Kameyer 1992, Classen and Meyr 1994].

Results for a system with combined equalisation, decoding and antenna diversity combining with feedforward synchronisation have been obtained by simulation [Fechtel and Meyr 1993]. The system works in the frequency-selective Rayleigh fading channel. The data aided feedforward synchronisation performs a channel estimate and the channel estimate can track a normalised carrier frequency offset of $\Delta fT = 0.0032$. However, the system does not explicitly estimate the carrier frequency offset.

A feedforward carrier recovery scheme has been proposed for the frequency-selective fading channel [Luise and Reggiannini 1995]. It was derived using maximum-likelihood techniques, and estimates the residual carrier frequency offset present in a received signal after down-conversion to baseband by a free-running local oscillator. However, it requires channel and data estimates in order to remove the modulation component of the signal, and leaving a signal from which to estimate the carrier frequency offset.

1.9 AIM OF THE THESIS

The study of mobile communication systems is extremely complicated, and tends to be approached from one of two directions. Either assumptions are made to simplify the problem so that relatively simple *real world* solutions can be found, or assumptions are made to simplify the problem so that *optimal* (but unrealisable) solutions can be found. For example, if the system parameters are chosen such that the channel fading is non-frequency-selective and there is not much interference from other users, then it is simpler to design systems that can be implemented. Conversely, if the channel fading is frequency-selective and there is a large amount of interference from other users, theoretical solutions usually involve ideal assumptions, such as ideal channel state information, ideal carrier recovery, non-causal filters, or unlimited processing power.

This thesis aims to continue existing study tending from the optimal, unrealisable solutions to the real world, realisable solutions.

Three distinct aspects are concentrated on:

- The degradation in performance of a receiver with finite length equalisers as opposed to infinite length equalisers, assuming ideal carrier recovery, ideal channel state information, ideal symbol timing.

- The design and performance analysis of a feed-forward carrier frequency offset recovery scheme for the diversity receiver that does not require a channel estimate.
- The extension of the time-invariant (pseudo-static) frequency-selective channel model to a more general time-variant frequency-selective channel model.

1.10 SUMMARY

This chapter has given a short introduction to the goals of universal mobile communications, and has provided a conceptual feeling for the task of a digital transmission system, a background of the current technologies available, a summary of some of the relevant literature, and the motivation and aims of this thesis. The remaining chapters cover the material specified in the aims.

Chapter 2

SYSTEM MODEL

The system model presented here is similar to that presented by Clark [1992] except for two aspects: the time-varying nature of the model and the structure of the receiver. Clark assumed a pseudo-static channel model, whereas this chapter presents a general time-varying channel model of which Clark's is a special case. The reason for the similarities is to readily allow comparison of performance results of the receiver studied here with those of Clark. The structure of the receiver to be analysed is covered in Chap. 3.

The reception of digital radio transmission in the mobile cellular environment is affected by distortions introduced by the environment. This chapter describes the parts of the physical environment that are considered, the distortion encountered in the signals received at the receiver, and develops a model of the channel between the transmitter and the receiver.

Section 2.1 describes the cellular subsystem that is considered in this thesis. Section 2.2 describes the data sources. Section 2.3 presents the transmission link from the transmitters to the receivers. Section 2.4 describes the time-varying multipath channel model. Section 2.5 describes computer simulation of the channel, and the chapter is concluded in Sec. 2.6.

2.1 RESTRICTED SUBSYSTEM OF THE GENERAL CELLULAR SYSTEM

In order to evaluate the performance of a radio link in a cellular system, it is necessary to consider only a small subsystem of the general system. The subsystem presented here is the same as the subsystem presented by Clark [1992]. The general cellular concepts have been described in Sec. 1.1, while this section describes the parts of the general cellular system that are considered here and the motivation for choosing the model.

Each base station will have a number of frequency bands assigned to the mobiles in its cell at any time. Attention is focussed on the reception of signals in a single

frequency band at a single base station. The general system will have a large number of radio links between mobiles and base stations, however it is necessary to consider only a single link and the distortions and interference it experiences. This is because the physical environment is not explicitly modelled, and all base stations and all frequency bands are assumed to have effectively equivalent expected performance.

Although not necessary, it is assumed that the diversity antennae are at the base station, as the base station receiver can be made relatively complex. The use of transmission diversity at the base station (allowing a simple receiver structure at the mobile) is not investigated. Since the base station is assumed to be the receiver, the mobiles are assumed to be transmitters and are referred to as sources. However, the mobile-to-base and base-to-mobile transmission statistics are almost identical [Glance and Greenstein 1983].

For any frequency band in any cell, there will be one *desired* source and many co-channel sources in distant cells. In the general cellular model, every mobile will be a desired source in its own cell, and the base station receiver will require separate processing for each desired source (i. e., on each frequency band) in its cell.

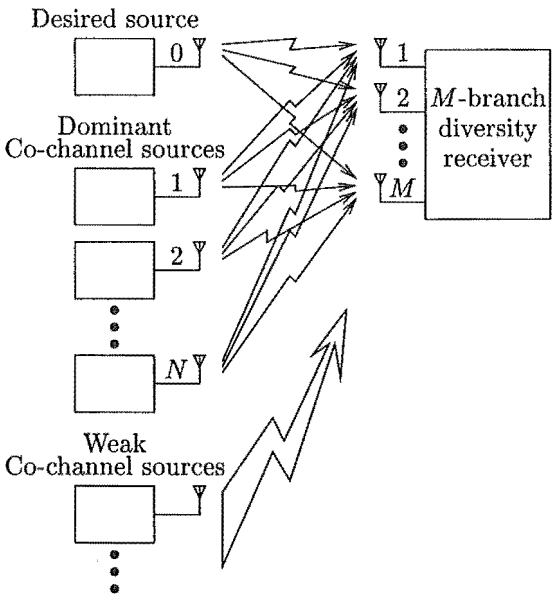

Figure 2.1 Restricted sub-system to be analysed

The resulting restricted subsystem is shown in Fig. 2.1. The following components are modelled: one desired (dominant) source, N *dominant co-channel* sources, and "a large number" of *weak co-channel* sources. Between the $N_d = 1 + N$ dominant sources (i. e., the desired source and the dominant co-channel sources) and the M receiver branches, $N_d M$ multipath channels are modelled. The dominant co-channel interferers contribute, in general, non-white, non-Gaussian interference which is explicitly modelled in the same manner as the desired source, whereas the weak co-channel interferers

are assumed to contribute noise which is assumed Gaussian (by the Central Limit Theorem) and can be handled as is usual for coloured noise. The distinction between the dominant and weak co-channel sources is that the dominant co-channel sources are assumed to have a large average power relative to the weak co-channel sources, as their names suggest. Denoting S_n as the average gain of the n^{th} transmitter, two average power ratios are used to specify the levels of interference [Clark 1992]:

- The signal-to-interference ratio, defined as the ratio of average desired signal power to average CCI power is given by

$$\text{SIR} = \frac{S_0^2}{\sum_{n=1}^{N} S_n^2 + \sum_{n>N} S_n^2} \tag{2.1}$$

- The dominant-to-weak-interference ratio, defined as the ratio of average dominant CCI power to average noise-like CCI power is given by

$$\text{DWR} = \frac{\sum_{n=1}^{N} S_n^2}{\sum_{n>N} S_n^2} \tag{2.2}$$

2.2 DATA SOURCES AND MODULATION

This section describes the characteristics of the signals that are transmitted from the sources.

The system is assumed to operate in burst mode, which means that bursts of tens or hundreds of symbols are transmitted in a burst rather than continuous transmission of symbols [Steele 1992]. This allows for the simple implementation of time division multiple access (TDMA), where different users transmit bursts on different timeslots one after another in the same frequency band. The use of TDMA increases the bandwidth which can be an advantage in the fading channel [Monsen 1971]. The system may also use frequency division multiple access (FDMA), although adjacent channel interference is not considered here.

Each of the sources is assumed to generate random uncorrelated binary message data. If this were not the case, then it would be possible to code the message data to remove any correlation. Efficient algorithms for compressing speech, images, or any other data will result in almost completely uncorrelated data. Hence the assumption of uncorrelated data is valid for any sort of digital transmission. The zero-mean uncorrelated data symbols have covariance

$$E[x_k^* x_{k'}] = \sigma_x^2 \delta(k, k') \tag{2.3}$$

where $\delta(k, k')$ is the Kronecker delta function [Kreyszig 1988, p. 219].

Note that channel coding is not considered, that is to say redundant bits are not included to improve transmission performance. The ability of the receiver to estimate raw data bits is all that is considered. If channel coding was used, then the assumption of uncorrelated transmitted data would not hold, and the analysis would have to allow for combined coding and equalisation [Gitlin *et al.* 1992, p. 108].

The transmitter is assumed to transmit symbols using a linear modulation technique, e. g., phase shift keying (PSK) or quadrature amplitude modulation (QAM). The binary message data are mapped onto a signal constellation as described in Sec. 1.2. The modulation is restricted to being linear, but the analysis is valid for any constellation shape. However, simulation results are obtained only for a symbol consisting of two bits, i. e., quadrature phase shift keying (QPSK). QPSK has similar characteristics to those of the bandwidth efficient Gaussian minimum shift keying (GMSK), however it is simpler to analyse because it is linear [Proakis 1989, p. 201].

2.3 TRANSMISSION LINK

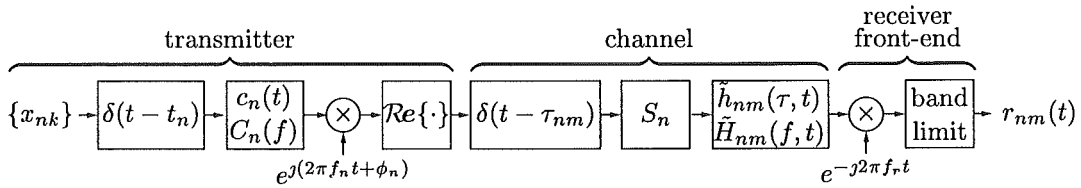

Figure 2.2 Passband system link model.

Figure 2.2 shows a block diagram of the link, $r_{nm}(t)$, from the n^{th} data source to the received signal on the m^{th} diversity branch. The sequence of complex data symbols, $\{x_{nk}\}$, is transmitted at time $t = kT$, where T is the symbol period, t_n is the symbol timing offset of the n^{th} source relative to the desired source ($t_0 = 0$) assumed to be uniformly distributed on $[-\frac{T}{2}, \frac{T}{2})$, $c_n(t)$ is the pulse shaping filter impulse response of the n^{th} transmitter with excess bandwidth β, f_n is the n^{th} transmitter oscillator frequency, ϕ_n is the n^{th} transmitter oscillator phase relative to the receiver oscillator assumed to be uniformly distributed on $[0, 2\pi)$, τ_{nm}, S_n, and $\tilde{h}_{nm}(\tau, t)$ describe the *passband* channel, the statistics of which are described in Sec. 2.4 and f_r is the receiver oscillator frequency. Note that all the pulse shaping is performed in the transmitter, and the receiver only has a noise-rejection filter, i. e., it has a flat response over the bandwidth of the received signal, but rejects noise outside this bandwidth.

The response of the time-varying frequency-selective multipath channel from the n^{th} transmitter (or source) to the m^{th} receiver branch is described by the input-delay spread function, $\tilde{h}_{nm}(\tau, t)$ [Bello 1963]. The input-delay spread function describes the passband response at time t of the channel, to an impulse transmitted at time $t - \tau$. In other words, t is the time instant when the response at the output of the channel

is observed, and τ is the delay beforehand when the signal was transmitted. However, $\tilde{h}_{nm}(\tau, t)$, is not defined to describe the total transmission delay from the transmitter to the receiver. Instead, it is defined so the first path has no delay, and the total transmission delay from the n^{th} transmitter to the m^{th} receiver branch is modelled separately by τ_{nm}.

The input-delay spread function is used to describe the channel, as opposed to either the output-delay spread function or the kernel functions described in Bello [1963], because the forms of the equations used here reduce to the time-invariant case simply by dropping the t variable, and can readily be compared to previous work.

2.4 CHANNEL MODEL

This section presents a general time-varying frequency-selective multipath channel model that may be used to analyse the system, and also to allow an efficient technique for computer simulation of the system. It is based on the pseudo-static model developed by Clark [1992], however, it extends this model into a general time-varying model.

It is assumed that the mobile is operating in a multipath environment, i. e., on each channel, plane waves travel from a transmitter antenna to a receiver antenna via many different *paths*, each wave reflecting off objects in the mobile environment. Each channel between the sources and the receiver diversity branches is assumed to be a frequency-selective multipath channel with identical Rayleigh fading statistics [Jakes, Jr. 1974, pp. 13–19]. The mobile is assumed to be operating in a dense urban environment, so there is no direct line-of-sight wave. The waves travelling over long paths have long delays and generally have larger losses because they have reflected off more objects. The frequency of each received wave has a Doppler shift associated with it, which is primarily a result of the movement of the mobile relative to the base station [Jakes, Jr. 1974, pp. 46–50]. For any particular delay many waves will contribute and may add constructively or destructively. The phase of each received wave depends on the length of the path taken by the wave. Small changes in path length produce rapid changes in phase, for instance, a change in path length equal to the carrier wavelength (e. g., 33 cm at 900 MHz) will change the phase by 2π. The phase of the sum of the contributions at a particular delay also varies rapidly and is highly dependent on the path taken (and hence the delay). The phase of the contributions at different delays are highly uncorrelated, and channel is therefore said to exhibit *uncorrelated scattering* [Proakis 1989, pp. 702–713]. The amplitude of both the in-phase and quadrature components of the sum of the contributions will have approximately a Gaussian distribution by the central limit theorem, so the distribution of the *envelope* of the received signal in each channel will be Rayleigh.

The frequency-selective nature of the channel means that different frequencies experience a different attenuation and phase through the channel. This occurs when the difference between the maximum and minimum transmission delays (the delay spread) experienced by the waves travelling via the multiple paths is not negligible relative to the symbol period [Proakis 1989, pp. 713–716]. This means that the bandwidth is large enough that, for example, waves at some frequency can arrive at the receiver and combine constructively, while waves at different frequencies can arrive at the receiver via the same paths and combine destructively. This could occur, for example, if the symbol period is reduced, the cell size is increased, or there are more scatterers in the environment.

As well as being assumed to exhibit uncorrelated scattering (US), the channel is assumed to be *quasi wide-sense stationary* (QWSS). The assumption of wide-sense-stationarity means that the second-order statistics remain constant over time. This is not the case in a mobile radio environment, because the channels exhibit slow shadow fading due to large features of the environment such as hills [Loo and Secord 1991]. However, the short term statistics can be assumed approximately constant, hence the assumption of QWSS. This implies that the complex response of the channel can be described by a single complex correlation function.

2.4.1 Complex Baseband Representation of the Channel

In order to simplify analysis, it is desirable to represent the system at baseband, i. e., representing the baseband signal at the receiver without using passband channel response functions [Bello 1963]. This is done by defining complex baseband representations of the passband channel functions. The passband channel input-delay spread function, $\tilde{h}_{nm}(\tau, t)$, is replaced by its complex baseband equivalent, $h_{nm}(\tau, t)$, using the following relation

$$\tilde{h}_{nm}(\tau, t) = 2\mathcal{R}e\{h_{nm}(\tau, t)e^{\jmath 2\pi f_n \tau}\} \tag{2.4}$$

The received signal on the m^{th} branch due to the n^{th} source is then

$$\begin{aligned} r_{nm}(t) = &\sum_k x_{nk} \int_{-\infty}^{\infty} c_n(t - \tau - \alpha_{nm} - kT) h_{nm}(\tau, t)\, d\tau \\ &\cdot e^{\jmath 2\pi (f_n - f_r)t} e^{-\jmath(2\pi f_n \tau_{nm} - \phi_n)} \end{aligned} \tag{2.5}$$

where $\alpha_{nm} = t_n + \tau_{nm}$. Notice the term *received signal* actually refers to the signal after the receiver front-end rather than the signal received on the antenna. It is a function of the complex baseband representation of the channel, the oscillator frequency mismatch, $(f_n - f_r)$, and the total transmission delay. As can be seen in Fig. 2.2, the receiver front-end only has band-limiting or noise-rejection filters, and does not perform any

pulse shaping. This is discussed in Chap. 3.

The received signal on the m^{th} branch due to all the sources is

$$r_m(t) = \underbrace{r_{0,m}(t)}_{\substack{\text{Desired} \\ \text{source}}} + \underbrace{\sum_{n=1}^{N} r_{nm}(t)}_{\substack{\text{Dominant} \\ \text{CCI}}} + \underbrace{\eta_m(t)}_{\substack{\text{Weak CCI and} \\ \text{additive noise}}} \tag{2.6}$$

where $\eta_m(t)$ is the complex baseband representation of the noise contributions of the weak co-channel interferers and the receiver noise, which is assumed Gaussian as described in Sec. 2.1. The passband noise signal, $\tilde{\eta}_m(t)$, and its complex baseband equivalent, $\eta_m(t)$, are related by the following

$$\tilde{\eta}_m(t) = 2\mathcal{R}e\{\eta_m(t)e^{\jmath 2\pi f_r t}\} \tag{2.7}$$

It is desirable in both the analysis and the simulation of the system to consider the combination of the pulse shaping filter function and the channel function as a single random process. Therefore the complex baseband *link* input-delay spread function, $q_m(\tau, t)$, is defined as

$$q_{nm}(\tau, t) = \int_{-\infty}^{\infty} c_n(\tau - \alpha - \alpha_{nm}) h_{nm}(\alpha, t)\, d\alpha \tag{2.8}$$

The link function from the n^{th} source to the m^{th} branch can be seen as the combined response (at time t to an impulse at time $t - \tau$) of the n^{th} pulse shaping filter time shifted by the total transmission delay, and the channel response.

The received signal on the m^{th} branch due to the n^{th} source becomes

$$r_{nm}(t) = \sum_k x_{nk} q_{nm}(t - kT, t) e^{\jmath 2\pi \Delta f_n t} e^{\jmath \phi_{nm}} \tag{2.9}$$

where $\Delta f_n = f_n - f_r$ and $\phi_{nm} = \phi_n - 2\pi f_n \tau_{nm}$. The received signal is composed of data symbols, the complex baseband link response, a linear phase term proportional to the carrier frequency offset, and a nominally constant phase offset that is dependent on oscillator mismatches and total channel transmission delays.

2.4.2 Orthogonal expansion of the complex baseband link response

The procedure is performed in the frequency domain and converted to the time domain for two reasons. First, a time shift, α_{nm}, is accomplished efficiently in the frequency domain by multiplying the channel time-varying transfer function by the linear phase trend term, $e^{\jmath 2\pi f \alpha_{nm}}$. Second, the algorithm involves eigenvalues that decay faster in

the frequency domain than in the time domain, and thus requires fewer terms for a given accuracy.

To compact notation, the input-delay spread function of the *channel shaped by the pulse shaping filter response* is denoted by

$$z_{nm}(\tau, t) = \int c_n(\tau - \alpha) h_{nm}(\alpha, t)\, d\alpha \tag{2.10}$$

and the time-varying transfer function (the corresponding frequency domain response) by

$$Z_{nm}(f, t) = C_n(f) H_{nm}(f, t) \tag{2.11}$$

Consider the autocorrelation of $Z_{nm}(f, t)$

$$\Xi(f_1, f_2; t_1, t_2) = E[Z_{nm}(f_1, t_1) Z^*_{nm}(f_2, t_2)] \tag{2.12}$$

The autocorrelation function, $\Xi(f_1, f_2; t_1, t_2)$, can be separated into two functions, one describing the frequency correlation, and one describing the time correlation, since the time correlation can be seen to be independent of frequency by considering the following. The time correlation is determined by the Doppler spectrum and for a fast moving mobile in a dense urban environment, the Doppler spectrum is almost totally determined by the vehicle speed and the transmission frequency. At carrier frequencies of 900 MHz and a signal bandwidth of a few hundred kilohertz, the transmission frequency is essentially the same across the signal bandwidth, so the Doppler spectrum shape would not change significantly as a function of frequency over the signal bandwidth.

Thus the autocorrelation function, can be written as.

$$\Xi(f_1, f_2; t_1, t_2) = \Xi_f(f_1, f_2) \Xi_t(t_1, t_2) \tag{2.13}$$

If shadowing is not considered, and the time correlation is assumed to be wide-sense stationary, then the autocorrelation of $Z_{nm}(f, t)$ becomes a function of three variables

$$\Xi(f_1, f_2; t_2 - t_1) = \Xi_f(f_1, f_2) \Xi_t(t_2 - t_1) \tag{2.14}$$

Since the autocorrelation of $Z_{nm}(f, t)$ can be separated into two functions describing the time and frequency correlations and since $Z_{nm}(f, t)$ is a zero-mean complex Gaussian random process, it can be expanded in a Karhunen-Loéve orthogonal expansion [Davenport and Root 1958] where the random coefficients become time-varying processes. (Appendix A contains a summary of the Karhunen-Loéve expansion with

coefficients that are not correlated in time.)

$$Z_{nm}(f,t) = \sum_{i=1}^{J_n} \sqrt{\lambda_{ni}} c_{nmi}(t) \phi_{ni}(f) \tag{2.15}$$

where $\{\lambda_{ni}\}$ is a set of J_n real eigenvalues (2.17), $\{c_{nmi}(t)\}$ is a set of independent zero-mean complex Gaussian random processes with unity variance, and $\{\phi_{ni}(f)\}$ is a set of orthonormal eigenfunctions (2.17), i. e., such that

$$\int_{-\frac{W}{2}}^{\frac{W}{2}} \phi^*_{n_1 i}(f) \phi_{n_2 i}(f)\, df = \delta(n_1, n_2) \tag{2.16}$$

The eigenvalues and eigenfunctions are found by solving the eigensystem given by [Clark 1992]

$$\int_{-\frac{W}{2}}^{\frac{W}{2}} \Xi_f(f_1, f_2) \phi_{ni}(f_2)\, df_2 = \lambda_{ni} \phi_{ni}(f_1), \qquad |f_1| \leqslant \frac{W}{2} \tag{2.17}$$

The time correlation of $Z_{nm}(f,t)$ is given by $\Xi_t(t_2 - t_1)$. It remains to determine the time correlation of $c_{nmi}(t)$, the weighting random processes. Note that $E[c_{nmi}(t_1) c^*_{nmj}(t_2)] = 0$ for $i \neq j$ [Davenport and Root 1958], i. e., the different indices represent different independent random processes.

From (2.12) and (2.15) we then have

$$\Xi(f_1, f_2; t_2 - t_1) = E\left[\sum_i \sum_j c_{nmi}(t_1) c^*_{nmj}(t_2) \sqrt{\lambda_{ni}} \sqrt{\lambda_{nj}} \phi_{ni}(f_1) \phi^*_{nj}(f_2) \right] \tag{2.18}$$

$$= \sum_i E[c_{nmi}(t_1) c^*_{nmi}(t_2)] \lambda_i \phi_{ni}(f_1) \phi^*_{ni}(f_2) \tag{2.19}$$

and since the functions $\phi_{ni}(f)$ are orthonormal they can be removed from the RHS by multiplying and integrating

$$\int \Xi(f_1, f_2; t_2 - t_1) \phi^*_{nj}(f_1)\, df_1 = \int \sum_i E[c_{nmi}(t_1) c^*_{nmi}(t_2)] \lambda_i \phi_{ni}(f_1) \phi^*_{ni}(f_2) \phi^*_{nj}(f_1)\, df_1 \tag{2.20}$$

$$= E[c_{nmj}(t_1) c^*_{nmj}(t_2)] \lambda_{nj} \phi^*_{nj}(f_2) \tag{2.21}$$

by (2.16) and the same technique gives

$$\frac{1}{\lambda_{nj}} \iint \Xi_f(f_1, f_2)\Xi_t(t_2 - t_1)\phi^*_{nj}(f_1)\phi_{nj}(f_2)\, df_2\, df_1$$

$$= \frac{1}{\lambda_{nj}} \int E[c_{nmj}(t_1)c^*_{nmj}(t_2)]\lambda_{nj}\phi^*_{nj}(f_2)\phi_{nj}(f_2)\, df_2 \tag{2.22}$$

$$= E[c_{nmj}(t_1)c^*_{nmj}(t_2)] \tag{2.23}$$

$$\tag{2.24}$$

Then by (2.17)

$$\frac{1}{\lambda_{nj}}\Xi_t(t_2 - t_1) \int \lambda_{nj}\phi^*_{nj}(f_1)\phi_{nj}(f_1)\, df_1 = E[c_{nmj}(t_1)c^*_{nmj}(t_2)] \tag{2.25}$$

$$\Xi_t(t_2 - t_1) = E[c_{nmj}(t_1)c^*_{nmj}(t_2)] \tag{2.26}$$

In other words, the time correlation of the weighting random processes, $c_{nmi}(t)$, is the same as the time correlation of the $Z_{nm}(f, t)$.

Then the link time-varying transfer function is given by

$$Q_{nm}(f, t) = S_n Z_{nm}(f, t)e^{j2\pi f_n \alpha_{nm}} \tag{2.27}$$

where S_n is the average gain of the n^{th} transmitter. Finally, the link input-delay spread function is given by

$$q_{nm}(\tau, t) = \mathcal{F}^{-1}\{Q_{nm}(f, t)\} \tag{2.28}$$

2.4.3 Specifying the frequency correlation function

The frequency correlation function, $\Xi_f(f_1, f_2)$, of the combination of the channel and the pulse shape filter, $Z_{nm}(f, t)$, can be determined from measurements of channels. Consider the autocorrelation of a time-invariant channel impulse response, $h_{nm}(t)$ [Clark 1992]. Since the channel is assumed to exhibit uncorrelated scattering, the autocorrelation function, or *delay power spectrum*, is a function of only one delay variable [Proakis 1989, Chap. 7].

$$E[h_{nm}(\tau_1)h^*_{nm}(\tau_2)] = P(\tau_1)\delta(\tau_2 - \tau_1) \tag{2.29}$$

The autocorrelation, or *coherence function*, of the time-invariant channel frequency response is given by the Fourier transform of the delay variable of the delay power spectrum

$$R(f) = \mathcal{F}\{P(\tau)\} \tag{2.30}$$

The uncorrelated scattering assumption of the channel gives rise to the fact that the autocorrelation of the time-varying transfer function, $R(\alpha)$, is a function only of frequency difference.

From experimental sounding of real (not necessarily time-varying) channels, the shape of the impulse response correlation function of typical channels can be found, and a curve that approximates this shape can be used to characterise the channel [Glance and Greenstein 1983].

Then the frequency correlation function of $Z_{nm}(f,t)$ is found from the channel coherence function, $R(f)$, as

$$\Xi_f(f_1,f_2) = C_n(f_1)C_n^*(f_2)R(f_2-f_1) \tag{2.31}$$

2.4.4 Distribution of the total transmission delay

The data symbols from each co-channel source are assumed to have the same period, T, which, in most systems, is a reasonable assumption. The symbols being transmitted from the n^{th} source have a timing offset relative to the desired source. There is also a timing offset which results from the different delays through the channels. Although the system is assumed to be burst-mode for reasons of equaliser and carrier acquisition, the analysis does not account for the fact that bursts are not synchronised among the desired sources. Instead, it is assumed that infinite streams of data symbols are being produced. Because of this, it is not important which random data symbol from the co-channel interferers is being considered, and therefore, the total timing offset can be assumed to be uniformly distributed over $[-\frac{T}{2},\frac{T}{2})$, even though the difference between the channel delays for the desired source and the co-channel interferer may be larger than this. In other words, should the total timing offset for a given co-channel source be larger than $\frac{T}{2}$, a different symbol could be considered which would reduce the phase offset by a multiple of T. The timing offset results in a phase offset in the received signal, which is combined with the oscillator phase offset between the n^{th} source and the receiver.

2.4.5 Comparison with Clark's pseudo-static channel model

The general time-varying channel model presented here reduces to the model presented by Clark [1992], if all functions of τ and t become functions of τ only by removing the t variable. The random processes $c_{nmi}(t)$ then become independent random variables, and $\Xi_t(t_2-t_1) = \delta(t_2-t_1)$

2.5 COMPUTER SIMULATION OF THE CHANNEL

Generating the time-varying frequency-selective channel responses on a computer must be fast and efficient. The method presented here uses the Karhunen-Loéve orthogonal expansion technique developed by Clark [1992] for his pseudo-static channel model, but also specifies the method of generating time-correlated weighting functions and thus results in a time-varying model.

The following steps are required for each simulation:

- Specify the time correlation function.
- Specify the frequency correlation function.
- Solve the eigensystem given by (2.17).
- Generate random phase offsets for each channel.

Then to generate the time-varying channel responses, perform the following steps:

- Generate independent weighting functions that are correlated in time.
- Generate $Z_{nm}(f,t)$ by (2.15).
- Generate $Q_{nm}(f,t)$ by (2.27).
- Convert to the time domain using the Fast Fourier Transform to obtain $q_{nm}(\tau,t)$.
- Use $q_{nm}(\tau,t)$ for ISI calculations directly or generate $r_m(t)$ using (2.9) and (2.6).

2.5.1 Correlation functions used in this thesis

In the simulations described in this thesis, only one of the power delay spectrum shapes presented by Clark has been used to describe the frequency correlation. It is the one-sided exponential shape

$$P(\tau) = \frac{1}{\tau_0} \exp\left(\frac{-\tau}{\tau_0}\right), \qquad \tau \geqslant 0 \tag{2.32}$$

where τ_0 is the rms delay spread of the channel and is a measure of how spread out the multipath components are, and determines the channel's frequency selectivity, where

$$\tau_0 = \sqrt{\int_{-\infty}^{\infty} (\tau - \overline{\tau})^2 P(\tau)\, d\tau} \tag{2.33}$$

and $\overline{\tau} = \int_{-\infty}^{\infty} \tau P(\tau)\, d\tau$ is the *mean delay.*

The corresponding frequency coherence function is

$$R(f) = \frac{1}{1 + j2\pi f \tau_0} \tag{2.34}$$

The reason for restricting the channel characteristics to one function is that Clark has already established trends for three different power delay spectrum shapes for the different receiver structures, and shows that the optimum linear receiver performance is not extremely sensitive to delay spectrum shape especially for continuous delay profiles, as opposed to discrete delay profiles. Also, choosing only one profile reduces the amount of simulation required.

Despite having developed a time-varying channel model, this thesis does not generate correlated random weighting processes for the simulations. Instead it uses independent identically distributed random variables in the same manner as Clark [1992]. The reason for this is that the results presented here are compared against those presented by Clark, and this thesis did not cover adapting equaliser weights which would require a time-varying channel model.

However, if a time-varying channel model was to be used, the time correlation function, (which is also the time correlation of the weighting functions, $c_{nmi}(t)$), can be determined from assumptions about the incident rays at the receiver. In a dense urban environment, the waves can be assumed to arrive at the receiver horizontally with uniformly distributed approach angles [Parsons 1992] in which case

$$\Xi_t(t_2 - t_1) = J_0\left(\frac{2\pi v(t_2 - t_1)}{\lambda}\right) \tag{2.35}$$

where $J_0(\cdot)$ is a Bessel function of the first kind of zero order, v is the vehicle speed, and λ is the carrier wavelength. Using a more general model in which the waves arrive at an angle from the horizontal [Aulin 1979], the correlation function is given by

$$\Xi_t(t_2 - t_1) = \int J_0\left(\frac{2\pi v(t_2 - t_1)}{\lambda}\cos\beta\right) p_\beta(\beta)\, d\beta \tag{2.36}$$

where $J_0(\cdot)$ is a Bessel function of the first kind of zero order, $p_\beta(\beta)$ specifies the distribution of the arrival angle of the incident waves.

2.6 CONCLUSION

This chapter has presented the system model to be analysed in this thesis. It has presented the subsystem of the general cellular model that is considered and discussed the data sources in the system. It clearly defines the extension of Clark's pseudo-static channel model to a general time-varying channel model. It presents the correlation

functions used in the simulations in this thesis. The next chapter presents the receiver structure that has been proposed to process the received signals.

Chapter 3

RECEIVER STRUCTURE

With the use of space diversity, the optimum minimum-mean-square-error (MMSE) linear receiver (i.e., best possible MMSE linear receiver) has already been shown to closely approximate the maximum likelihood receiver (i.e., best possible non-linear receiver) [Clark 1992]. In this thesis, attention is concentrated on a linear diversity receiver structure rather than a non-linear structure because it has a lower complexity, is simpler to analyse, and also, is closer to being implemented. The receiver structure presented here approximates the optimum linear receiver [Clark 1992]. In Chap. 4, results show the degradation in performance of the sub-optimal, but physically realisable, receiver from that of the optimum linear receiver, however ideal carrier recovery is assumed in both cases to allow for easy comparison. In Chap. 5, the performance of a carrier frequency recovery scheme is presented.

This chapter describes the receiver structure studied in this thesis. It discusses the motivation behind the choice of receiver structure and the assumptions made about the receiver functionality in the two separate studies on equalisation and carrier recovery. Section 3.1 describes how the optimum linear *filter* can be synthesized by a single fractionally-spaced equaliser. Section 3.2 goes on to show how this fact can be used to derive a receiver structure that is a realisable approximation to the optimum linear diversity *receiver* structure (which consists of many optimum linear filters). Section 3.4 discusses some practical considerations concerning the chosen receiver structure.

3.1 SYNTHESIS OF THE OPTIMUM LINEAR FILTER

It is well known [Qureshi 1985] that a cascade consisting of a filter that is matched to the channel followed by a symbol-spaced sampler and an infinite-length tapped-delay-line (TDL), or equaliser, is the optimum linear receive filter for an additive white Gaussian noise channel with linear distortion. This means that the output of the cascade of matched filter and infinite-length TDL is a set of sufficient statistics for estimating the transmitted data. The filter is optimum for the same criterion of optimality as the equaliser. In other words if the equaliser is optimised for minimum mean-square-error

(MMSE), then the cascade is optimum in the MMSE sense. It is possible to achieve better performance using a *non-linear* structure such as a decision-feedback-equaliser, but the cascade of matched filter and TDL is the best possible *linear* structure.

Figure 3.1 shows a cascade of a filter matched to a link response, followed by an infinite length equaliser. The output of the matched filter is sampled synchronously, (at multiples of the symbol period, T), and these samples are fed into the delay elements. The stored samples are weighted by the equaliser weights (or taps), w_l, and summed to produce an output sample every symbol period.

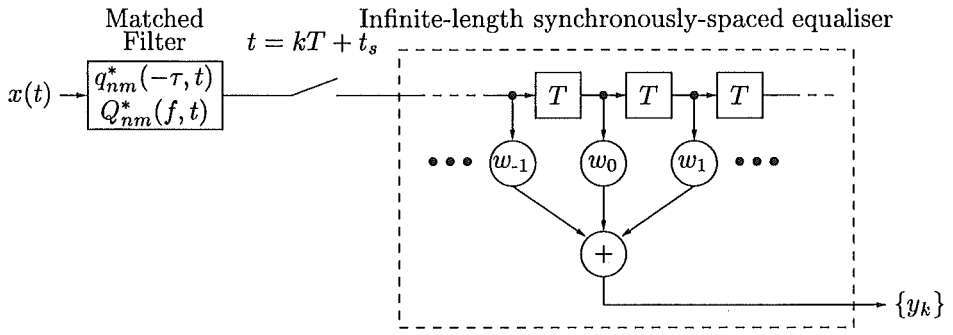

Figure 3.1 Cascade of matched filter followed by infinite length equaliser

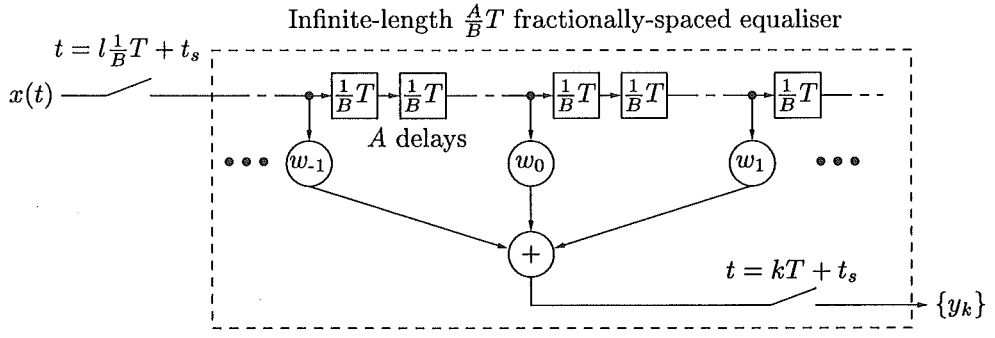

Figure 3.2 Infinite length fractionally spaced equaliser

A fractionally spaced equaliser can synthesize the cascade of a matched filter and a symbol spaced equaliser [Qureshi 1985]. Figure 3.2 shows an equaliser structure that can synthesize the overall filter cascade shown in Fig. 3.1 for bandlimited input signals. In a digital implementation, the fractional spacing is limited to $\frac{A}{B}T$, where A and B are integers. Every T seconds, B samples are fed into the delay elements, and samples spaced by A delay elements are weighted by the weights, w_l, to give the output, y_k.

The matched filter compensates for phase distortion introduced by the channel, while the infinite-length TDL equalises amplitude distortion. To see how this happens, it is instructive to view the complex frequency responses of the link, the combination

of the link and matched filter, the MMSE equaliser, and the combination of the link, the matched filter, and the MMSE equaliser.

Figure 3.3(a) shows an example of a complex baseband link frequency response. The radial lines from the frequency axis are plotted on planes parallel to the plane containing the real and imaginary axes. So vertical lines represent purely real quantities, while lines that are parallel to the imaginary axis represent purely imaginary quantities. It should be possible to see how the phase changes across the frequency band, and that there is a deep fade to the left of 0 Hz frequency.

Figure 3.3(b) shows the sampled output of a filter that is matched to the link frequency response of Fig. 3.3(a). It can be seen that the matched filter compensates for the phase distortion making the filter output purely real. The sampling process causes the frequency spectra to be repeated at multiples of the sampling frequency, and the repeated spectra are shown in different line styles. Although the link response is quite faded at the band edges, it is still possible to see aliasing occurring where the tails of the repeated spectra overlap. However, since the matched filter output has zero phase, the aliasing does not result in loss of information.

Figure 3.3(c) shows the response of the infinite-length equaliser that has been optimised for minimum-mean-square-error (MMSE). Note the high gain at the frequency corresponding to the deep fade. Figure 3.3(d) shows the response of the cascade of the link, the matched filter, and the equaliser. It can be seen that the resulting response approximates a Nyquist response. (If the system was noise free, and the equaliser could have infinite gain, then the combined response would be a Nyquist response.)

In order to understand how a fractionally spaced equaliser can synthesize the combination of a matched filter and a symbol spaced equaliser, it is necessary to understand the concept of aliasing. Aliasing occurs when a lowpass signal is sampled at a sampling rate that is less than twice the highest frequency component in the signal. When a system uses a pulse shape with excess bandwidth [Gitlin *et al.* 1992, p. 493] the band edges are aliased when the received signal is sampled at the symbol rate. This can clearly be seen in Fig. 1.2(c) where the solid pulse overlaps both dashed pulses. When the pulses are transmitted through a channel with frequency selective distortion, the band edges experience differing phase changes. For example, Fig. 3.3(a) shows the combined frequency response of a channel and pulse shape filter where the symbol experiences a negative phase change at the positive frequency band edge and a positive phase change at the negative frequency band edge. If a signal transmitted on this channel was sampled at the symbol rate, the band edges would cancel when they are aliased.

As the sampling rate is increased, the repeated spectra become further apart. So when the received signal is sampled, any excess bandwidth due to pulse shaping is not aliased by the sampling process, as is the case for symbol spaced samples. It is

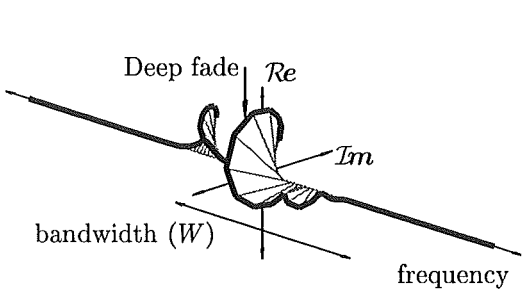

(a) Link frequency response

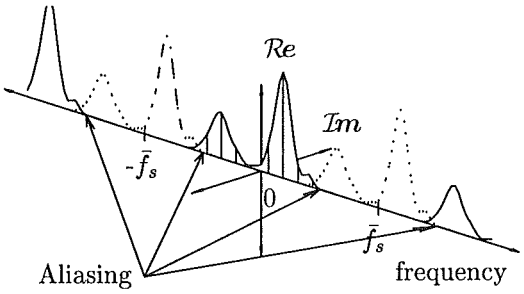

(b) Matched filter output synchronously sampled

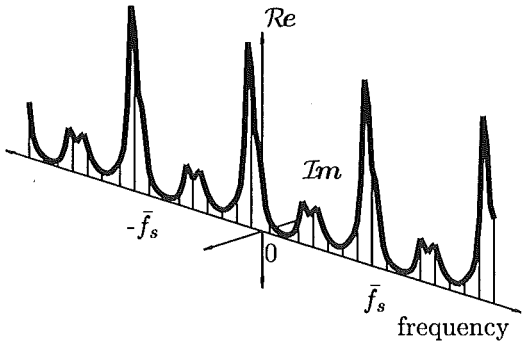

(c) MMSE synchronously spaced equaliser response

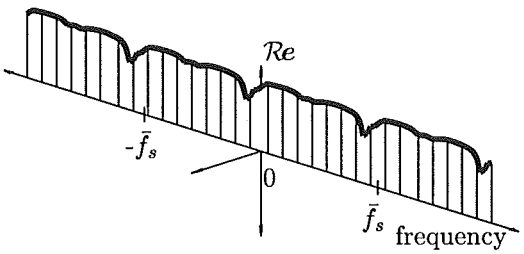

(d) Equalised link frequency response

Figure 3.3 Complex baseband frequency responses describing cascade of matched filter and synchronously-sampled equaliser

important to realise that since the repeated spectra appear at multiples of the sampling frequency, the increased sampling frequency of the fractionally spaced equaliser, relative to the symbol spaced equaliser, allows it to effectively deal with band edge phase distortion before the band edges are aliased. In other words, the fractionally spaced equaliser can compensate for the phase distortion (and also the amplitude distortion) before the spectrum is aliased by symbol spaced sampling at the output. As a result, the symbol-spaced output contains negligible phase distortion.

Figure 3.4(a) shows the complex baseband frequency response of the same example link which has been sampled at a fractional sample period, with sampling frequency, f_s. It can be seen that for an ideal bandlimited pulse shaping filter, no aliasing occurs. For a realisable pulse shaping filter, the aliasing can be reduced by increasing the sampling frequency.

Figure 3.4(b) shows the complex baseband response of a *fractionally-spaced* equaliser, with infinite-length, optimised for MMSE. It also exhibits a large gain corresponding to the channel fade, but has non-zero phase to compensate for the phase

response of the link which has not been matched filtered. The combined response of the link and the fractionally-spaced equaliser is shown in Fig. 3.4(c). It can be seen that the equaliser has compensated for both the phase and amplitude distortion. Finally, the frequency response is aliased by subsampling the fractionally-spaced samples (Fig. 3.4(d)), resulting in the same frequency response as for the cascade of the matched filter and synchronously-spaced equaliser (Fig. 3.3(d)). However, note that the aliasing experienced by the subsampling at the output of the fractionally-spaced equaliser does not result in loss of information, provided the equaliser has corrected for the phase distortion of the channel.

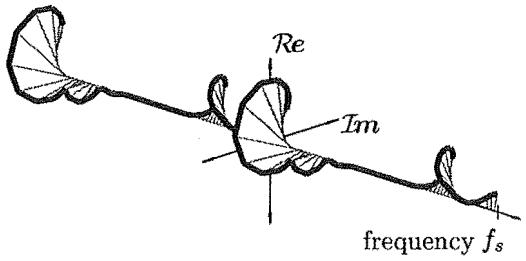

(a) Fractionally spaced sampled link frequency response

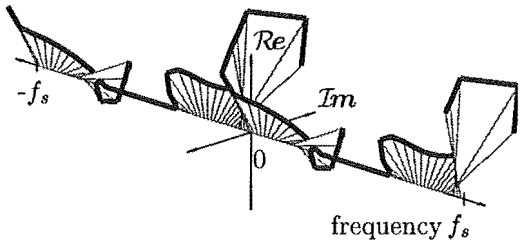

(b) MMSE fractionally spaced equaliser response

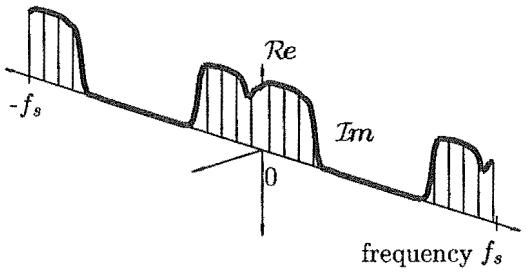

(c) Fractionally spaced sampled equalised link response

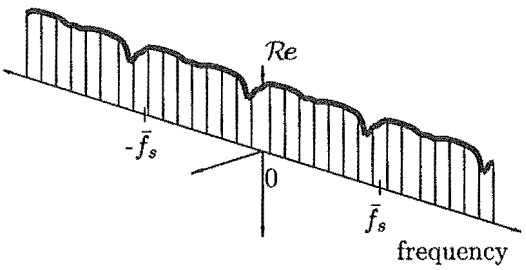

(d) Synchronously spaced sampled equalised link frequency response

Figure 3.4 Complex baseband frequency responses describing fractionally-spaced equaliser

In a time-varying channel, a matched filter is required that evolves with time as the channel varies. However, a filter like this is very difficult to build because there are no simple methods for designing continuous filters with generalised responses in real time. Using a fractionally-spaced equaliser instead of the cascade of matched filter and synchronously-spaced equaliser is better because it does not require a time-varying continuous matched filter. Since the equaliser is realised in the digital domain and its structure is well defined, it is relatively easy to design adaptive algorithms that can be used to update the coefficients, w_l, to effectively match the time-varying channel. There is much literature on the topic — see Qureshi [1985] for a thorough overview.

3.2 REALISABLE APPROXIMATION TO THE OPTIMUM LINEAR RECEIVER

Section 1.7 has presented the optimum linear space diversity receiver operating in a multipath fading channel with dominant co-channel interference. However, it is not possible to build an infinite length equaliser as required by the optimum linear receiver, so it is necessary to evaluate the degradation in performance of a receiver containing finite-length equalisers.

The following discusses the justification for the transition from the optimum linear receiver to the finite-length fractionally-spaced equaliser receiver studied here.

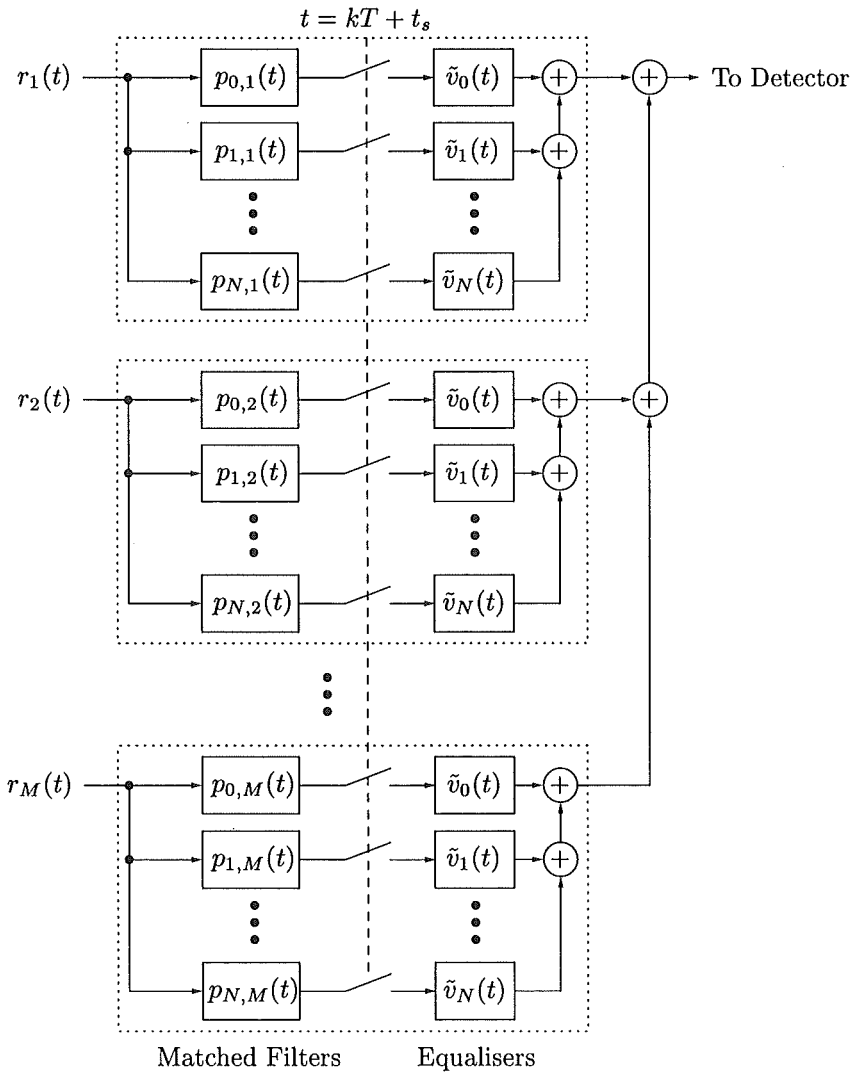

Figure 3.5 Optimum Linear Receiver

Figure 3.5 shows a diagram of the M-branch optimum linear receiver structure for the desired source [Clark 1992]. It shows matched filter responses, $p_{n,m}(t) = q^*_{n,m}(t_s - t)$,

which are matched to the link response between the n^{th} source and the m^{th} receiver branch, and the infinite-length symbol-spaced equalisers, $\tilde{v}_n(t)$. Note that it differs from the original diagram [Clark 1992, Fig. 5.1] as the order of summations has been changed, the equalisers have been deliberately copied into each branch, and some notation has changed. From this configuration, it can easily be seen that each dotted box can be synthesized by a single infinite-length fractionally-spaced equaliser. This is because each cascade of matched filter and symbol-spaced equaliser can be replaced by a fractionally-spaced equaliser, and the linear combination of the resulting equalisers in each branch can be replaced by a single equaliser. Therefore, the optimum linear space diversity receiver operating in a multipath fading channel with dominant co-channel interference can be synthesized by a receiver with one infinite-length fractionally-spaced equaliser in each branch, the outputs of which are summed by a combiner. An approximation to the optimum linear receiver is obtained if the length of each equaliser is limited to J taps, with the quality of approximation improving as J increases.

Inspection of (2.9) reveals that the received signals also contain a linear phase trend term proportional to the carrier frequency offset, Δf_n. The receiver, therefore, requires carrier frequency offset compensation, whereas the optimum linear receiver assumes ideal carrier recovery. The linear phase trend could be compensated by equaliser tracking, however, the frequency offset can be much larger than the fade rate, making equaliser tracking far more difficult. It is better to estimate the carrier frequency offset and remove it from the received signals, and possibly remove the need for equaliser tracking altogether. The constant phase term, ϕ_{nm}, is easily compensated by the equalisers during training.

Figure 3.6 shows the receiver structure to be analysed in this thesis. The signal flow is from left to right, with the passband signals being received on the diversity antennae, down-converted, and processed. The receiver front-end (consisting of noise-rejection filters, mixers, and samplers) is analog, while the remaining processing is assumed to be performed digitally. No explicit pulse shaping filters are present in the receiver because the fractionally spaced equalisers adapt to compensate for the distortion in the link responses, and therefore effectively perform pulse shaping. The passband signals on the diversity branches are assumed to be mixed to approximately baseband by a free-running local oscillator. (The use of intermediate frequency (IF) stages in the actual hardware is irrelevant to the analysis.) The received complex baseband signals are fractionally sampled and processed in a burst-mode fashion, i. e., the carrier frequency offset is estimated and the equalisers are trained once per burst, both from the same training sequence. The carrier frequency offset estimator uses synchronously-spaced samples of the received signals, so the received samples, $\hat{r}_{ml}$, are sub-sampled to give $\bar{r}_{ml}$. The carrier frequency offset estimate is removed from the received samples to give r_{ml}. The fractionally-spaced received samples with carrier offset removed are then filtered by the finite-length fractionally-spaced equalisers, with tap weights v_{mkl}. The

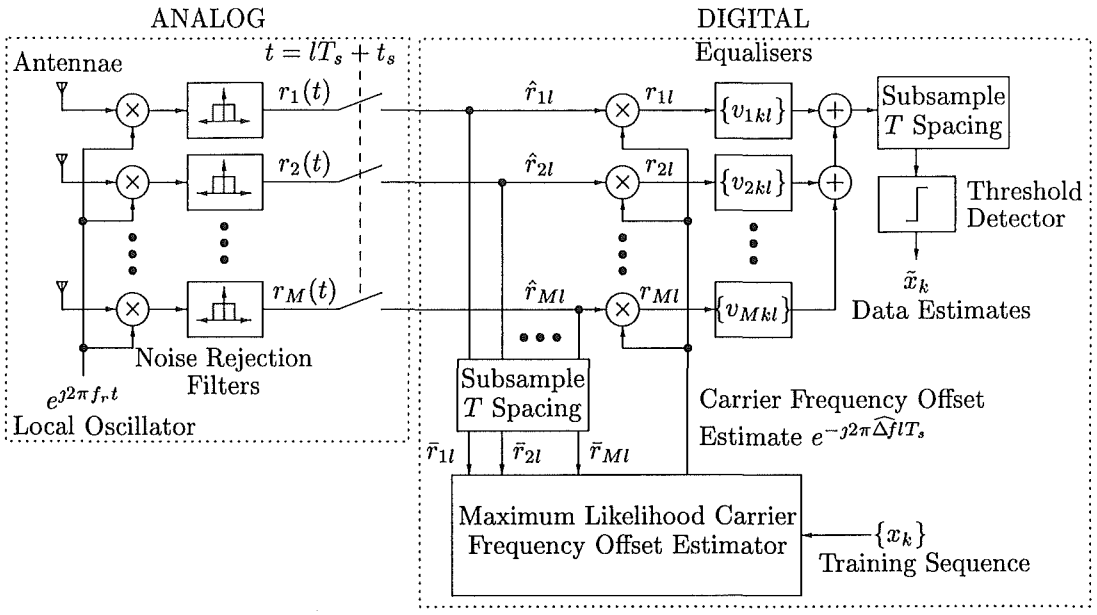

Figure 3.6 Receiver Structure

outputs of the equalisers are combined, and sub-sampled to symbol spacing to produce a linear estimate of the transmitted data. The threshold detector then gives a data estimate depending on which decision region the linear estimate is in.

It should be noted that the entire receiver is linear except for the threshold detector. The current data estimate is determined from the current linear estimate, and no past estimates are used to reduce ISI or influence the decision of the current estimate.

The receiver achieves synchronous reception in the following ways:

- The *carrier frequency* is not estimated, however, a free-running local oscillator is used and the carrier frequency *offset* is estimated (The carrier frequency offset is the difference between the transmitted carrier frequency plus Doppler shift, and the local oscillator frequency).

- The quasi-static *carrier phase*, ϕ_{nm}, is not estimated, but is cancelled by appropriate rotations of the equaliser taps during the equaliser training.

- *Burst synchronisation* is assumed to be performed by control channels and guard bits at the end of the burst timeslot.

- The *symbol period* is assumed to be known at the receiver with high accuracy, and so it is not estimated. This is a valid practical assumption in almost all systems [Ungerboeck 1976].

- The *symbol timing* is assumed known. Although this is not a valid assumption, it has been shown that fractionally-spaced equalisers are relatively insensitive to

symbol timing [Gitlin and Weinstein 1981], and the frequency offset estimator is shown in Chap. 5 to be relatively insensitive to symbol timing over a wide range (on the order of symbol periods). Thus the receiver does not have stringent requirements for symbol timing estimation.

3.3 RECEIVER FUNCTIONALITY FOR THE TWO STUDIES

Two separate studies have been carried out on the receiver structure shown in Fig. 3.6, namely, the effect of finite-length equalisers on the performance of the diversity receiver, and the performance of a carrier frequency offset estimator operating in a diversity receiver.

The first study on the effect of equaliser length is carried out assuming that the carrier frequency offset is estimated exactly in the receiver. It is equivalent to analysing a system that does not introduce a carrier frequency offset. The reason for this assumption is to concentrate solely on the effect of equaliser length on the performance of the diversity receiver, to readily allow comparison with previous results, and also to simplify the analysis.

In the second study, the effect of diversity on the performance of the carrier frequency offset estimator was determined solely from the carrier frequency offset estimate error, and not from the receiver bit error probability. This means that the remainder of the receiver including the equalisers, combiner, and threshold detector is not considered in the study of the carrier frequency offset estimator.

3.4 PRACTICAL CONSIDERATIONS

Although this study is concerned with obtaining performance results assuming various ideal conditions, the receiver structure has been chosen to be essentially what would be used in a practical implementation. A practical implementation would require equaliser training, and possibly tracking, algorithms, whereas here the best possible equaliser responses are determined using knowledge of the channels. In addition, the receiver does not have stringent requirements on symbol timing and is likely to require only burst synchronisation. Other than these two considerations which have been well studied in other applications [Falconer and Ljung 1978, Cioffi and Kailath 1984, Gitlin *et al.* 1992, D'Aria *et al.* 1992], the basic structure of the receiver is physically realisable.

The main aim in the choice of receiver structure was to enable implementation of as much as possible of the design in the digital domain using one or more digital signal processors (DSP). As can be seen in Fig. 3.6 only the noise rejection filters, the down converters, and the diversity branch samplers are analog components. The remaining carrier offset estimation and removal, equalisation, and detection is performed by digital components. This choice provides for a simpler, more flexible and possibly cheaper

solution than if more of the design were analog. Different designs can be implemented simply by changing the software in the DSP. More complicated algorithms can be implemented as DSP speeds increase without changing the hardware design. Also production costs would reduce as DSP prices reduce. (Note however that this study does not consider required DSP speeds or processing power.)

If the training sequence is transmitted in the middle of the burst, e.g., as in the GSM protocol [Steele 1992], then some or all of the burst would have to be stored in memory and could be processed from the middle to the start and also from the middle to the end. This has the advantage that only half a burst period of channel evolution is encountered at either end of the burst relative to the state at the middle. Therefore, if the equalisers are trained to equalise the channel state at the middle of the burst, they will be closer to the required responses at either end of the burst, than they would be at the end of the burst if they were trained at the start of the burst. In the analysis, the training sequence was assumed to be midamble (rather than a preamble), as ISI was considered affecting the training sequence bits at both ends. However, the algorithm would perform at least as well using a preamble training sequence instead of a midamble, because the guard time between the bursts would only reduce the ISI present at the start of the burst.

3.5 CONCLUSION

This chapter has described the receiver structure to be analysed in this thesis. It presents the motivation for the choice of receiver structure as being a realisable approximation to the optimum linear receiver. It describes the functionality of the receiver for the two studies presented in subsequent chapters, and it specifies how the receiver is to achieve synchronous reception in the multipath fading channel. Also discussed are the practical considerations in building a real receiver. Essentially, the receiver structure is physically realisable, however, equaliser training and tracking algorithms, and burst synchronisation will be required. These are not considered in this thesis.

Chapter 4

MINIMUM-MEAN-SQUARE ERROR OPTIMISATION OF THE DIVERSITY RECEIVER

This chapter describes the minimum-mean-square error optimisation technique and a performance analysis for the receiver structure described in Sec. 3.2. The analysis is limited to the case where the carrier frequency offset is assumed to be known exactly at the receiver, and the receiver has ideal channel state information. (An analysis of a carrier frequency offset estimator is presented in Chap. 5.) The aim of the performance analysis is to determine the effect of diversity and equaliser length on the performance of the receiver structure in Fig. 3.6. Using the assumption of ideal carrier recovery and ideal channel state information, the best possible performance of the receiver structure can be found, given the number of diversity branches and number of weights (or taps) per branch equaliser. Knowing the best possible performance of the receiver is important because it can be used as a benchmark for further studies into equaliser training and adaptive tracking algorithms where the channel state is not known at the receiver.

The receiver will be analysed in a similar manner to that presented by Clark [1992]. The M diversity equalisers will be globally optimised under the criterion of minimum mean-square-error (MMSE) at the output of the combiner, i. e., the equaliser tap weights are calculated using the ideal channel state information. The global MMSE optimisation, as applied to diversity [Hebley *et al.* 1994], is a novel extension to the standard single equaliser optimisation [Qureshi 1985]. It means that all the branch equalisers will be optimised so that the sum of their outputs produces a signal that is as close as possible to the transmitted signal in the mean-square-error sense. To understand what this means, it must be realised that the optimisation only depends on the channel state and not the transmitted data. The equalisers are optimised so that the *expected* squared-error between the transmitted signal and the output of the combiner is the smallest possible when averaged over all the possible transmitted data sequences.

This chapter consists of the following sections. Section 4.1 presents the derivation of the formula for the equaliser tap weights that result in the minimum mean-square-error at the combiner output. Section 4.2 presents the performance measures used

to evaluate the performance of the receiver. The method of simulating the system to obtain the performance results follows in Sec. 4.3.1. Then the chapter is concluded.

4.1 MINIMUM MEAN-SQUARE-ERROR RECEIVER OPTIMISATION

The ideal criterion for optimising the receiver would be minimum bit-error-rate of the receiver's data estimates. However, a receiver under this criterion is extremely difficult to analyse. Instead, the criterion of minimum mean-square-error has been chosen for three reasons. First, the equation for the mean-square-error has a quadratic form, which allows for simple minimisation. Second, the performance of the receiver under the criterion of minimum mean-square-error closely approaches that of a receiver under the criterion of minimum bit-error-rate [Qureshi 1985]. Third, the criterion of minimum mean-square-error was used in the performance analysis of the optimum linear diversity receiver [Clark 1992], and thus using the same criterion of optimality readily allows for comparison of results.

4.1.1 Receiver mean-square-error

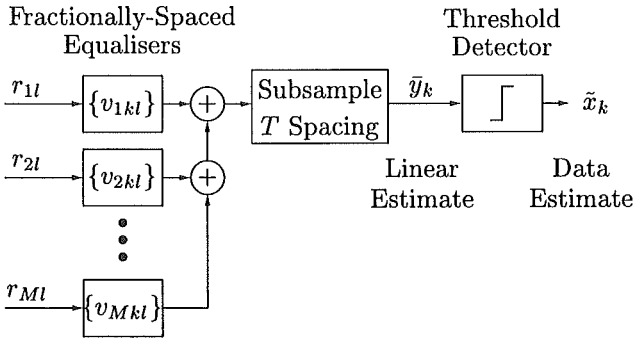

Figure 4.1 Relevant parts of the receiver structure showing finite-length fractionally-spaced equalisers, and combiner.

The analysis follows that of Qureshi [1985] and extends it to M branches. As discussed in Chap. 3, only a part of the whole receiver structure (Fig. 3.6) is considered in the analysis of the diversity equalisers. Figure 4.1 shows the relevant parts of the receiver structure. It shows how the M-branch receiver operates on the fractionally-spaced baseband received samples, r_{ml}, to obtain the sampled output linear estimates, $\bar{y}_k$. In this chapter, the received samples are assumed to have no residual carrier frequency offset ($\Delta f = 0$). The received samples are filtered by the fractionally-spaced equalisers, and the equaliser outputs are summed to obtain the linear estimates. Every symbol interval, the receiver makes a *symbol estimate*, $\hat{x}_k$, by mapping the *linear estimate*, $\bar{y}_k$, to a symbol which corresponds to the decision region containing the linear estimate.

The global optimisation of the diversity equalisers is clarified by defining the following vectors: The received sample vector stored in the m^{th} equaliser is defined as

$$\boldsymbol{r}_{mk} = \left[r_m\left(kT + \left\lfloor \frac{J-1}{2} \right\rfloor T_s + t_s\right), \ldots, r_m\left(kT + \left\lfloor \frac{-(J-1)}{2} \right\rfloor T_s + t_s\right) \right]^T \tag{4.1}$$

where the floor function, $\lfloor \cdot \rfloor$, is defined as the largest integer less than or equal to $\cdot$. The vector of T_s-spaced tap weights of the m^{th} fractionally-spaced equaliser at time $t = kT + t_s$ is defined as

$$\boldsymbol{v}_{mk} = \left[v_{mk\left\lfloor \frac{J-1}{2} \right\rfloor}, \ldots, v_{mk\left\lfloor \frac{-(J-1)}{2} \right\rfloor} \right]^T \tag{4.2}$$

The receiver's linear estimate which is the output of the combiner at time $t = kT + t_s$ is then given by

$$\bar{y}_k = \sum_{m=1}^{M} \boldsymbol{v}_{mk}^T \boldsymbol{r}_{mk} \tag{4.3}$$

and the mean-square-error at time $t = kT + t_s$ of the linear estimate, $\bar{y}_k$, is

$$\epsilon_k = E[|\bar{y}_k - x_k|^2] \tag{4.4}$$

$$= E\left[\left| \sum_{m=1}^{M} \boldsymbol{v}_{mk}^T \boldsymbol{r}_{mk} - x_k \right|^2 \right] \tag{4.5}$$

$$= \sum_{m=1}^{M} \sum_{m'=1}^{M} \boldsymbol{v}_{mk}^H E[\boldsymbol{r}_{mk}^* \boldsymbol{r}_{m'k}^T] \boldsymbol{v}_{m'k} - \sum_{m=1}^{M} \boldsymbol{v}_{mk}^H E[\boldsymbol{r}_{mk}^* x_k] - \sum_{m=1}^{M} \boldsymbol{v}_{mk}^T E[\boldsymbol{r}_{mk} x_k^*] + E[x_k^* x_k] \tag{4.6}$$

where the superscripts ^{T}, *, and ^{H} stand for matrix transpose, conjugate and Hermitian transpose respectively, $E[\cdot]$ indicates expectation (in this instance, over all possible input data sequences), and $|\cdot|$ means absolute value.

4.1.2 Minimisation of the mean-square-error

In order to optimise the receiver for MMSE, the equaliser tap weights, $\boldsymbol{v}_{mk}$, must be chosen to minimise (4.6). This can be performed by standard linear algebra techniques when (4.6) is rewritten in matrix form. This is done with two levels of matrix notation: the expectation terms are first defined as matrices, and then the sums over the diversity branches are performed by matrices consisting of the first level sub-matrices.

The covariance matrix of the received samples between the m^{th} and m'^{th} branch

is defined as,

$$\mathbf{A}_{mm'k} = E[\boldsymbol{r}^*_{mk}\boldsymbol{r}^T_{m'k}] \tag{4.7}$$

and the cross correlation vector of the received samples on the m^{th} branch and the transmitted message data is defined as,

$$\boldsymbol{\alpha}_{mk} = E[\boldsymbol{r}^*_{mk}x_k] \tag{4.8}$$

where the expectation is taken over all the possible data sequences.

Using (2.6) and (2.9), assuming that the data symbols are uncorrelated, and that both the channel responses and weak coloured noise processes are uncorrelated between branches, the (r, c) element of $\mathbf{A}_{mm'k}$ is given by

$$\begin{aligned} A_{mm'krc} = &\sum_{n=0}^{N} \sigma_x^2 \sum_i q^*_{nm}((k-i)T - rT_s + t_s, kT + t_s) \\ &\cdot q_{nm'}((k-i)T - cT_s + t_s, kT + t_s)e^{-\jmath(\phi_{nm} - \phi_{nm'})} \\ &+ E[\eta^*_m(kT - rT_s + t_s)\eta_{m'}(kT - cT_s + t_s)]\delta(m, m') \end{aligned} \tag{4.9}$$

and the r^{th} element of $\boldsymbol{\alpha}_{mk}$ is given by

$$\alpha_{mkr} = \sum_{n=0}^{N} \sigma_x^2 q^*_{nm}(kT - rT_s + t_s, kT + t_s)e^{-\jmath 2\pi \Delta f_n(kT + t_s)}e^{-\jmath\phi_{nm}} \tag{4.10}$$

where $\sigma_x^2 = E[x^*_k x_k]$ is the symbol energy. (Note that in this chapter, the carrier frequency offset, Δf_n, is assumed to be zero.)

The minimisation process, applied to a single equaliser, is a standard procedure [Qureshi 1985]. (Appendix B presents the MMSE optimisation of a single finite-length fractionally-spaced equaliser.) However in order to globally optimise the M branch equalisers of the diversity receiver, the following vectors and matrices are constructed from the previously defined subvectors and submatrices: $\boldsymbol{v}_k$ is a column vector of all the equaliser tap weights in the receiver, $\boldsymbol{\alpha}_k$ is the cross correlation vector of the transmitted data with all the received samples being processed in the equalisers, and $\mathbf{A}_k$ is the covariance matrix of the received samples across all the diversity branches. The subscript k indicates the time is $t = kT + t_s$.

The definitions are described by the following equations

$$\boldsymbol{v}_k = \begin{bmatrix} \boldsymbol{v}_{1,k} \\ \boldsymbol{v}_{2,k} \\ \vdots \\ \boldsymbol{v}_{M,k} \end{bmatrix} \tag{4.11}$$

$$\boldsymbol{\alpha}_k = \begin{bmatrix} \boldsymbol{\alpha}_{1,k} \\ \boldsymbol{\alpha}_{2,k} \\ \vdots \\ \boldsymbol{\alpha}_{M,k} \end{bmatrix} \tag{4.12}$$

and

$$\mathbf{A}_k = \begin{bmatrix} \mathbf{A}_{1,1,k} & \mathbf{A}_{1,2,k} & \cdots & \mathbf{A}_{1,M,k} \\ \mathbf{A}_{2,1,k} & \mathbf{A}_{2,2,k} & & \\ \vdots & & \ddots & \vdots \\ \mathbf{A}_{M,1,k} & & \cdots & \mathbf{A}_{M,M,k} \end{bmatrix} \tag{4.13}$$

Then the mean-square-error at time $t = kT + t_s$ is given by rewriting (4.6) in matrix form as

$$\epsilon_k = \boldsymbol{v}_k^H \mathbf{A}_k \boldsymbol{v}_k - \boldsymbol{v}_k^H \boldsymbol{\alpha}_k - \boldsymbol{\alpha}_k^H \boldsymbol{v}_k + E[x_k^* x_k] \tag{4.14}$$

In order to minimise the mean-square-error, (4.14) must be differentiated with respect to the equaliser tap weights, and the result set to zero. Since the differentiation is with respect to a *vector* of *complex* numbers, a gradient operator must be used. The gradient operator is defined as [Haykin 1996]

$$\nabla = \begin{bmatrix} \frac{\partial}{\partial \iota_0} + \jmath \frac{\partial}{\partial \kappa_0} \\ \frac{\partial}{\partial \iota_1} + \jmath \frac{\partial}{\partial \kappa_1} \\ \vdots \\ \frac{\partial}{\partial \iota_{M*(J-1)}} + \jmath \frac{\partial}{\partial \kappa_{M*(J-1)}} \end{bmatrix} \tag{4.15}$$

where ι_l and κ_l are the real and imaginary parts of v_l, respectively.

Using the gradient operator on (4.14) and setting the result to zero yields

$$\nabla \epsilon_k = 2\mathbf{A}_k \boldsymbol{v}_k - 2\boldsymbol{\alpha}_k = 0 \tag{4.16}$$

and so the receiver is optimised for minimum MSE when

$$\boldsymbol{v}_{k(\text{opt})} = \mathbf{A}_k^{-1} \boldsymbol{\alpha}_k \tag{4.17}$$

It should be noted that this global optimisation automatically biases towards the diversity branches that are least distorted, i. e., it is the best possible way of combining the received samples. This is in contrast to the case where each equaliser is optimised individually, because some method of biasing towards the least distorted channels would then be required.

Gitlin and Weinstein [1981] show that for fractionally-spaced equalisers operating on signals with less than 100% excess bandwidth (as determined by $c_n(t)$, Sec. 2.3), $\mathbf{A}_k$ is non-singular even for vanishingly small noise. Therefore (4.17) is unique and exists.

4.2 RECEIVER BIT-ERROR-RATE

The receiver bit-error-rate (BER) is a useful performance measure because it estimates the probability that a particular message bit will be recovered correctly at the receiver. In an additive noise channel the BER is a simple parameter—it is simple to calculate, and it has a simple meaning. It depends only on the ratio of signal power to noise power, and it means the expected rate of errors encountered due to the additive noise in the system.

In a system with frequency-selective fading, the probability that a particular message bit will be in error depends not only on the signal-to-noise ratio, but also on the channel responses and the *actual message symbols transmitted.* The message symbols transmitted adjacent to the desired symbol and by the co-channel interferers determine whether the ISI and CCI distortion interferes constructively making an error likely even for high SNR, or destructively making an error mainly dependent on the noise sample value. However, a probability of error measure would have little use if it was specified for a given set of channel responses *and a given set of message bits.* Even if the probability of error is averaged over all possible message bit sequences, it still remains a random process, which changes as the channel evolves. On the other hand, if the probability of error is also averaged over the channel ensemble, the resulting performance measure does not describe the receiver performance adequately. For instance, the receiver could perform exceedingly well most of the time yet exceeding poorly some of the time, or it could perform adequately all of the time, and have a similar average probability of error in both cases. The second case would be preferable, but the performance measure does not describe the difference between the two cases.

Following Clark [1992], this thesis uses a BER measure which is defined as the probability that a message bit will be recovered incorrectly given a particular set of channel responses, i. e., averaged over all possible transmitted sequences. The average bit-error-rate, $\langle \mathrm{BER} \rangle$, is defined as the bit-error-rate averaged over the ensemble of channel responses, and the outage probability, P_{out}, is the probability that the BER is less than some threshold, BER_0.

The BER is calculated as follows. Once the fractionally-spaced equaliser tap weights have been calculated as described in Sec. 4.1, the overall system impulse response can be calculated. The overall system impulse response is the impulse response from the transmitter, including the pulse shaping filter, to the output of the combiner. This response gives the weight of the desired symbol and the weights of the intersymbol interference terms (ISI) in the linear estimate, i. e., after the equalisation. In a similar

manner the co-channel interference (CCI) weights are given by the impulse responses from each of the dominant sources to the output of the combiner.

Rewriting (4.3) in full using (2.9) to show the components of ISI, CCI and noise, yields

$$\bar{y}_i = \sum_{m=1}^{M} \sum_{l} v_{mil} r_m(kT - lT_s + t_s) \tag{4.18}$$

$$= \sum_{m=1}^{M} \sum_{l} v_{mil} \Big(\sum_{n=0}^{N} \sum_{k} x_{nk} q_{nm}\big((i-k)T - lT_s + t_s, iT - lT_s + t_s\big) e^{\jmath\phi_{nm}} + \eta_m(iT - lT_s + t_s) \Big) \tag{4.19}$$

$$= \sum_{n=0}^{N} \sum_{k} x_{nk} \sum_{m=1}^{M} \sum_{l} v_{mil} q_{nm}\big((i-k)T - lT_s + t_s, iT - lT_s + t_s\big) e^{\jmath\phi_{nm}} + \sum_{m=1}^{M} \sum_{l} v_{mil} \eta_m(iT - lT_s + t_s) \tag{4.20}$$

where the sums over l contain the terms in (4.2).

The overall system impulse response is defined as

$$g_{nki} = \sum_{m=1}^{M} \sum_{l} v_{mil} q_{nm}\big((i-k)T - lT_s + t_s, iT - lT_s + t_s\big) e^{\jmath\phi_{nm}} \tag{4.21}$$

which is the response of the links and receiver equalisation from the n^{th} source at time $iT + t_s$ to a symbol transmitted at time kT. Similarly, the equalised weak noise term at time $iT + t_s$ is given by

$$\rho_i = \sum_{m=1}^{M} \sum_{l} v_{mil} \eta_m(iT - lT_s + t_s) \tag{4.22}$$

Thus the receivers linear estimate can be written as the combination

$$\bar{y}_i = \underbrace{x_{0i} g_{0i}}_{\substack{\text{Desired} \\ \text{symbol}}} + \underbrace{\sum_{k \neq i} x_{0k} g_{0k}}_{\text{ISI}} + \underbrace{\sum_{n=1}^{N} \sum_{k} x_{nk} g_{nk}}_{\text{CCI}} + \underbrace{\rho_i}_{\text{Gaussian Interference}} \tag{4.23}$$

which shows the weightings of the symbols, x_{ni}, that contribute ISI and CCI. Ideally,

$$g_{nk} = \begin{cases} 1 & n = 0,\ i = k \\ 0 & \text{otherwise} \end{cases} \tag{4.24}$$

If the receiver is performing well, this condition will be approximated.

As described in Sec. 2.1, the non-white non-Gaussian interference (dominant CCI) is modelled separately from the non-white Gaussian interference (weak CCI). The BER for any particular set of data sequences transmitted over a particular set of channels (i. e., the contribution of the dominant sources is defined) is obtained from the Gaussian probability-density-function (pdf) of the weak interference.

Calculating the BER for each possible data sequence and then averaging is a prohibitively expensive computation. However, there is an iterative algorithm [Metzger 1987, Pokrajac and Nikolic 1995] that calculates the probability distribution of the ISI terms and CCI terms, allowing simple calculation of the BER averaged over all transmitted sequences.

For a rectangular constellation, the decision regions are bounded by lines parallel to the real and imaginary axes of the constellation plane. Therefore, the BER can be estimated by considering either the real part or the imaginary part of the linear estimate. The real part of (4.23) becomes

$$\mathcal{R}e\{\bar{y}_i\} = \underbrace{a_{0i}\mathcal{R}e\{g_{0i}\}}_{\substack{\text{Desired}\\ \text{bit}}} + \underbrace{-b_{0i}\mathcal{I}m\{g_{0i}\} + \sum_{k\neq i} a_{0k}\mathcal{R}e\{g_{0k}\} - \sum_{k\neq i} b_{0k}\mathcal{I}m\{g_{0k}\}}_{\text{Adjacent bit interference (from ISI)}}$$
$$+ \underbrace{\sum_{n=1}^{N}\sum_{k} a_{nk}\mathcal{R}e\{g_{nk}\} - \sum_{n=1}^{N}\sum_{k} b_{nk}\mathcal{I}m\{g_{nk}\}}_{\text{CCI}} + \underbrace{\mathcal{R}e\{\rho_i\}}_{\text{Gaussian Interference}} \tag{4.25}$$

Metzger's algorithm can be briefly summarised by the following

- Assume the data to consist of uncorrelated equiprobable symbols where $a_{nk}, b_{nk} = \pm 1$. (The pdf can be readily extended to higher order constellations.)

- Define the interference terms, p_k, as being the real and imaginary parts of all the response terms $\mathcal{R}e\{g_{nk}\}$ and $\mathcal{I}m\{g_{nk}\}$, while letting $p_0 = \mathcal{R}e\{g_{0i}\}$.

- Sort the interference terms, p_k, $k > 0$, into decreasing order.

- The interference from the ISI and CCI will then be a random variable,

$$z_{\text{interference}} = \sum_{k=1}^{\infty} \pm p_k \tag{4.26}$$

where the plus or minus will depend on the associated message bit.

- Define the remainder of the interference beyond the K^{th} term as

$$z_{K+1} = \sum_{k=K+1}^{\infty} \pm p_k \tag{4.27}$$

- Start with an arbitrary probability density function (pdf) for the smallest term, z_{K+1}.
- Since $z_K = z_{K+1} \pm p_K$, it is easy to iteratively obtain the pdf of the next term, z_K, by convolution.
- The algorithm specifies a numerical method for normalising the pdf at each step.
- The final pdf is the pdf of z_1.

The BER is then given by

$$\text{BER} = \frac{1}{2} \int f_1(x) \operatorname{erfc}\left[\frac{p_0 - x}{\sigma\sqrt{2}}\right] dx \tag{4.28}$$

where $f_1(x)$ is the pdf of z_1, p_0 denotes the decision threshold, erfc[·] is defined by $2\sqrt{\pi}\int_x^{\infty} \exp(-u^2)\, du$ and σ_e^2 denotes the filtered noise variance at time $kT + t_s$,

$$\sigma_e^2 = \sigma^2 \sum_m \sum_l |v_{mkl}|^2 \tag{4.29}$$

where σ^2 is the variance of the weak CCI noise lumped with receiver thermal noise.

4.3 SIMULATION RESULTS OF THE MSE ANALYSIS

The following sections present simulation results which show the trade-off between performance and complexity of the receiver described in section Sec. 3.2. Essentially, the number of diversity branches and the number of taps per branch determines the receiver complexity. The diversity order has a significant impact on the required hardware because a complete analog front end is needed for each diversity branch. Each front end consists of mixers, filters, and samplers which require room in the receiver thereby increasing its physical size and also increasing power consumption and cost. On the other hand, the number of taps indirectly influences the required processing capabilities and storage. The required processing power will depend on the specific algorithms used to train the equalisers, but will increase as the number of taps increases. Whether the equaliser training is performed globally or individually for each branch, the total number of taps will be a significant parameter indicating complexity.

The effect of diversity order and equaliser length on the performance of the finite-length fractionally-spaced equaliser receiver are compared with those of the optimum linear receiver studied by Clark [1992], and described in Sec. 1.7.

The results are classified in seven sections as follows:

- A description of the channel modelling parameters, and other parameters that are held constant throughout the simulation of the MMSE receiver.
- The influence of symbol timing offset on the bit-error-rate, BER, for some example sets of fixed channel snapshots.
- The influence of the bit-error-rate threshold, BER_0, on the outage probability, P_{out}, for fixed signal-to-interference ratio, SIR.
- The influence of the signal-to-interference ratio, SIR, on the outage probability, P_{out}, for fixed bit-error-rate threshold, BER_0.
- The influence of the signal-to-interference ratio, SIR, on the average bit-error-rate, $\langle \mathrm{BER} \rangle$.
- The influence of diversity order, M, on the signal-to-interference ratio, SIR, for fixed outage probability, bit-error-rate threshold, and fixed total number of taps in the receiver.
- The influence of signal-to-interference ratio, SIR, on the error burst nature of the receiver.

4.3.1 Simulation method

An expression has been derived, (4.17), that describes the best possible tap weight values for the finite-length fractionally-spaced receiver given the channel state information between each source and each receiver diversity branch. Given the optimum tap weight values for the set of channel responses, the bit-error-rate of the receiver can be found using Metzger's algorithm as described in Sec. 4.2. Note that, by calculation, this BER measure is the BER averaged over the *transmitted data*, i. e., no random binary data are generated, only random channel snapshots. The single system snapshot results in a single BER value, and simulation is required to observe how the receiver performs over the channel ensemble.

To minimise computation in the simulations, the channel model is reduced from a general time-varying frequency-selective channel to a *quasi-static* frequency-selective model, as described in Sec. 2.5.1. This means that the channel is assumed static over the duration of a burst, but changes from burst to burst. Each simulation run then consists of generating static *channel snap-shots* and evaluating the performance of the receiver for the given set of channel snap-shots. This assumption results in the following

simplifications

$$\begin{aligned} h_m(\tau,t) &\longrightarrow h_m(\tau) \\ q_m(\tau,t) &\longrightarrow q_m(\tau) \\ P(\tau,t) &\longrightarrow P(\tau) \\ Q_m(f,t) &\longrightarrow Q_m(f) \end{aligned}$$

The simulation performs the following steps:

- Define the parameters: M, N_d, J, SIR, DWR, τ_0, delay spread profile, B.
- Generate the set of $M \times N_d$ random independent channel snapshots.
- Optimise the receiver tap weights for MMSE at the receiver output using (4.17)
- Calculate the BER using Metzger's algorithm.
- Store the BER sample.
- Repeat previous four steps N_{mc} times.

4.3.1.1 Parameters held constant in the MSE simulations

The simulations made use of the efficient channel modelling techniques described in Sec. 2.4 and critical routines that were efficiently coded in the C programming language. However, as the Monte Carlo technique was used to obtain the receiver performance over the channel statistics, simulation run time was still rather lengthy. In an effort to reduce the amount of simulation required, the following parameters were held constant throughout the simulations presented in this chapter:

- The constellation was QPSK (2 bits-per-symbol). It is presumed that higher order constellations could improve bandwidth efficiency, but this was not investigated.
- The transmit pulse shaping filter was raised cosine in all of the dominant sources. This is a likely scenario, although it is possible that filters with asymmetrical impulse responses may give better results. However, as the channel varied, the equalisers would still have to compensate for the overall distortion and may not benefit from a different pulse shape.
- The transmit pulse shaping filter excess bandwidth was $\beta = 0.5$ (50%). This is a realistic figure, although systems may use values down to about 30% [Long *et al.* 1988].

- One channel characteristic was chosen from those presented by Clark. The delay spectrum shape used was "exponential" and the normalised delay spread used was $\tau_0/T = 1$ (see Sec. 2.5.1). One of Clark's findings was that the performance was not extremely sensitive to the choice of delay spectrum shape, so all the results here use the exponential shape. The choice of normalised delay spread was to show the receiver's ability to combat a large level of ISI because the more ISI the receiver can handle, the higher the symbol rate can be or the more dispersive the channel can be.

- For scenarios where there were dominant interferers, the choice of dominant-to-weak-interference ratio, DWR, was 20 dB. The signal-to-total-interference ratio, SIR, determines the amount of interference, while the DWR determines how much of the interference is non-Gaussian. The figure of 20 dB was chosen so that comparisons could be made with the optimum linear receiver.

- The number of Monte Carlo runs was 10000. This was established by increasing the number until consistent results were obtained.

Also, for simplicity in the simulations, the dominant interferers are assumed to have the same average power,

$$S_n = S_0\sqrt{N\text{SIR}(\frac{1}{\text{DWR}}+1)}, \qquad n = 1, 2, ..., N \tag{4.35}$$

4.3.2 Influence of symbol timing offset

The receiver is assumed to have a highly accurate estimate of the symbol period, T, and therefore it can be assumed that the receiver can sample the incoming received samples without extracting the symbol period from the signals. It remains to discuss the symbol timing phase, t_s.

Fractionally-spaced equalisers are relatively insensitive to symbol timing phase [Ungerboeck 1976]. This is because a timing phase error of some delay, τ_e for example, is equivalent to multiplying the channel frequency response by $e^{-j2\pi f\tau_e}$. To cancel such a timing phase error, the equaliser must have its frequency response multiplied by $e^{j2\pi f\tau_e}$ over the bandwidth of interest. (As described in Sec. 3.1, a fractionally-spaced equaliser can do this before the excess bandwidth of the signal's pulse shape is aliased, whereas a symbol-spaced equaliser cannot.) However, a frequency response of $e^{j2\pi f\tau_e}$ requires that the equaliser has infinite-length, and a finite-length equaliser can only approximate the correct response. This would make the symbol timing phase somewhat more sensitive for finite-length equalisers than for infinite-length equalisers. Ungerboeck [1976] suggested that since the receiver can know the symbol period to a high accuracy, the received data can just be sampled at an arbitrary, but fixed, symbol

phase and the equalisers will automatically train to whatever symbol phase has been acquired.

In this section, the effect of varying the symbol timing phase is presented, and it is found that the assumption of an arbitrary fixed sampling phase is adequate for the receiver being studied, as long as suitable burst synchronisation has been achieved. In other words, the finite-length equalisers can withstand symbol timing errors on the order of symbol periods, but the extent is limited by the length of the equalisers. As long as the receiver knows roughly where in time the burst is, to within a few symbol periods, the equalisers will compensate for the symbol timing error.

It is extremely difficult to obtain an expression for the optimum symbol timing offset because it involves minimising the expression for the mean-square-error (MSE) at the receiver output written as a function of the symbol timing offset. The minimisation must also be performed simultaneously with the minimisation of the equation for the receiver's mean-square-error with respect to the equaliser weights.

The minimisation presented in Sec. 4.1 was performed assuming the symbol timing offset, t_s, was zero. The equations optimise the receiver's equalisers using the sampled channel impulse responses. If the channel responses are sampled at an arbitrary fixed symbol timing offset, the equalisers become optimised for this symbol timing offset.

For a given set of $N_d \times M$ channel snapshots, (where a *set* indicates one response for each channel between the dominant sources and diversity branches), the receiver can be optimised, and the receiver's BER can be calculated, for a range of symbol timing offsets. Then the BER can be plotted against the timing offset. However, it is not possible to average the effects of altering the symbol timing offset over the channel ensemble, and a feeling for the sensitivity must be obtained by looking at many such plots.

In this section, eight plots are presented to give an idea of the receiver's sensitivity to a symbol timing offset. The plots have been categorised to show how the receiver performs with a combination of the following system attributes:

- No diversity, $M = 1$, or high diversity, $M = 4$.
- Weak noise-like interference, $N_d = 1$, or dominant interference, $N_d = 2$.

An example is given of a "good" and a "poor" set of channel snapshots for each combination, where "good" implies a relatively low BER and "poor" implies a relatively high BER. To reduce the number of plots, only a single channel characterisation was used, i. e., one with a large delay spread ($\tau_0/T = 1$). From looking at many plots with different delay spreads, it is apparent that the sensitivity to timing offset is similar for different delay spreads, and all arguments presented here apply to a certain extent. However, the plots of BER versus timing offset become more symmetrical as the delay spread is decreased. (It should be noted that it is difficult to compare the sensitivities

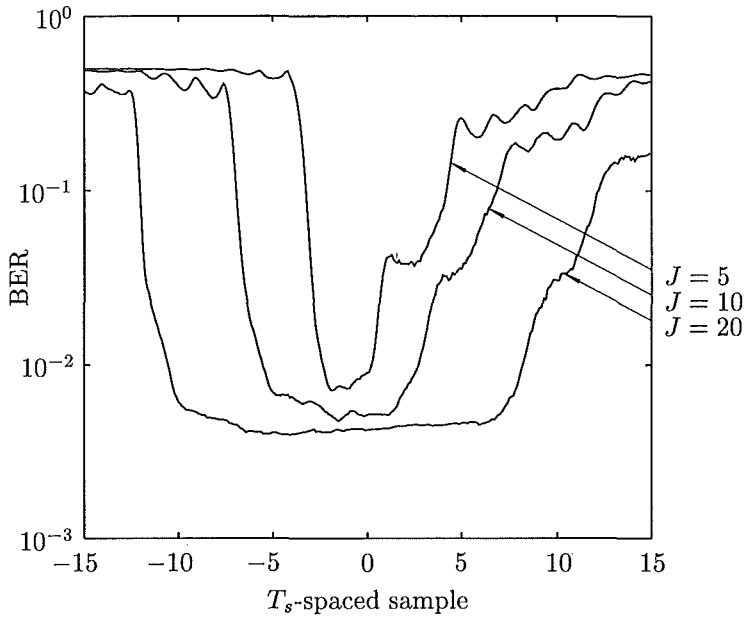

Figure 4.2 Performance of M-branch finite-length equaliser receiver. Bit-error-rate for single set of channel snapshots: Effect of symbol timing offset. Results for one dominant source (i. e., weak noise-like interference). Example of "good" channel snapshot. Diversity order $M = 1$ and SIR = 10 dB.

at different delay spreads since the channel snapshots are randomly generated.) The x-axes have units of $T_s = T/2$ which is the tap spacing of the equaliser, and the zero timing reference excludes the delay from the transmitter.

Figure 4.2 through Fig. 4.9 show how sensitive the BER is to the choice of symbol timing offset, for receivers with equaliser lengths of $J = 5, 10, 20$. (Note that the equalisers are optimised at each timing offset.) A curve with a wide flat bottom on it is desirable because it means that the BER is insensitive over a wide range of offsets, whereas a narrow spiky curve is undesirable because it means that the symbol timing is critical, and the receiver's performance is highly dependent on the choice of timing offset. It can be seen that the receiver with fractionally-spaced equalisers can compensate for a wide range of symbol timing offsets, where the range is dependent on the length of the equalisers.

Figure 4.2 through Fig. 4.5 are for weak, noise-like interference. The curves are reasonably flat for offsets on the order of half the equaliser length. The receiver becomes more sensitive to the timing offset when the set of channel snapshots is "good", however, the overall performance is better compared to that for a "poor" set of channels. The receiver is also less sensitive with higher diversity because of the averaging effect of the different channels between the sources and the diversity branches.

Figure 4.6 through Fig. 4.9 are for a single dominant interferer. Figure 4.6 and Fig. 4.7 show curves that are not smooth indicating that the receiver is more sensitive

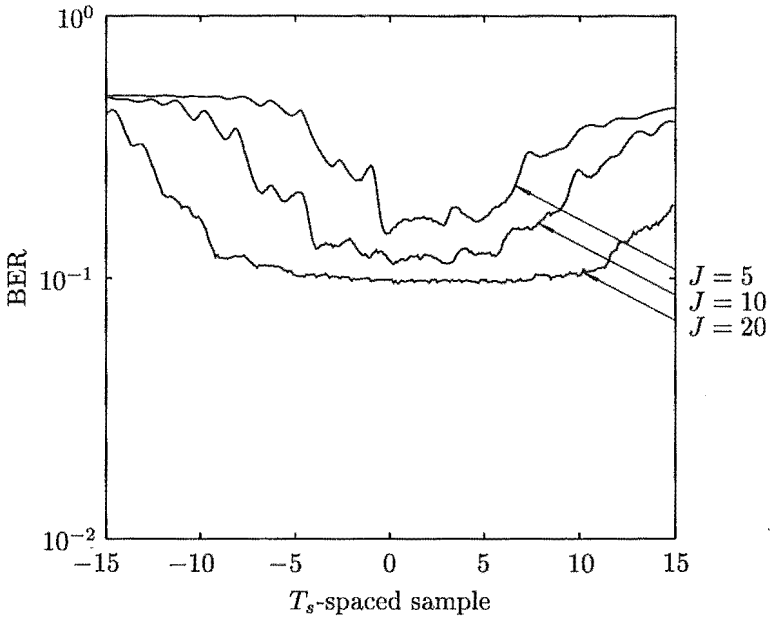

Figure 4.3 Performance of M-branch finite-length equaliser receiver. Bit-error-rate for single set of channel snapshots: Effect of symbol timing offset. Results for one dominant source (i. e., weak noise-like interference). Example of "poor" channel snapshot. Diversity order $M = 1$ and SIR = 10 dB.

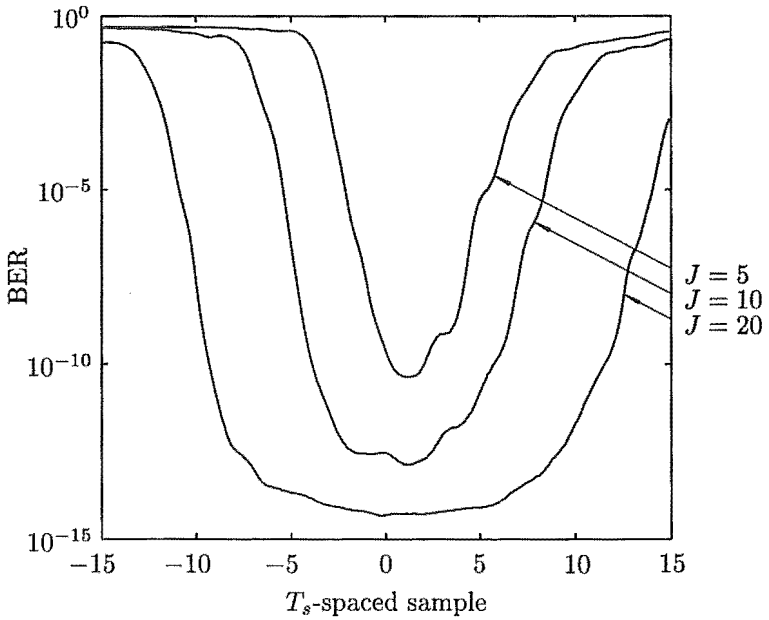

Figure 4.4 Performance of M-branch finite-length equaliser receiver. Bit-error-rate for single set of channel snapshots: Effect of symbol timing offset. Results for one dominant source (i. e., weak noise-like interference). Example of "good" set of channel snapshots. Diversity order $M = 4$ and SIR = 10 dB.

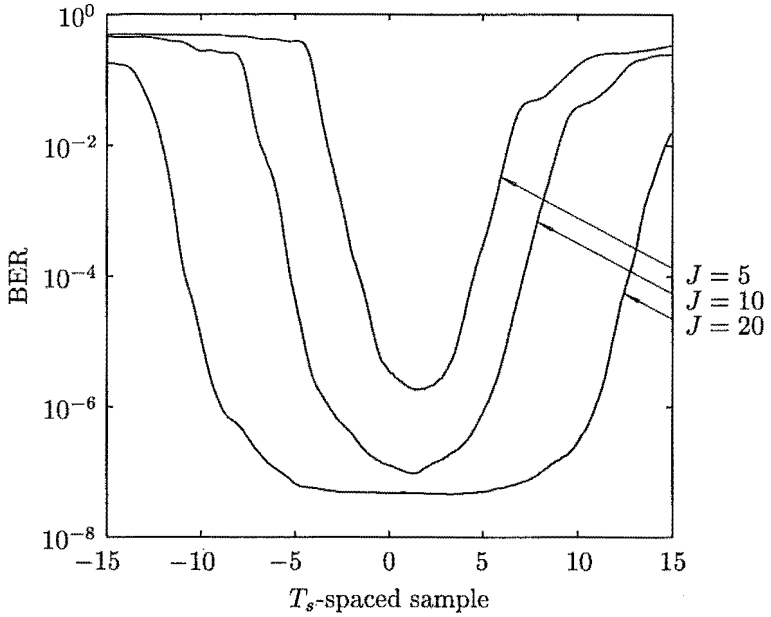

Figure 4.5 Performance of M-branch finite-length equaliser receiver. Bit-error-rate for single set of channel snapshots: Effect of symbol timing offset. Results for one dominant source (i. e., weak noise-like interference). Example of "poor" set of channel snapshots. Diversity order $M = 4$ and SIR = 10 dB.

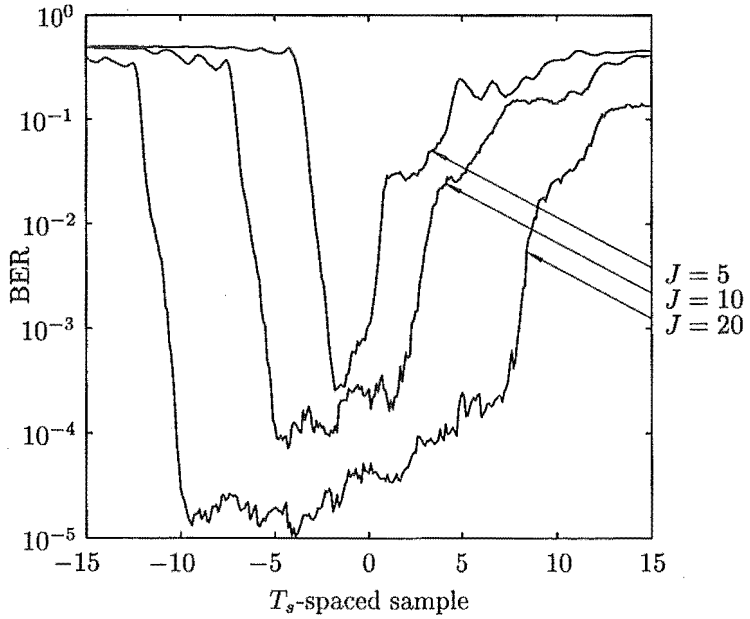

Figure 4.6 Performance of M-branch finite-length equaliser receiver. Bit-error-rate for single set of channel snapshots: Effect of symbol timing offset. Results for two dominant sources (i. e., one dominant interferer). Example of "good" channel snapshot. Diversity order $M = 1$ and SIR = 10 dB.

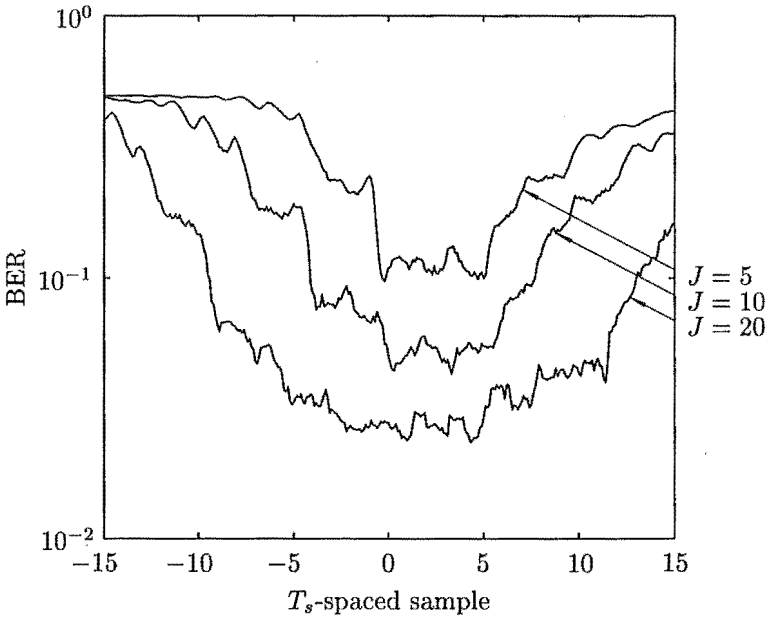

Figure 4.7 Performance of M-branch finite-length equaliser receiver. Bit-error-rate for single set of channel snapshots: Effect of symbol timing offset. Results for two dominant sources (i. e., one dominant interferer). Example of "poor" channel snapshot. Diversity order $M = 1$ and SIR = 10 dB.

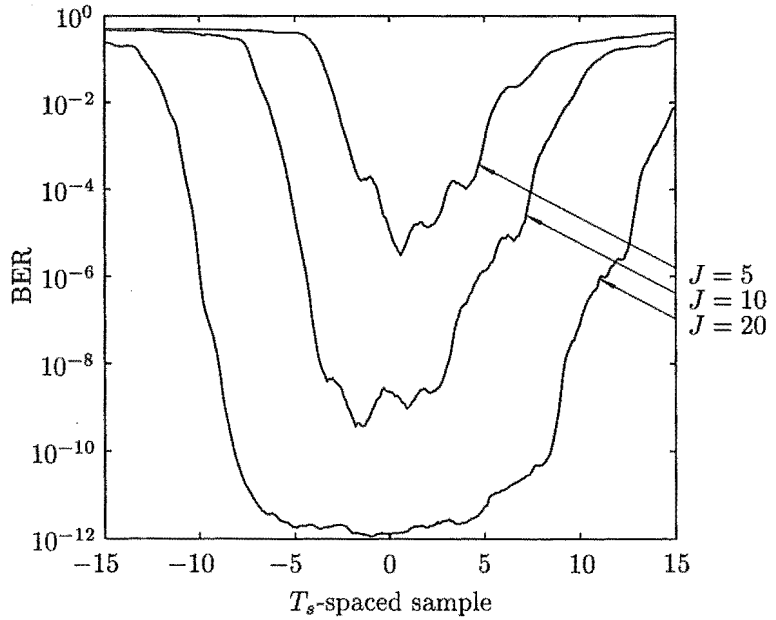

Figure 4.8 Performance of M-branch finite-length equaliser receiver. Bit-error-rate for single set of channel snapshots: Effect of symbol timing offset. Results for two dominant sources (i. e., one dominant interferer). Example of "good" set of channel snapshots. Diversity order $M = 4$ and SIR = −10 dB.

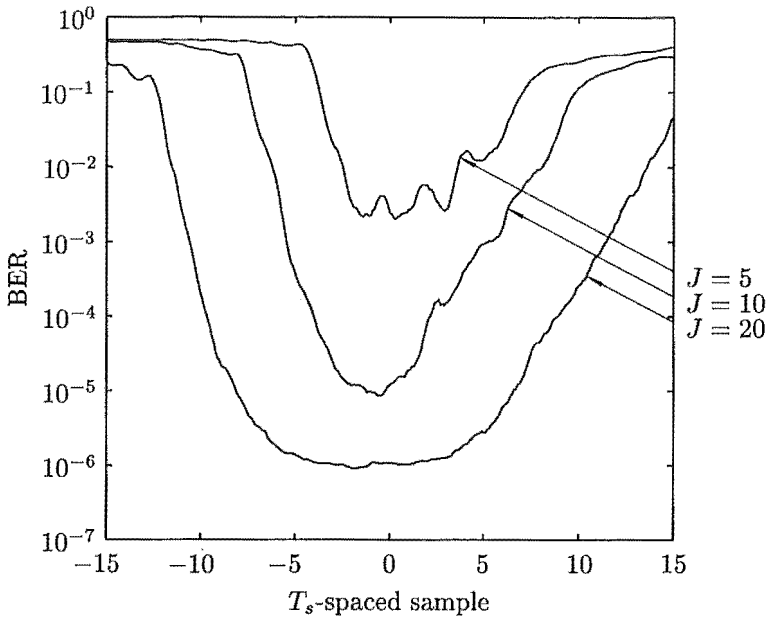

Figure 4.9 Performance of M-branch finite-length equaliser receiver. Bit-error-rate for single set of channel snapshots: Effect of symbol timing offset. Results for two dominant sources (i. e., one dominant interferer). Example of "poor" set of channel snapshots. Diversity order $M = 4$ and SIR $= -10$ dB.

to symbol timing offset when the interference is dominant rather than weak. Despite being less smooth, the curves are still reasonably flat over a similar range of symbol timing offsets. As for the case of weak interference, the receiver experiencing dominant interference becomes more sensitive to the timing offset when the set of channel snapshots is "good", however, the overall performance is better compared to that for a "poor" set of channels. Similarly, the receiver is also less sensitive with higher diversity. (Note that in Fig. 4.8 and Fig. 4.9, the SIR has been reduced to -10 dB because the diversity receiver performs much better against dominant interference, as will be shown in later sections.)

Only one SIR value has been presented for each combination of receiver diversity and type of interference, however, after looking at many such plots with different SIR values, it appears that the receiver is more sensitive and the curve is likely to become more skewed as the SIR is increased. Of course, the BER values are usually better in this case. The point here is that when the channel responses are "good", so the receiver is performing well, and the receiver becomes more sensitive to the choice of symbol timing, a poor choice of timing offset will still result in an adequate receiver performance. But when the channel responses are "poor", the receiver is not very sensitive to symbol timing offset, and will perform approximately the same (but not very well) for a range of timing offsets. It is difficult to quantify labels, "good" and "poor", because the receiver BER values are dependent on the system parameters.

Nevertheless, for any set of parameters, the receiver will have some range of BER values over the channel ensemble, i. e., ranging from "good" to "poor". The use of the snapshots presented in Fig. 4.2 through Fig. 4.9 are useful for illustrating the receiver's sensitivity to symbol timing qualitatively, rather than quantitatively.

All the figures in this section show curves that are skewed to one side somewhat. This is a result of the asymmetrical nature of the channel delay power profile (described in Sec. 4.3.1.1), which, in turn, determines the shape of the channel impulse response.

Channels with low delay spread (e. g., $\tau_0/T = 0.1$) result in curves that are almost completely symmetrical.

The optimum symbol timing offset can vary from the zero reference by up to plus or minus half the equaliser length. Since the channels are assumed to be uncorrelated among the antennae, the best timing on one antenna may be several symbols from that on another antenna. However, it is unlikely that a practical diversity receiver will have separate timing circuitry on each branch because of the added complexity, so it is assumed in the simulations that all branches have the same timing.

Therefore, for the remaining performance results, it was decided to perform a search over a number of symbol intervals to obtain the BER that was closest to the minimum. A five point search at $t_s = 0, \pm 1, \pm 2$ sample periods was chosen as a compromise that would give approximately the minimum BER most of the time, but not increase simulation time too much.

In an actual receiver the symbol timing offset may be determined by some combination of control/synchronisation channel signals and some processing of the received signal such as a correlation between the received signal and a known training sequence [D'Aria *et al.* 1992]. It appears that whatever method is used, it will probably involve a limited amount of searching which will not necessarily find the exact optimum timing offset.

The effects of symbol timing offset on the performance of the diversity receiver can be summarised by the following:

- The receiver is relatively insensitive to timing offset over a wide range, in most cases almost equal to the length of the equalisers.
- The receiver is less sensitive to timing offset when a higher diversity order is employed.
- The receiver is less sensitive to timing offset when the channel responses are "poor" or the SIR is low, however, the performance is poor in these cases.
- The receiver is more sensitive to timing offset when the interference is dominant as opposed to weak, although the receiver performs better in this case.

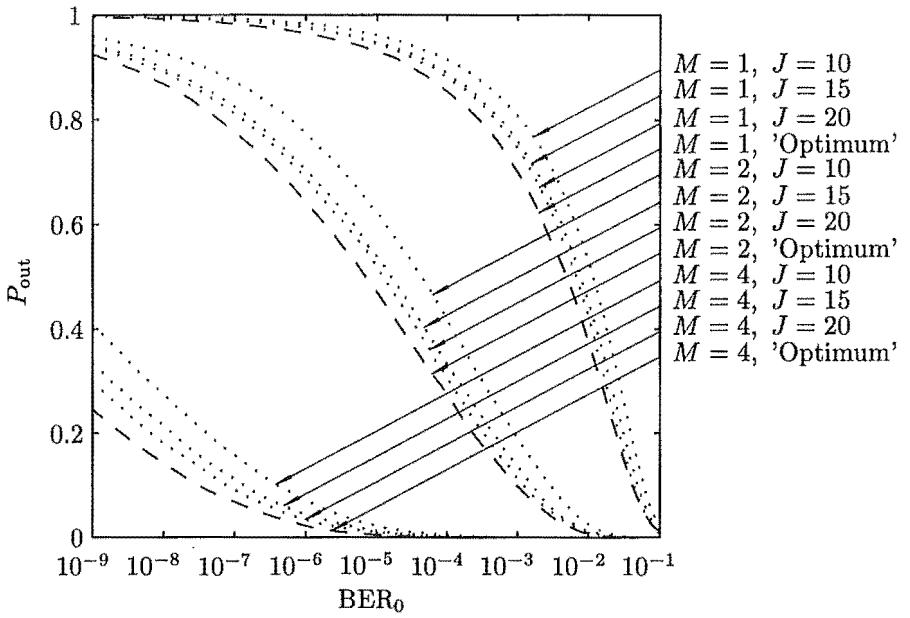

Figure 4.10 Performance of M-branch finite-length equaliser receiver (dotted) compared with optimum linear receiver (dashed). BER distribution: Influence of diversity order, M, and equaliser length, J. Results for one dominant source (i. e., weak noise-like interference) and SIR = 10 dB.

- The receiver is more sensitive to timing offset when the channel exhibits high delay spread.

4.3.3 Influence of Bit-Error-Rate threshold

A given service on a cellular system will require a certain transmission bit-error-rate (BER) in order to operate satisfactorily. It is commonly accepted that speech can be transmitted with a BER of 10^{-3}, while data transmission requires a BER of 10^{-6} [Glance and Greenstein 1983]. It should be noted that the system would usually employ error detecting and error correcting codes to improve the overall BER, however, values of 10^{-3} and 10^{-6} are regarded as important benchmarks for uncoded transmission. A probability of outage can be defined as the proportion of the time that the BER exceeds the requirement (BER_0). It gives an indication of the proportion of message bursts that would have too many bit errors to be useful and would require retransmission. Figure 4.10 through Fig. 4.12 show graphs of outage probability versus the bit-error-rate threshold. The results are for the diversity receiver for the cases of a) no dominant interferers, b) one dominant interferer, and c) two dominant interferers. The diversity receiver performs poorly when there are no dominant interferers (Fig. 4.10) and the performance improves significantly with one dominant interferer, but slowly degrades as more dominant interferers become present and the interference tends to noise-like. Also, a higher order of diversity allows the receiver to better cope with the larger

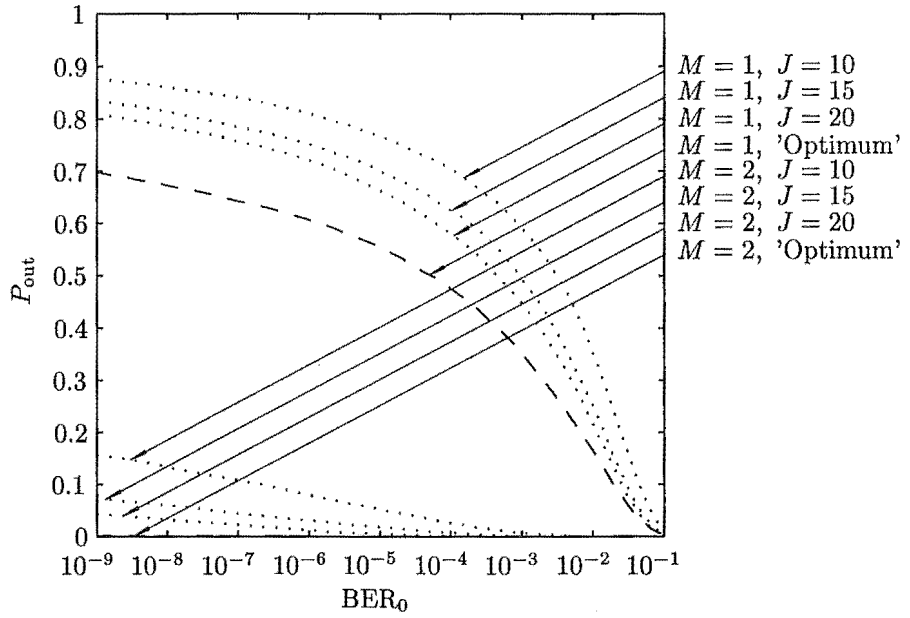

Figure 4.11 Performance of M-branch finite-length equaliser receiver (dotted) compared with optimum linear receiver (dashed). BER distribution: Influence of diversity order, M, and equaliser length, J. Results for two dominant sources (i. e., one dominant interferer) and SIR = 10 dB.

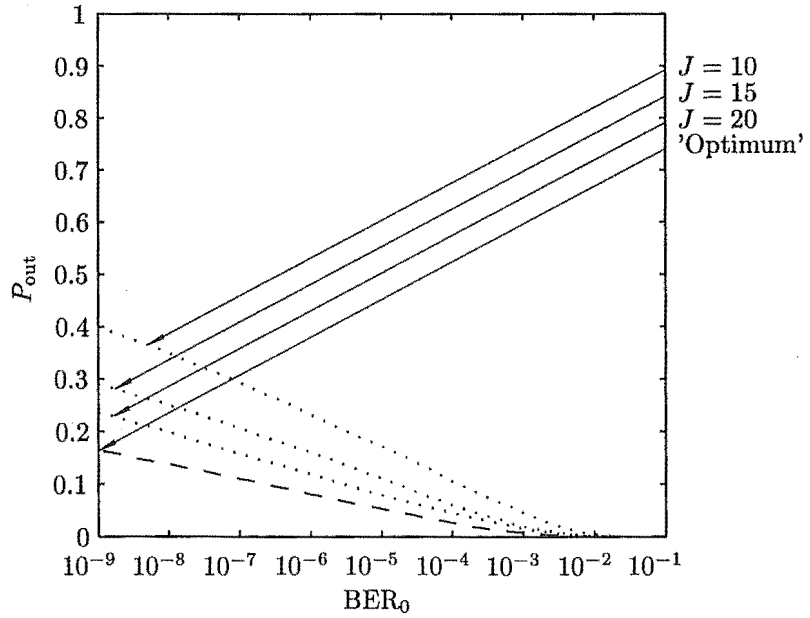

Figure 4.12 Performance of M-branch finite-length equaliser receiver (dotted) compared with optimum linear receiver (dashed). BER distribution: Influence of equaliser length, J. Results for diversity order $M = 1$, three dominant sources (i. e., two dominant interferers) and SIR = 10 dB.

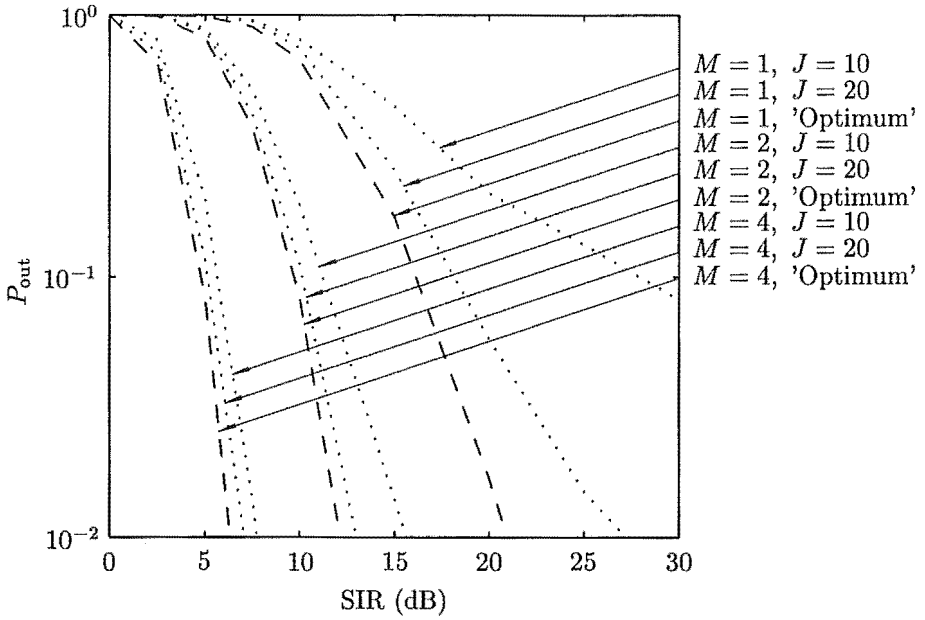

Figure 4.13 Performance of M-branch finite-length equaliser receiver (dotted) compared with optimum linear receiver (dashed). Outage probability ($BER_0 = 10^{-3}$): Influence of diversity order, M, and equaliser length, J. Results for one dominant source (i. e., weak noise-like interference).

number of dominant interferers.

More taps are required in each equaliser in order to obtain a close approximation to the optimum linear receiver when there are dominant co-channel interferers. A receiver with 10 taps per branch suffers an degradation in P_{out} of up to 0.1 over the optimum linear receiver when all the interference is noise-like (Fig. 4.10), but the receiver requires 20 taps per branch, for a similar degradation, when the interference is dominant (Fig. 4.11 and Fig. 4.12). Both the optimum linear receiver and the finite-length equaliser receiver can combat dominant CCI more effectively than noise-like CCI because the contribution of the dominant CCI sources can be minimised in the MSE sense by appropriate tap settings as the channel responses from the dominant CCI sources are known, whereas the noise-like CCI is assumed to be Gaussian coloured noise so its noise power can not be cancelled. However, the ability of the finite-length equaliser receiver to reduce the effects of dominant CCI is more severely limited by the finite-length of the equalisers, than for noise-like CCI. Hence there is a need for greater equaliser length to approach the optimum linear receiver in the case of dominant CCI.

4.3.4 Influence of Signal-to-Interference Ratio

Since the object of a cellular system is to enable as many users as possible within a certain area, a system that can withstand a large amount of interference from other users is desirable. Therefore, the SIR of signals in a cellular radio environment is

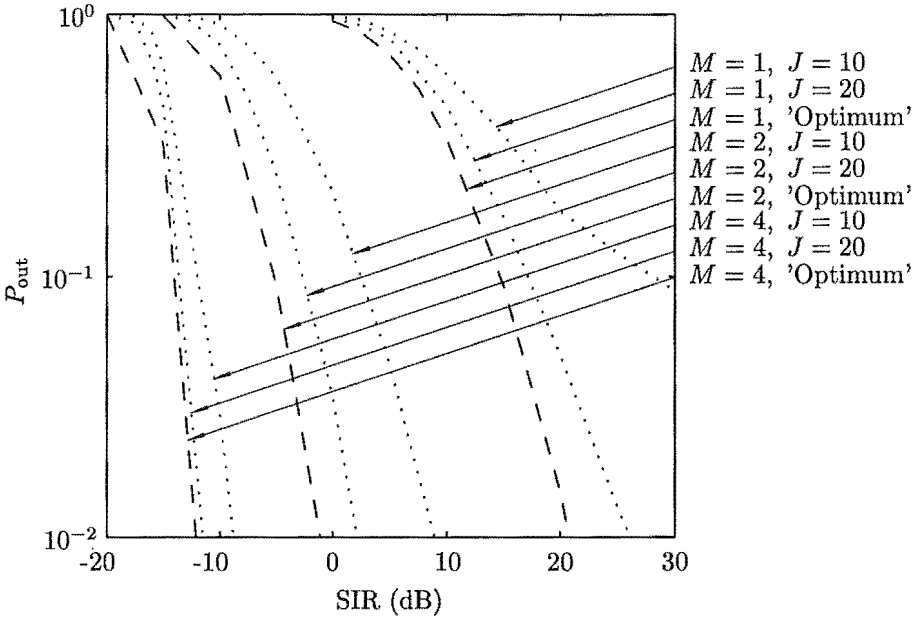

Figure 4.14 Performance of M-branch finite-length equaliser receiver (dotted) compared with optimum linear receiver (dashed). Outage probability ($\mathrm{BER}_0 = 10^{-3}$): Influence of diversity order, M, and equaliser length, J. Results for two dominant sources (i. e., one dominant interferer).

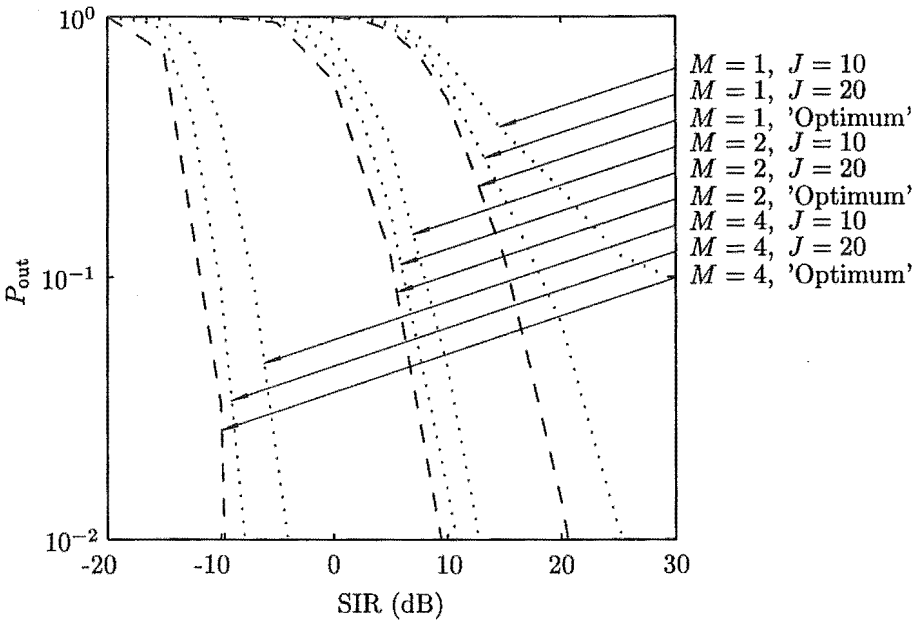

Figure 4.15 Performance of M-branch finite-length equaliser receiver (dotted) compared with optimum linear receiver (dashed). Outage probability ($\mathrm{BER}_0 = 10^{-3}$): Influence of diversity order, M, and equaliser length, J. Results for three dominant sources (i. e., two dominant interferers).

determined primarily by the relative strengths of the desired source and the co-channel interference at the receiver. The graphs in this section show how the outage probability changes for a fixed BER threshold of 10^{-3}, (speech quality), as the SIR is varied. The results show the required SIR for a given set of parameters to obtain a required P_{out}. (Again the results obtained for the finite length equaliser receiver are compared against the results of the optimum linear receiver.)

Figure 4.13 through Fig. 4.15 show three plots of outage probability versus signal-to-interference ratio. The plots illustrate how the finite length equaliser receiver can more closely approximate the optimum as the diversity is increased.

Figure 4.13 is for one desired source only, and all the interference is noise-like. It shows that diversity is not very effective against noiselike CCI, and as a result all the receiver configurations must operate above a SIR of 0 dB. However, the finite length equaliser receiver closely approximates the optimum linear receiver for diversity order of two or more, being within 1 dB when there are 20 taps per branch filter.

With dominant interference, the optimum linear receiver can operate with a much lower SIR value, down to -10 dB with four branches. However, the finite-length equaliser receiver has a reduced ability to approximate the optimum linear receiver in this case. The diversity receiver with 20 taps per branch requires an extra 2 or 3 dB over the optimum linear receiver when the interference is dominant. It should be noted that although the finite-length equaliser receiver performs more poorly when compared to the optimum linear receiver with dominant interference, both receivers still perform significantly better than with noiselike interference.

In the case of both dominant and noise-like interference, the finite-length equaliser receiver performs very poorly without diversity and requires 20 taps to be within approximately 5 dB of the optimum linear receiver at P_{out} =0.02. There is also a floor in the outage probability, when the receiver has one branch and an equaliser length of 10, indicating that the performance of the receiver is interference limited in this case.

4.3.5 Influence of Signal-to-Interference Ratio on the average BER

The average bit-error-rate, $\langle \text{BER} \rangle$, is defined as the average of the BER for each channel snapshot set. It indicates the expected BER of the bit stream rather than the proportion of bursts that must be retransmitted, and is particularly relevant to fast moving mobile users. Figure 4.16 through Fig. 4.18 show plots of average BER versus SIR for the cases of no dominant interference, one dominant interferer, and two dominant interferers, respectively. Similar trends to those found in the previous sections are evident. Namely, the receiver can compensate for dominant interference at a significantly lower SIR than for noise-like interference, but the finite-length equaliser receiver approximates the optimum linear receiver more closely when exposed to noise-like interference because of the difficulty both receivers have in combating noise-like

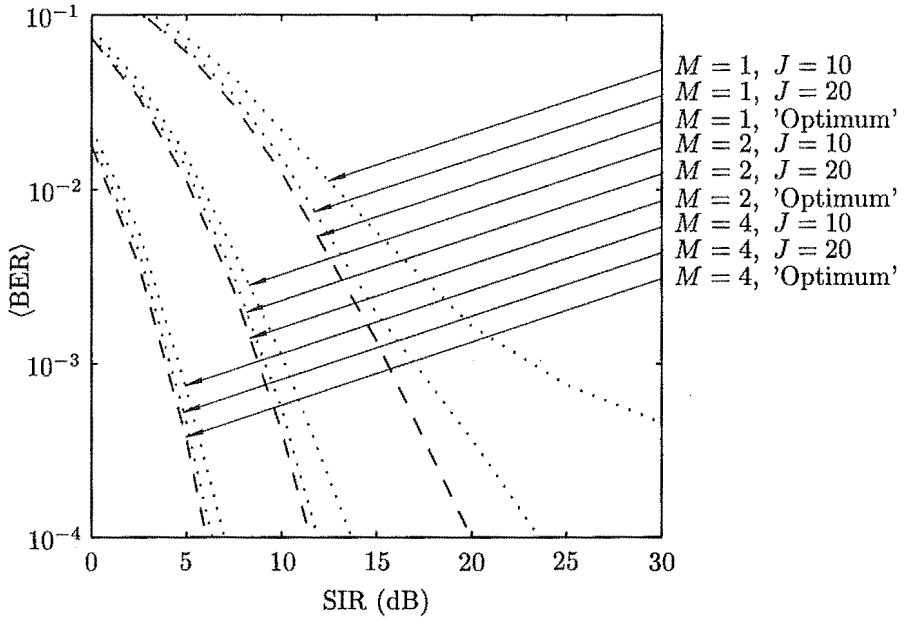

Figure 4.16 Performance of M-branch finite-length equaliser receiver (dotted) compared with optimum linear receiver (dashed). Average bit-error-rate: Influence of diversity order, M, and equaliser length, J. Results for one dominant source (i. e., weak noise-like interference).

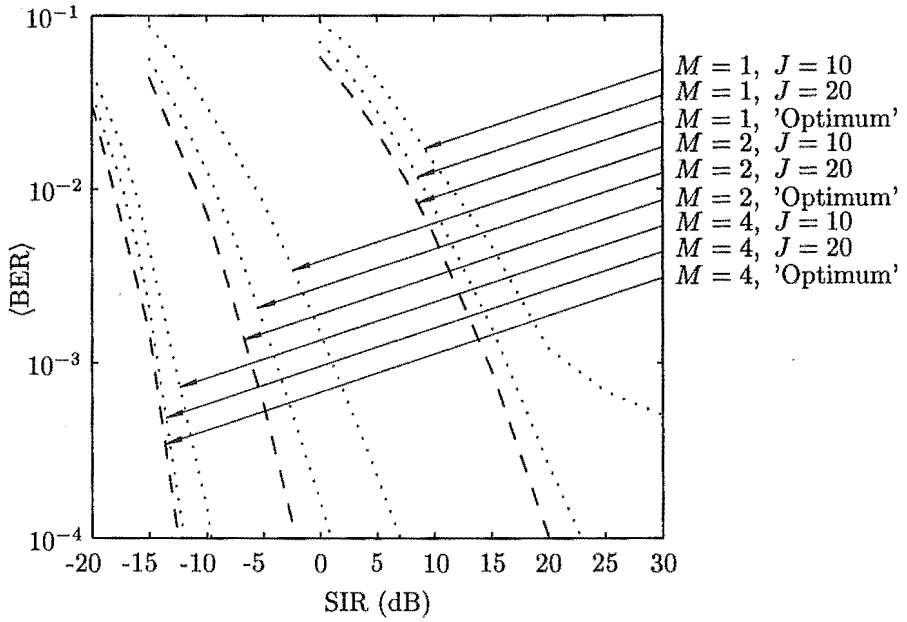

Figure 4.17 Performance of M-branch finite-length equaliser receiver (dotted) compared with optimum linear receiver (dashed). Average bit-error-rate: Influence of diversity order, M, and equaliser length, J. Results for two dominant sources (i. e., one dominant interferer).

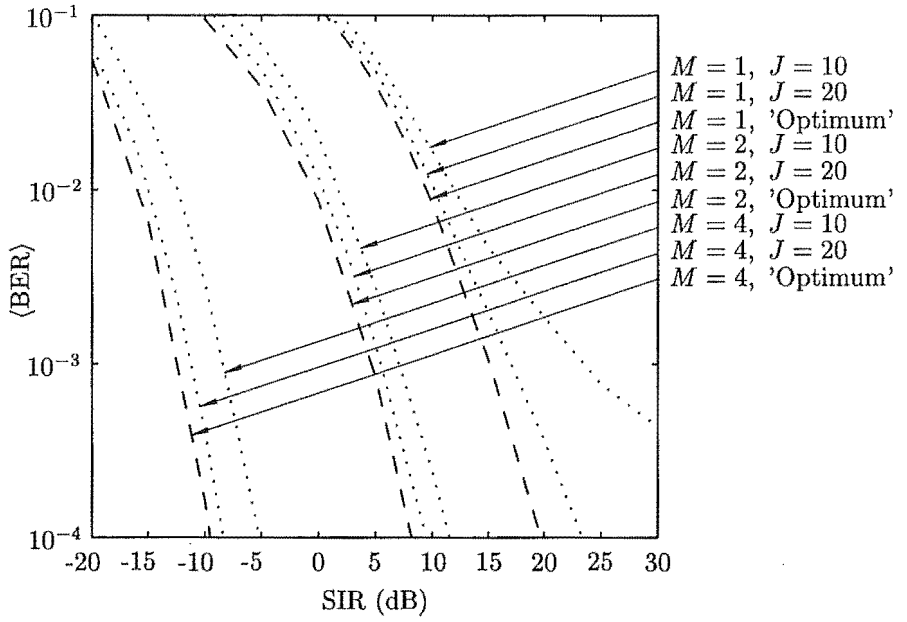

Figure 4.18 Performance of M-branch finite-length equaliser receiver (dotted) compared with optimum linear receiver (dashed). Average bit-error-rate: Influence of diversity order, M, and equaliser length, J. Results for three dominant sources (i. e., two dominant interferers).

interference. Also, again the receiver performs best with one dominant interferer, and more poorly as more dominant interferers are present.

The receiver with no diversity performs poorly, requiring an SIR of more than 15 dB to achieve an average bit-error-rate of 10^{-3}, and requires more than 10 taps per branch to reduce an error floor at about that error rate.

4.3.6 Influence of Diversity with constant total number of taps

This section highlights the effectiveness of diversity in a receiver assuming a fixed total number of taps. Figure 4.19 shows three curves of P_{out} versus SIR indicating the performance of three receiver configurations which all have the same total number of 20 taps. The increased diversity improves the performance even though each branch equaliser has less distortion correcting capability due to a shorter length (i. e., fewer taps). This trend could be noticed from the previous sections, but is highlighted here.

Figure 4.20 shows a plot of required SIR versus diversity order for a fixed outage probability, $P_{\text{out}} = 10^{-2}$, for a bit-error-rate threshold, $\text{BER}_0 = 10^{-3}$. Three curves are show for the finite-length equaliser receiver with a fixed total number of taps, $M \times J$. The curve for the optimum linear receiver is included as a comparison (dashed).

It can be seen that large gains in performance can be achieved by using two diversity branches (more than 18 dB depending on the number of taps), and further significant

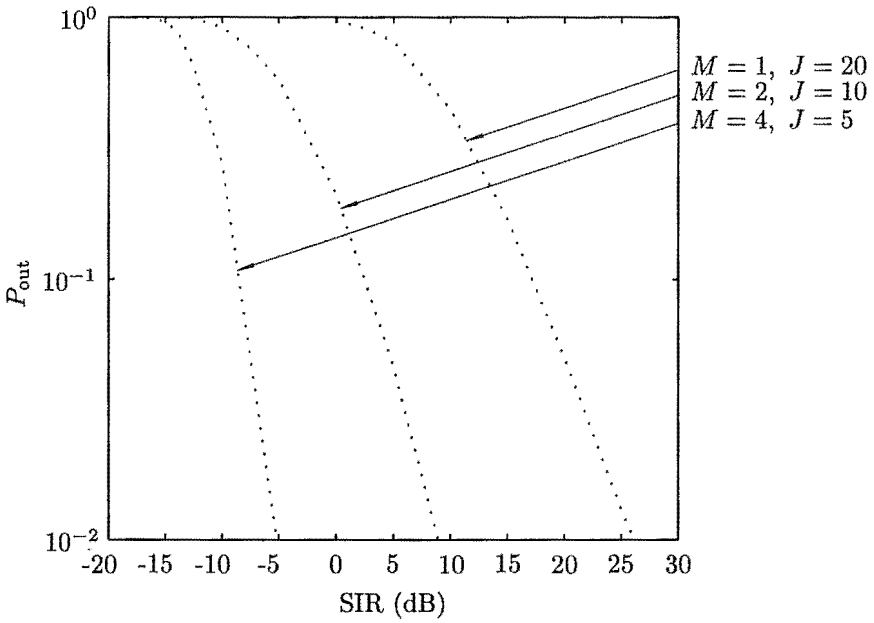

Figure 4.19 Performance of M-branch finite-length equaliser receiver (dotted). Outage probability ($\mathrm{BER}_0 = 10^{-3}$): Influence of diversity order, M, and equaliser length, J, for constant total number of taps ($M \times J$). Results for two dominant sources (i. e., one dominant interferer).

gains can be achieved with four diversity branches (more than 12 dB). Higher order diversity results in diminishing returns, as it takes a further four branches to achieve another 5 dB.

The gain in SIR as the total number of taps is increased from 8 to 16 is $\approx$ 12 dB for two, four, and eight branches, and similarly the gain from 16 taps to 32 taps for a given diversity is $\approx$ 6 dB. However, high order diversity with a small number of taps per branch improves the performance over low order diversity with a greater *total* number of equaliser taps even though each branch equaliser has less distortion correcting capability due to a shorter length. For example, a receiver with a total of eight taps and four branches (i. e., two taps/branch) has approximately the same performance as a receiver with 16 taps and two branches (eight taps/branch). Thus there is more potential performance improvement through using a larger number of diversity branches with shorter equalisers.

4.3.7 Influence of Diversity on the error burst nature of the receiver

A communication system operating in a time-varying fading channel experiences significant variation in performance, and it is difficult to quantify how the performance varies. Sections 4.3.3 and 4.3.4 show how the receiver is expected to perform by presenting the proportion of time that successful transmission can be made (outage probability). Section 4.3.5 shows how the receiver is expected to perform by presenting the expected

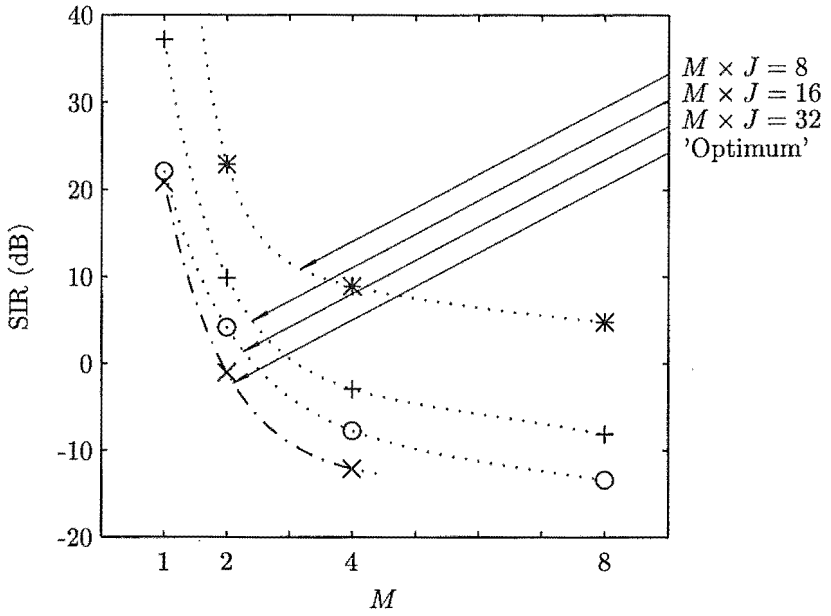

Figure 4.20 Performance of M-branch finite-length equaliser receiver (dotted) compared with optimum linear receiver (dashed). Required SIR: Influence of diversity order, M, and equaliser length, J, for constant total number of taps ($M \times J$). Results for two dominant sources (i. e., one dominant interferer).

proportion of message symbols that can be transmitted correctly (bit-error-rate). These two measures can be used together to give an indication of whether the errors occur in bursts or more intermittently. Here the term *burst* is used to imply sequences of symbols that are incorrect, rather than a burst of symbols in a burst-mode system. A knowledge of whether errors occur together in bursts, or not, is important in the design of error-correcting codes.

A measure of the error burst nature is given by the outage probability when $\text{BER}_0 = \langle \text{BER} \rangle$. When the errors are spread out evenly through the transmission, P_{out} is close to 0.5, (its maximum value when $\text{BER}_0 = \langle \text{BER} \rangle$). The more the errors tend to bunch together, the more P_{out} tends to $2\langle \text{BER} \rangle$, (its minimum value when $\text{BER}_0 = \langle \text{BER} \rangle$) [Clark 1992].

This measure of the error burst nature can be plotted by calculating the average bit-error-rate, $\langle \text{BER} \rangle$, setting the BER threshold to $\langle \text{BER} \rangle$, calculating the outage probability, P_{out}, and scaling its maximum and minimum values to 1 and 0 respectively.

Figures 4.21 and 4.22 show the error burst nature measure plotted against signal-to-interference ratio, for receivers with equaliser length 10 and 20 respectively. Results for weak noise-like interference are shown in solid lines, while results for dominant interference are shown in dot-dashed.

Similar trends are shown for both equaliser lengths. First, the errors are reason-

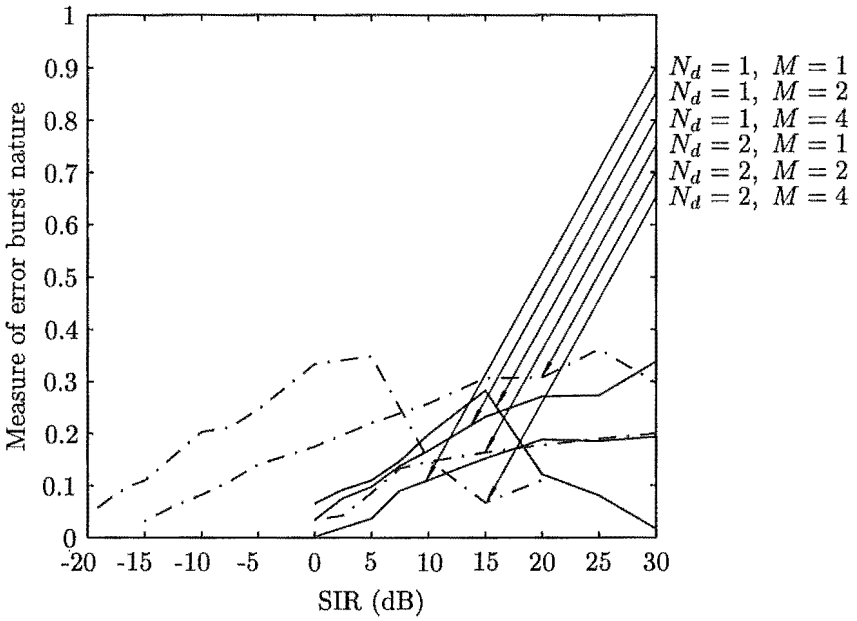

Figure 4.21 Performance of M-branch finite-length equaliser receiver. Measure of error burst nature: Influence of diversity order, M, and number of dominant sources, N_d. Results for equaliser length, $J = 10$.

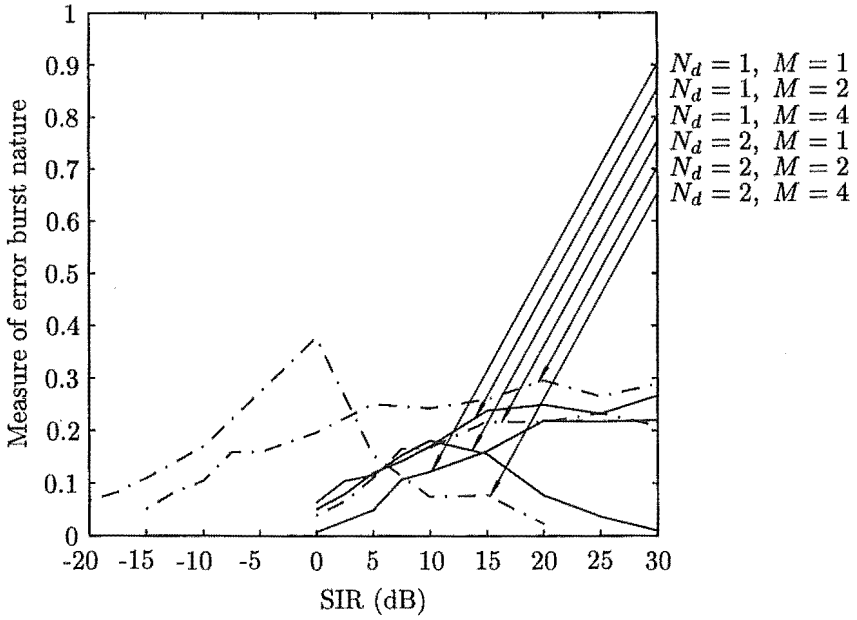

Figure 4.22 Performance of M-branch finite-length equaliser receiver. Measure of error burst nature: Influence of diversity order, M, and number of dominant sources, N_d. Results for equaliser length, $J = 20$.

ably well spread out, with the maximum burst measure being less than 0.4 in all cases. Second, the receiver with four diversity branches has an increase in the burst measure as the SIR is increased, followed by a decrease in the burst measure. The lower order diversity receiver experiences an increase in the burst measure as the SIR is increased, and may experience a decrease, although the simulations did not evaluate the burst measure at a high enough SIR because it would be impractical in a real system. However, the trend of the burst measure with a peak in the middle indicates that the receiver experiences a lot of errors (which are therefore spread out) at low SIR, manages to compensate for mildly distorted channels at medium SIR (which therefore decreases the BER during the mildly channels and increases the burst measure), and manages to compensate for more distorted channels at high SIR (which reduces the BER over the mildly and the more distorted channels). The receiver with only one or two branches does not manage to compensate for the more distorted channels (perhaps until a very high SIR is present). This implies that a real system would require four fold diversity to overcome the channel distortions.

The nature of the interference (i. e., weak or dominant) does not have significant influence over the error burst nature of the receiver. In Fig. 4.21 and 4.22, the results for weak interference show the same trends as for dominant interference except that the required level of SIR is different, as already discussed in previous sections.

4.4 CONCLUSION

This chapter has presented the minimum-mean-square-error optimisation of the finite-length equaliser diversity receiver. The optimisation is carried out assuming ideal channel-state-information, and ideal carrier frequency recovery. The global optimisation, as applied to the diversity receiver, is a novel extension to previous single equaliser optimisations. An outline of the algorithm for numerically calculating the receiver's bit-error-rate is given, and the simulation procedure is presented. The definitions of the performance measures $\langle \text{BER} \rangle$ and P_{out} are the same as those presented by Clark [1992], but here are applied to a receiver with finite-length equalisers. Performance results for the diversity receiver structure described in Chap. 3 are given for a receiver assumed to have ideal carrier recovery and ideal channel state information. Monte Carlo simulation techniques were used to average the performance over the channel fading statistics, while an efficient iterative algorithm was used to calculate the BER for a given set of channel snapshots.

The results highlighted the following points:

- The diversity receiver with fractionally-spaced equalisers is relatively insensitive to symbol timing offsets over a wide range, on the order of half the equaliser

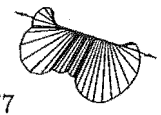

length. The sensitivity is reduced when the diversity is increased, and when the interference is weak and noise-like.

- Neither the optimum receiver nor the finite-length equaliser receiver is particularly effective against noise-like CCI, so the finite-length receiver closely approximates the optimum linear receiver even with a small number of taps (e. g., 10) per branch.

- The receiver is effective in combating dominant interference when the diversity is greater than or equal to the number of dominant sources (i. e., the number of dominant interferers plus the desired source), but as the number of dominant interferers increases, the receiver performance tends to the noise-like interference case.

- The finite-length equaliser receiver approximates the optimum linear receiver more closely for higher order diversity because the gains achieved by diversity reduce the requirement on the sub-optimal finite-length equalisers.

- Higher order diversity improves performance even when the total number of taps remains the same, indicating that the highest feasible diversity should be used.

- An error burst measure was obtained by setting $\mathrm{BER}_0 = \langle \mathrm{BER} \rangle$. The measure indicated that as the SIR was increased the errors became less spread out, meaning that the receiver was able to compensate for some of the channel distortion more effectively than at other times. Presumably, the receiver could compensate for mild channel distortion and fading more easily than severe distortion and fading. In the case of the receiver with four diversity branches, the error burst measure reduced again as the SIR was further increased, indicating that the receiver could compensate for mild and severe distortion.

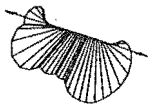

Chapter 5

CARRIER FREQUENCY OFFSET RECOVERY

The study of the effect of finite equaliser length (Chap. 4) assumed ideal carrier recovery which allowed for simple analysis and simulation, and highlighted, in isolation, the effect of equaliser length on the receiver performance. However, a real receiver would not have ideal knowledge of the carrier used at the transmitter. This chapter presents the derivation of a maximum likelihood carrier frequency offset estimation algorithm, and investigates the performance of the estimator. The main aim of this chapter is to determine the effect of diversity on the carrier offset estimator. As discussed in Sec. 3.2, the algorithm estimates the carrier *frequency* offset, but does not estimate the carrier *phase* offset.

The chapter is organised as follows. Section 5.1 discusses the problems associated with carrier recovery in the fading channel, and how the estimator proposed in this thesis operates in the multipath environment. Section 5.2 presents the method of evaluating the performance of the estimator. The performance measures are indicated by the tracking range of the algorithm and the expected value and variance of the estimate. The derivation of the estimator equation is presented in Sec. 5.3. The simulation procedure is outlined in Sec. 5.4, together with the parameters that are held constant throughout the entire simulation are presented. The results of the simulations are presented in the following section. Finally, the chapter is concluded.

5.1 ESTIMATOR OPERATION

In a channel with only additive noise and no distortion, recovering the carrier from a linearly modulated digital received signal is relatively simple. In the majority of linear modulation schemes, the modulation of the carrier can be removed from the received signal by a non-linear device, such as a power-law device, to give a signal with which to estimate the carrier frequency [Gitlin *et al.* 1992, p. 422].

In a frequency-selective fading channel, the recovery of the carrier is made difficult because of intersymbol interference (ISI) introduced by the channel (Sec. 1.4), and by a decrease in signal-to-interference ratio when the channel is faded. The presence of

ISI makes it very difficult to remove the effects of the modulation because, even at the ideal sampling instants, the samples are a function of many data symbols that have been weighted by the link impulse response.

The carrier recovery scheme developed here is suited to burst-mode systems where several users are each allocated a timeslot within a frame [Steele 1992]. As discussed in Chap. 3, the receiver operates by translating the RF signals received on the antennae to approximately baseband with a free-running local oscillator, sampling the baseband signals based on a symbol period known with high accuracy, calculating the carrier frequency offset estimate, and removing it from the received samples. The carrier frequency offset is the difference between the transmitter's oscillator frequency plus Doppler shift frequency and the receiver's local oscillator frequency. The Doppler shift is caused by relative motion between the transmitter and receiver, but is not present if the received rays are uniformly distributed around the mobile as assumed in a dense urban environment. The received signal may also experience Doppler spreading which is caused by the time-varying nature of the channel, which also modulates the transmitted signal. In any case, the receiver forms an estimate of the difference between the effective carrier frequency in the received signal (which includes any Doppler shift, and is within the Doppler spread bandwidth), and the receiver's oscillator frequency. The distortions due to the Doppler spreading appear as phase jitter in the received signals and can ideally be removed by equaliser tracking.

The received signal on each diversity branch is down-shifted by the same local oscillator frequency, and the carrier frequency offset is assumed to be the same on each branch. This is a valid assumption if there is a Doppler shift because all branches will be moving in the same direction relative to the transmitter resulting in the same Doppler shift on each branch. It is also valid in a dense urban environment because the effect of Doppler spreading does not introduce a distinct carrier frequency offset. The fact that each received signal is down-shifted by the same local oscillator implies that the receiver employs micro-diversity [Cox 1987], (i. e., the diversity antennae are close enough such that the average received power from a given co-channel source is the same on every diversity branch, yet far enough apart to ensure independent fading on each branch). The maximum likelihood technique for deriving the carrier frequency offset estimate could be modified to apply to a system with macro-diversity, (i. e., the diversity branches are separated by a much greater distance), where each branch would have a different local oscillator, and would require an independent offset estimate on each branch.

The carrier frequency offset estimate algorithm presented here is based on work by Luise and Reggiannini [1995]. The algorithm presented there builds a reconstruction at the receiver of the modulated and faded message data using an estimate of the channel and the known training sequence. This reconstructed signal is then removed from the received signal to obtain a noisy estimate of the carrier offset. The estimated

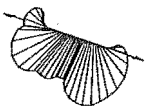

carrier offset can then be removed from the received signal before it is demodulated. The algorithm presented in this thesis is novel in two respects. First, a channel estimate is not required, rather it only requires knowledge of the *channel auto-correlation function.* Second, it has been applied to the M-branch diversity receiver. The use of the channel auto-correlation function is a significant improvement because it is simpler for a practical implementation to estimate the correlation of a channel instead of the actual channel response.

The carrier phase may be determined as part of an equaliser training process. Using the training sequence as a reference, the phases of the filter taps are appropriately rotated to cancel the carrier phase offset present in the received signals. Burst synchronisation is assumed, but may be achieved fairly simply in a real system using methods such as the use of control channels, correlating the received signal with the known training data, or a search method [D'Aria *et al.* 1992].

5.2 PERFORMANCE MEASURES FOR THE CARRIER FREQUENCY OFFSET ESTIMATOR

The estimator described in this chapter estimates the offset or difference between the carrier frequency apparent in the received signals and the local oscillator frequency. Due to the fading characteristics of the channel and noise, the estimate is not the same as the true offset that is present. The performance, or amount by which the estimate varies from the true offset, must be determined. Ideally the most desirable performance measure for the estimator is the degradation in receiver performance from the case of known offset to the case where the offset is estimated. The receiver performance can be quantified as before by average BER or outage probability. However, the performance of the estimator becomes obscured by the interactions of the equalisers in the receiver, and more useful performance measures are obtained simply by comparing the offset estimate directly with the actual offset present.

Therefore the three main performance indicators of the carrier estimation algorithm are:

- The expected value of the estimate.
- The variance of the estimate.
- The tracking range which is the extent by which the actual or received carrier frequency can differ from the local oscillator frequency while the algorithm remains able to estimate the offset.

It must be emphasized that the estimator functions in open-loop mode and estimates the carrier frequency offset every burst. It does not operate like a phase locked-loop and does not have a locking time [Lindsey and Chie 1981]. The estimate could

be averaged over several bursts to improve the variance [Luise and Reggiannini 1995], however, this may only be performed for bursts corresponding to the same transmitter, and will depend on the stability of the oscillators, and variability of the Doppler shift.

5.3 DERIVATION OF THE CARRIER FREQUENCY OFFSET ESTIMATOR

This section presents the derivation of the carrier frequency offset estimator based on maximum likelihood techniques. In other words, an expression for the probability of receiving the signals on the diversity branches, given a set of hypothesized parameters, is maximised. The parameters that maximise the expression are those that are most likely to have resulted in the received signals, and are therefore chosen to be the estimates of the actual parameters. In this case, the parameter to be estimated is the carrier frequency offset.

The drawback of using maximum likelihood techniques for developing this estimator is that the analysis involves finding squares of double summations which quickly becomes intractable. Therefore, the system model must be simplified. Instead of considering dominant CCI, or even weak CCI (which is coloured), all CCI interference is assumed to be white and Gaussian. This may be considered, perhaps, as a rather gross simplification, however the estimator should still operate in the presence of non-Gaussian interference and merely does not take full advantage of this information. It must be remembered that the estimator operates in the presence of large amounts of ISI without the need for channel estimates, so the assumption of the noise being only white and Gaussian does not greatly simplify the problem. In any case, since the estimator does not rely on channel estimates, the maximum likelihood estimator assuming dominant CCI is unlikely to perform much better than the one described here. The reason for this is that the receiver gets information about the dominant CCI from the modelling of the channels between dominant co-channel sources and the diversity branches. So if the algorithm only uses the channel correlation, then it would not have this information in the case of dominant interference.

Using the assumption that the all interference is white and Gaussian, the received symbol-rate sample on the m^{th} branch at time $t = lT + t_s$ (2.6) becomes

$$\bar{r}_{ml} = \sum_k x_k \bar{q}_{mkl} e^{\jmath(2\pi\Delta f lT + \phi_m)} + \eta_{ml} \tag{5.1}$$

where $\phi_m = \phi_0 + 2\pi(\Delta f t_s - f_c \tau_{0m})$ is the phase offset on the m^{th} branch due to the transmitter oscillator phase offset, sampling instant, and total transmission delay, $\bar{q}_{mkl} = q_{0m}(lT + t_s - kT, lT + t_s)$ is the link response on the m^{th} branch at time $t = lT + t_s$ to an impulse at time $t = kT$ (i.e., synchronous samples), and η_{ml} is a complex noise sample assumed to be of a zero-mean white Gaussian random process.

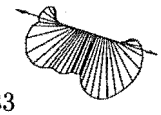

The carrier phase offsets, ϕ_m, are assumed to be uniformly distributed on $[0, 2\pi)$, and are uncorrelated across the branches.

To facilitate the maximum likelihood derivation, vector notation is employed by defining $\bar{r}$ to be a vector of ML synchronously-spaced received samples, $\bar{r}_m$ to be a vector of L synchronously-spaced received samples on the m^{th} branch, and $\boldsymbol{u}_m$ to be a vector of L noiseless hypothesized samples where u_{ml} is defined as

$$u_{ml} = \sum_k \tilde{x}_k \tilde{\bar{q}}_{mkl} e^{\jmath(2\pi\widetilde{\Delta f} lT + \tilde{\phi}_m)} \tag{5.2}$$

and $\tilde{x}_k, \tilde{\bar{q}}_{mkl}, \widetilde{\Delta f}$, and $\tilde{\phi}_m$ are hypothesized data symbols, link responses, carrier frequency offset, and carrier phase offsets, respectively. Similarly, $\tilde{\boldsymbol{x}}$, $\tilde{\bar{\boldsymbol{q}}}$, and $\tilde{\boldsymbol{\phi}}$ are defined as vectors of hypothesized data symbols, link impulse responses, and carrier phase offsets, respectively.

The conditional likelihood function of receiving $\bar{r}$, given hypothesized data, link responses, carrier frequency offset and carrier phase offset is derived from the standard Gaussian multi-variate probability distribution function [Davenport and Root 1958],

$$\Lambda(\bar{r}|\tilde{\boldsymbol{x}}, \tilde{\bar{\boldsymbol{q}}}, \widetilde{\Delta f}, \tilde{\boldsymbol{\phi}}) = \exp\left[\frac{-1}{2\sigma^2} \sum_m (\bar{r}_m - \boldsymbol{u}_m)^H (\bar{r}_m - \boldsymbol{u}_m)\right] \tag{5.3}$$

The multiplying constants of the probability distribution function have been ignored because the value of $\widetilde{\Delta f}$ that *maximises* the probability distribution function must be found, but the actual *maximum value* is not of interest. For this reason, constants or terms independent of $\widetilde{\Delta f}$ are dropped in this section of the analysis.

5.3.1 Maximisation of the Likelihood Function

To remove the unwanted parameters, the expectation of the likelihood function, Λ, is found with respect to the unwanted parameters: the unknown link responses, $\tilde{\bar{\boldsymbol{q}}}$; and the unknown phase offsets, $\tilde{\boldsymbol{\phi}}$. Then the result is maximised with respect to the carrier frequency offset, $\widetilde{\Delta f}$, and rearranged to solve for $\widetilde{\Delta f}$ to obtain the maximum likelihood carrier frequency offset estimate.

In order to take the expectation of (5.3) the exponential must be removed. It seems intuitive at this step to take the natural logarithm of both sides which would cancel with the exponential, however, if a non-linear function such as $\log_e$ is applied to both sides of the equation the expectation of the result is not the same as the desired expectation of Λ. Therefore the exponential in (5.3) is approximated by a Maclaurin series [Kreyszig 1988] and truncated to the squared term, which is valid at high SNR.

The likelihood function then becomes

$$\Lambda(\bar{r}|\tilde{x},\tilde{\bar{q}},\widetilde{\Delta f},\widetilde{\phi}) \approx 1 - \frac{1}{2\sigma^2}X + \frac{1}{8\sigma^4}X^2 \tag{5.4}$$

where

$$X = \sum_m (\bar{r}_m - \boldsymbol{u}_m)^H (\bar{r}_m - \boldsymbol{u}_m) \tag{5.5}$$

$$= \sum_m \sum_l |\bar{r}_{ml} - u_{ml}|^2 \tag{5.6}$$

$$= \sum_m \sum_l |\bar{r}_{ml}|^2 - 2\mathcal{R}e\{\bar{r}^*_{ml} u_{ml}\} + |u_{ml}|^2 \tag{5.7}$$

The terms in (5.4) are expanded and the expectation over the unknown phase offsets, $\widetilde{\phi}$, is taken, discarding the terms independent of $\widetilde{\Delta f}$. After much tedious algebra the likelihood function becomes

$$\Lambda(\bar{r}|\tilde{x},\tilde{\bar{q}},\widetilde{\Delta f}) = \sum_m \sum_l \sum_{l'} \bar{r}_{ml}\bar{r}^*_{ml'} \sum_k \sum_{k'} \tilde{x}^*_k \tilde{\bar{q}}^*_{mkl} \tilde{\bar{q}}_{mk'l'} \tilde{x}_{k'} \cdot e^{-\jmath 2\pi \widetilde{\Delta f}(l-l')T} \tag{5.8}$$

Taking the expectation of (5.8) with respect to the link impulse response yields

$$\Lambda(r|\tilde{x},\widetilde{\Delta f}) = \sum_m \sum_l \sum_{l'} \bar{r}_{ml}\bar{r}^*_{ml'} \sum_k \sum_{k'} \tilde{x}^*_k \bar{\psi}_{l-k,l'-k';l'-l} \tilde{x}_{k'} \cdot e^{-\jmath 2\pi \widetilde{\Delta f}(l-l')T} \tag{5.9}$$

where the link impulse response correlation function is defined as

$$\bar{\psi}_{l-k,l'-k';l'-l} = E[\bar{q}^*_{mkl}\bar{q}_{mk'l'}] \tag{5.10}$$

$$= \int_{-\infty}^{\infty} c^*((l-k)T + t_s - \alpha - \tau_m) \cdot c((l'-k')T + t_s - \alpha - \tau_m) P(\alpha,(l'-l)T)\, d\alpha \tag{5.11}$$

Equation (5.9) is the likelihood of receiving the samples $\bar{r}$, given the hypothesized data, $\tilde{x}$, and the hypothesized frequency offset, $\widetilde{\Delta f}$. Remember, it is not necessary to average over the hypothesized data because the training sequence is available at the receiver.

The likelihood function (5.9) is maximised by taking the derivative with respect to $\widetilde{\Delta f}$, and setting the result to zero to obtain

$$\sum_m \sum_l \sum_{l'} \bar{r}_{ml}\bar{r}^*_{ml'} \sum_k \sum_{k'} \tilde{x}^*_k \bar{\psi}_{l-k,l'-k';l'-l} \tilde{x}_{k'} (l-l') \cdot e^{-\jmath 2\pi \widetilde{\Delta f}(l-l')T} = 0 \tag{5.12}$$

This can be rearranged as

$$\mathcal{I}m\left\{\sum_m \sum_{l=1}^{L-1} l(L-l)\Phi_m(l)e^{-\jmath 2\pi \widetilde{\Delta f} lT}\right\} = 0 \tag{5.13}$$

where the correlation of the received samples weighted by data and link correlation terms is defined as

$$\Phi_m(l) \triangleq \frac{1}{L-l}\sum_{i=l+1}^{L} \bar{r}_{mi}\bar{r}^*_{m,i-l}\sum_j\sum_{j'}\tilde{x}^*_{i-j}\bar{\psi}_{j,j';-l}\tilde{x}_{i-l-j'}, \qquad 0 \leqslant l \leqslant L-1 \tag{5.14}$$

5.3.2 Solution for the Maximum Likelihood Carrier Frequency Offset Estimator

The maximum likelihood carrier frequency offset estimator is the solution to (5.12) or (5.13). However, this cannot be solved simply. Instead an approximation to (5.13) is solved by assuming that noise terms can be neglected. This method suffices to arrive at a carrier offset estimator which approximates the maximum likelihood estimator and its effectiveness is determined by simulation.

Following Luise and Reggiannini [1995] (5.13) is approximated by replacing the parabolic weighting, $\{l(L-l),\ l = 1, 2, \ldots, L-1\}$ by a truncated rectangular weighting, $\{1,\ l = 1, 2, \ldots, P$, and zero elsewhere$\}$ for some $P \leqslant L-1$ to obtain

$$\mathcal{I}m\left\{\sum_m \sum_{l=1}^{P} \Phi_m(l)e^{-\jmath 2\pi \widetilde{\Delta f} lT}\right\} = 0, \qquad P \leqslant L-1 \tag{5.15}$$

This can be rewritten as

$$\mathcal{I}m\left\{\sum_m \left[\sum_{l=1}^{P}\sum_{l'=1}^{P} \Phi_m(l)e^{-\jmath 2\pi \widetilde{\Delta f} l'T}\right] - \sum_{l=1}^{P}\sum_{\substack{l'=1 \\ l'\neq l}}^{P} \Phi_m(l)e^{-\jmath 2\pi \widetilde{\Delta f} l'T}\right]\right\} = 0, \qquad P \leqslant L-1 \tag{5.16}$$

For zero interference and noise, $\Phi_m(l)$ is sinusoidal, so following [Luise and Reggiannini 1995], the weighted correlation of the received samples is assumed to approximate a sinusoid, $\Phi_m(l) \approx A_m e^{\jmath 2\pi \Delta f lT} + \xi_{ml}$, where A_m is a fading term, and ξ_{ml} is an appropriate interference term. This has been seen to be the case in simulations of $\Phi_m(l)$. As the interference term tends to zero, then for $\Delta f = \widetilde{\Delta f}$ the imaginary part of the cross terms in (5.16) tends to zero. So an approximate solution for (5.15) is the solution of

$$\mathcal{I}m\left\{\left[\sum_m \sum_{l=1}^{P} \Phi_m(l)\right]\left[\sum_{l'=1}^{P} e^{-\jmath 2\pi \widetilde{\Delta f} l'T}\right]\right\} = 0, \qquad P \leqslant L-1 \tag{5.17}$$

This final approximation can now be solved to find an expression for $\widetilde{\Delta f}$. It is unfortunate that the likelihood function, Λ, had to be approximated by a Maclaurin Series, and that several more approximations were required to solve for the maximum value because the resulting expression does not give the actual maximum likelihood estimate. However, it should prove to be close to the maximum likelihood estimate, and its performance can be determined by simulation, (although it cannot be compared to the true maximum).

Applying a standard trigonometric identity [Gradshteyn and Ryzhik 1980, p. 29], (5.17) becomes

$$\mathcal{I}m\left\{\left[\sum_m \sum_{l=1}^{P} \Phi_m(l)\right] \frac{\sin(P\pi\widetilde{\Delta f}T)}{\sin(\pi\widetilde{\Delta f}T)} e^{-\jmath(P+1)\pi\widetilde{\Delta f}T}\right\} = 0, \qquad P \leqslant L-1 \tag{5.18}$$

For $|\widetilde{\Delta f}| < 1/PT$ the ratio $\sin(P\pi\widetilde{\Delta f}T)/\sin(\pi\widetilde{\Delta f}T)$ is positive, so (5.18) may be solved intuitively when the angle of the term in square brackets equals the negative of the angle of the exponential (in other words making the product real),

$$\arg\left\{\sum_m \sum_{l=1}^{P} \Phi_m(l)\right\} = (P+1)\pi\widetilde{\Delta f}T \tag{5.19}$$

Finally, rearranging (5.19), the equation for the carrier frequency offset estimate is given by

$$\widehat{\Delta f} = \frac{1}{(P+1)\pi T} \arg\left\{\sum_m \sum_{l=1}^{P} \Phi_m(l)\right\} \tag{5.20}$$

In order to avoid solutions to (5.15) which are not estimates of the true carrier offset frequency, the argument of the right-hand side of (5.20) must be limited to $\pm\pi$. This implies that the system parameters should be chosen so that

$$|\Delta f| < \frac{1}{(P+1)T} \tag{5.21}$$

confirming the above assumption used to obtain (5.19).

Note that (5.20) reduces to the solution obtained by Luise and Reggiannini [1995, eqn. (12)] for estimating a single (unfaded) carrier offset in noise, where, in their case, the function corresponding to $\Phi_m(l)$ is simply the correlation function of the received samples. In this thesis, $\Phi_m(l)$ is the correlation of the received samples weighted by message data and channel correlation terms, as in (5.14), and the estimate (5.20) has been extended to M-branches. Also, Luise and Regiannini arrive at an approximate solution for the maximum likelihood estimator [Luise and Reggiannini 1995, eqn. (9)] by expanding the exponential in a Taylor series and truncating to the linear term. They

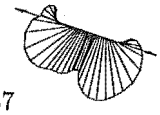

then apply a further approximation to obtain a solution corresponding to (5.20) "which is better oriented to a straightforward DSP implementation". However, the second approximation appears to cancel the effects of the first approximation because the simpler solution performs far better and is far less biased over a much wider frequency range than the original solution that it approximates. Here, an attempt has been made to show the solution (5.20) directly by considering suitable assumptions.

5.4 SIMULATION PROCEDURE

Due to the complicated nature of the mobile radio system being studied, simulation must be resorted to in order to evaluate the performance of the carrier frequency offset estimator. In establishing the performance of the receiver assuming ideal carrier recovery as in Chap. 4, Monte Carlo techniques were used to average over the channel fading, but message data symbols were not generated. Since the probability distribution function of the ISI could be found, the probability of error could be determined using only the link impulse response functions. In other words, for each set of channels, the probability of error could be found, averaged over all the possible data symbol sequences. In the performance evaluation of the carrier frequency offset estimate described in Sec. 5.3, it is necessary to generate data symbols as well as link impulse response functions. This is because the equation for the carrier frequency offset estimate (5.20) combines the channel functions in a far more complicated way than the equation for the symbol estimate (2.6).

The simulations aim to establish the expected value of the carrier frequency offset estimate, μ, and the standard deviation of the error, σ_ε, between the carrier frequency offset estimate and the actual offset. However, the simulations can only estimate these parameters. The effect of varying system parameters can be seen by plotting μ and σ_ε against another parameter.

For any particular set of parameters, the following loop is performed N_{mc} times:

- Generate random channel responses.
- Generate random phase offsets.
- Generate random noise.
- Generate random data symbols.
- Compute received signals using (2.6).
- Compute and store the i^{th} frequency offset estimate, $\widehat{\Delta f}_i$, using (5.20) and (5.14).

The first parameter, the estimate of the expected value of $\widehat{\Delta f}$, is given by

$$\mu = \frac{\sum_{i=1}^{N_{\text{mc}}} \widehat{\Delta f}_i}{N_{\text{mc}}} \tag{5.22}$$

If the i^{th} carrier frequency offset estimate *error* sample (from the i^{th} simulation run) is defined as

$$\varepsilon_i = \Delta f - \widehat{\Delta f}_i \tag{5.23}$$

then an estimate of the *expected value* and *variance* of the *estimate error*, ε, can be found, respectively, by the following

$$\mu_\varepsilon = \frac{\sum_{i=1}^{N_{\text{mc}}} \varepsilon_i}{N_{\text{mc}}} \tag{5.24}$$

and

$$\sigma_\varepsilon^2 = \frac{\sum_{i=1}^{N_{\text{mc}}} (\varepsilon_i - \mu_\varepsilon)^2}{N_{\text{mc}}} \tag{5.25}$$

The choice of N_{mc} was made by choosing a large number and increasing it if repeated simulations did not return consistent estimates of the mean and variance. In most of the simulations $N_{\text{mc}} = 10000$ was found to give consistent results. Because of the complexity of the problem, it was not possible to evaluate the confidence of the estimate mean and variance, however, they suffice to illustrate trends.

As in the previous study on equaliser length, the channel model is reduced from a general time-varying frequency-selective channel to a *quasi-static* frequency-selective model, as described in Sec. 2.5.1.

5.4.1 Definition of Signal-to-Noise Ratio

The Signal-to-Noise Ratio (SNR) used in the simulation is the average SNR. The Gaussian noise samples, η_{ml}, have a variance which gives the desired SNR if the signal were to be transmitted across an unfaded channel. Channels that are severely faded result in a decrease in actual SNR, and the estimator will reflect this by being more likely to give a large estimate error.

5.4.2 Evaluation of the offset estimate

The estimator, (5.20), requires P terms of (5.14) for each of the M branches. Following Luise and Reggiannini [1995], $P = L/2$. However, (5.14) assumes a double sum of an infinite number of terms of the link correlation function, $\bar{\psi}$, and the data, x. Only a small finite number of data symbols are known at the receiver, therefore the number of

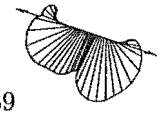

terms in the double summation in (5.14) is limited in practice. Therefore each index, j and j', in (5.14) takes on the values $-\left\lfloor \frac{N_{\bar{\psi}}}{2} \right\rfloor$ to $\left\lfloor \frac{N_{\bar{\psi}}-1}{2} \right\rfloor$, inclusive ($N_{\bar{\psi}}$ in total). If L_{TS} is defined as being the length of the training sequence, then

$$N_{\bar{\psi}} = L_{\mathrm{TS}} - L + 1 \tag{5.26}$$

5.5 SIMULATION RESULTS

There is a large number of parameters required to describe the system. In simulation, the following parameters were held constant:

- The transmit constellation = quadrature-phase-shift-keying (QPSK).
- The transmit pulse shaping filter = raised-cosine.
- The transmit pulse shaping filter roll-off factor = 50%.
- The number of samples used to represent the channel response = 32.
- The channel delay-power-spectrum function = exponential.

and the following parameters were varied:

- The normalised delay spread of the channel delay-power-spectrum, $\tau_0/T \in [0, 1]$.
- The number of branches of the diversity receiver, $M = 1, 2, 4$.
- The observation interval, $L \in [12, 26]$.
- The size of the parameter $N_{\bar{\psi}} \in [4, 18]$.
- The signal-to-noise ratio, SNR $\in [5, 20]$ dB.
- The normalised frequency offset, $\Delta f T \in [-0.072, 0.072]$.

With such a large number of parameters to vary, the following strategy was adopted to minimise the amount of simulation. The main interest is the effect of diversity on the estimator, so all simulations were performed for diversity of $M = 1, 2, 4$. First the expected value of the estimate and variance of the estimate error were found for fixed L, $N_{\bar{\psi}}$ and SNR, for both a low and high level of delay spread, and for a range of carrier frequency offsets. Then the effects of individually varying the SNR, delay spread, training sequence length, and symbol timing offset, were investigated while holding the other parameters constant.

To avoid calculating $\bar{\psi}$ as a function of τ_m in every simulation, (5.10) was calculated once by setting $\tau_m = 0$, so the results will be suboptimal. However, the matrix used for $\bar{\psi}$ in a real system will not be exact because the channel statistics are unknown. It is therefore satisfying that the carrier frequency offset estimator works with the simpler form of $\bar{\psi}$.

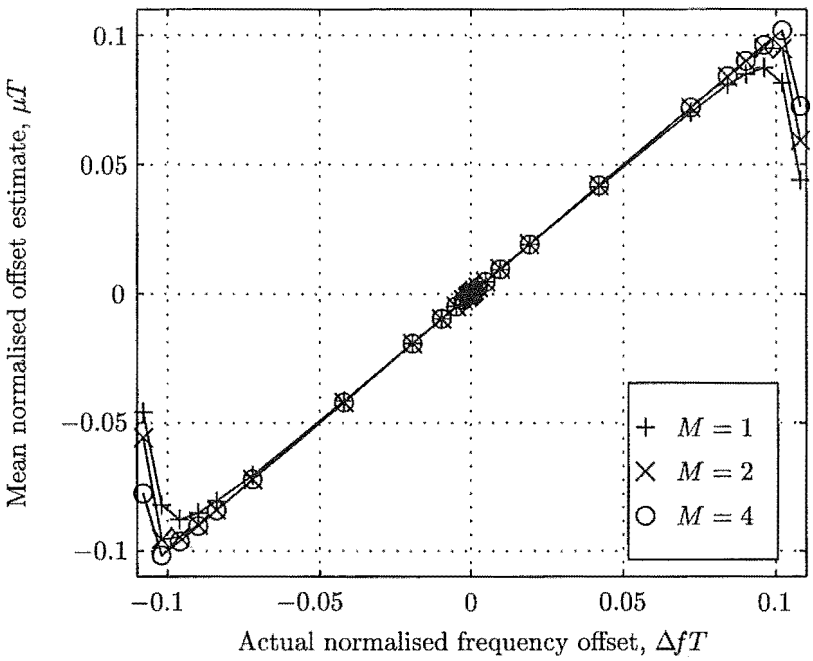

Figure 5.1 Normalised expected value of the carrier frequency offset estimate. $L = 16, N_{\bar{\psi}} = 8, \text{SNR} = 10\,\text{dB}, \tau_0/T = 0.1$

5.5.1 The effect of diversity on the mean and standard deviation of the error

The results presented here show that the estimator is unbiased over a wide range of carrier frequency offsets. This is an important characteristic of an estimator because the estimate tends to the actual offset as the standard deviation is reduced by changing parameters of the estimator. The theoretical range over which the estimator will function is given by (5.21). In these results, $L = 16$, and $P = L/2$, so the normalised offset is limited by $|\Delta fT| < 1/(P+1) = 0.11111$. Figure 5.1 and Fig. 5.2 show the expected value of the estimate versus actual offset for a low and high value of the channel delay spread, τ_0, respectively. Both figures show that the expected value of the estimate is equal to the actual value of the offset, however, the useful range is less than the theoretical range. The expected value of the estimator varies from the actual normalised offset outside the range of approximately ± 0.1 for low delay spread, and ± 0.075 for high delay spread. This is because the $\arg\{\cdot\}$ operator in (5.20) is cyclic on 2π, so the estimator is cyclic on $1/(P+1)T$ and must become non-linear.

It is clear that the diversity order does not significantly influence the expected value of the estimator, except to widen the range of operation slightly. This can be seen in Fig. 5.1 and Fig. 5.2, as all the lines are in the same position. However, in the case of no diversity, $(M = 1)$, the curve stops being linear at a lower offset frequency.

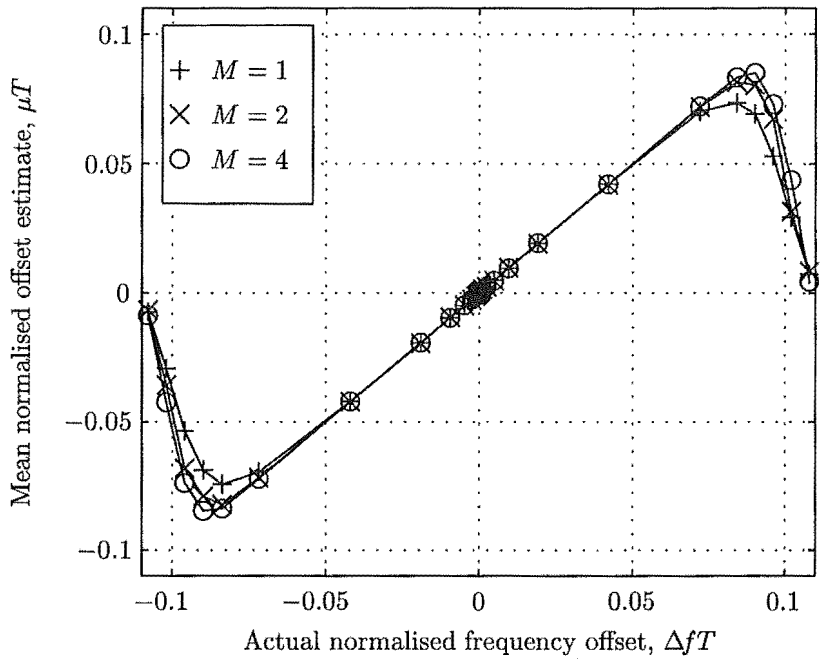

Figure 5.2 Normalised expected value of the carrier frequency offset estimate. $L = 16, N_{\tilde{\psi}} = 8, \mathrm{SNR} = 10\,\mathrm{dB}, \tau_0/T = 1$

Figure 5.3 and Fig. 5.4 show detail about the origin to highlight that there is no bias in the expected value of the estimator.

The $M = 1$ case also illustrates the performance of the carrier frequency estimator in a macro-diversity system, where each base station would independently estimate the carrier frequency offset (and have an estimate error variance as for the $M = 1$ case).

Although diversity does not significantly affect the expected value of the estimator, it does have a significant impact on the standard deviation of the estimate error. Figure 5.5 and Fig. 5.6 show the effect of diversity of the standard deviation of the estimate error versus actual offset for a low and high value of the channel delay spread, respectively. In both figures, the observation interval length, L, is 16 symbols and the signal-to-noise ratio is 10 dB. At low delay spread, $\tau_0/T = 0.1$, (Fig. 5.5), a large improvement is obtained increasing the diversity from one branch to two (the standard deviation of the error is reduced by approximately one third for small frequency offsets and even more for large frequency offsets), and a further improvement, reducing the standard deviation by approximately one half, is obtained when the diversity is increased from two branches to four branches. The "useful" range of the carrier frequency offset estimator is also more apparent from the standard deviation rather than the expected value of the estimate. Figure 5.5 shows that the estimator has a flat standard deviation of 0.0015 almost across the entire theoretical frequency offset range for a receiver with four branches. As the diversity order is reduced, the standard

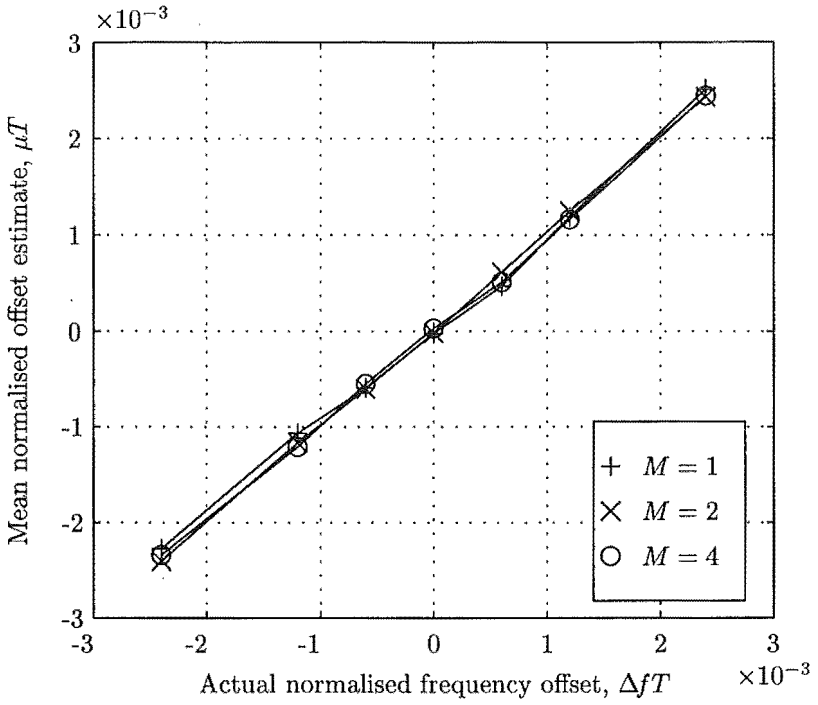

Figure 5.3 Normalised expected value of the carrier frequency offset estimate. $L = 16, N_{\tilde{\psi}} = 8, \mathrm{SNR} = 10\,\mathrm{dB}, \tau_0/T = 0.1$. Detail about origin.

deviation of the estimate error is less flat across the offset range, which limits the useful range, e. g., for $M = 1$, the useful range is approximately half to three quarters of the theoretical range.

At high delay spread, $\tau_0/T = 1$ (Fig. 5.6), the improvements are not quite as large, but still significant. The same trends of improving the standard deviation of the estimate error with diversity are apparent in Fig. 5.6, except that the standard deviation is not as flat across the offset range, even for high diversity order. The estimator is not as capable of compensating for high frequency offsets when the channel has high delay spread as it is when the channel has low delay spread.

To summarise, Fig. 5.5 and Fig. 5.6 show that the standard deviation of the estimator error is relatively insensitive to the actual carrier frequency offset over a range of half the theoretical range, and almost the entire theoretical range for low delay spread and high diversity.

5.5.2 The effect of signal-to-noise ratio on the standard deviation of the error

Having established that the estimator is essentially unbiased, and the variance of the estimator is relatively insensitive to carrier frequency offset, especially for small offsets, the normalised carrier frequency offset was set to 0 for the remaining investigations.

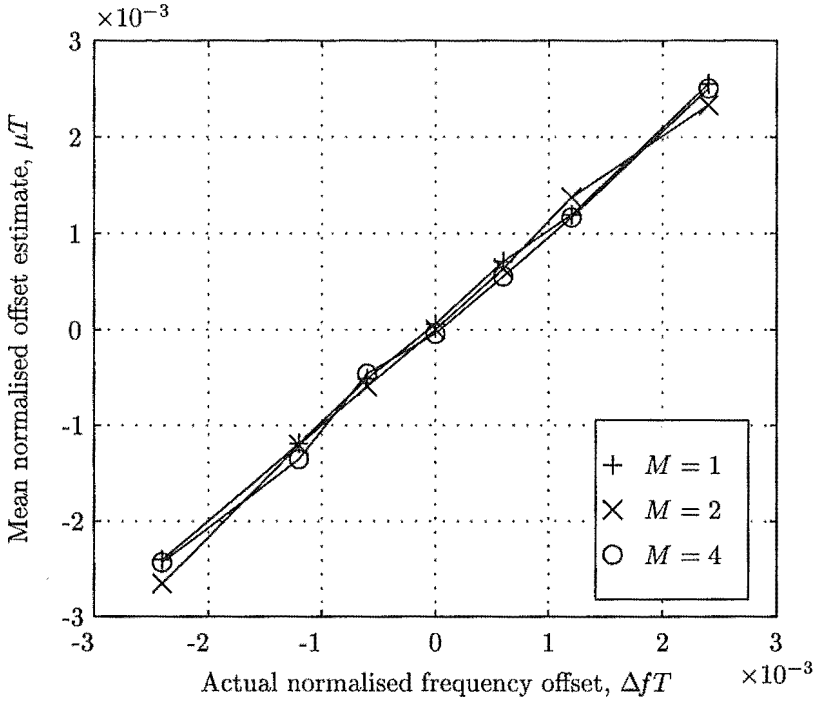

Figure 5.4 Normalised expected value of the carrier frequency offset estimate. $L = 16, N_{\tilde{\psi}} = 8, \mathrm{SNR} = 10\,\mathrm{dB}, \tau_0/T = 1$. Detail about origin.

Figure 5.7 and Fig. 5.8 show the effect of varying the SNR on the carrier frequency offset estimate error standard deviation, for constant observation interval length, carrier frequency offset and low and high delay spread, respectively. Increasing the SNR has a significant effect on the error standard deviation. Doubling the diversity from $M = 1$ to $M = 2$, and also from $M = 2$ to $M = 4$, reduces the error standard deviation by up to a factor of 2, and even more for low delay spread. The curves tend to a floor indicating that, as expected, the performance is limited by the fading and not the noise level. It can be seen that increasing the SNR has less effect when the delay spread is large, especially for higher diversity, as indicated by the reduced slope of the curves in Fig. 5.8. The trends of reducing the standard deviation by between one third and one half by doubling the diversity order are maintained as the signal-to-noise ratio is varied.

The Cramér-Rao Lower Bound (CRLB) for an estimator in a time and frequency-selective diversity system is extremely difficult to obtain, however, as a comparison, Fig. 5.7 and Fig. 5.8 show curves for the CRLB for the *additive white Gaussian noise* (AWGN) channel with the same SNR (dashed). The CRLB variance is given by [Luise and Reggiannini 1995, Rife and Boorstyn 1974]

$$\sigma^2_{\mathrm{CR}} = \frac{3}{2\pi^2 T_s^2} \frac{1}{\rho L(L^2-1)} \tag{5.27}$$

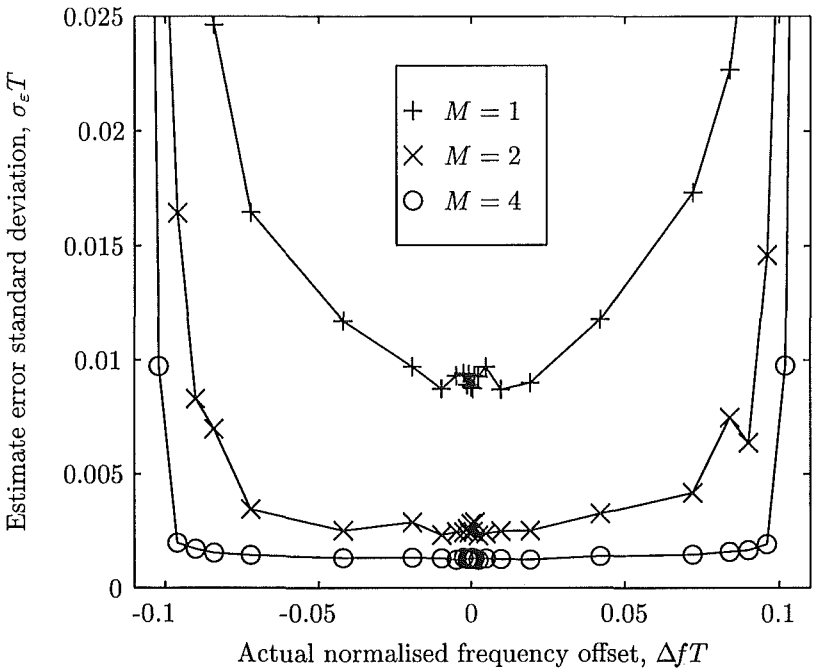

Figure 5.5 Normalised standard deviation of the carrier frequency offset estimate error. $L = 16, N_{\tilde{\psi}} = 8, \text{SNR} = 10\,\text{dB}, \tau_0/T = 0.1$

where ρ is the carrier-to-noise ratio. Also included, is the standard deviation of [Luise and Reggiannini 1995, eqn. (12) with $M = 47$ and $N = 96$] applied directly to the distorted received signal, (2.6), presented here (dot-dashed, labelled 'Luise'). Note single diversity is implied in this last case.

With four diversity branches the estimator presented here closely approaches the CRLB for the AWGN channel, and even does better than the CRLB for low channel delay spread. This is because the diversity receiver can make use of the channels which are above the average SNR due to constructive interference, due to the averaging effect of the noise across the diversity branches, and also because the CRLB is not exact in this situation.

The estimator presented in [Luise and Reggiannini 1995] is clearly not designed to handle data-modulated and ISI distorted signals, as its standard deviation is significantly higher than the single branch diversity case presented here, even with a significantly longer observation interval (96 as opposed to 16 symbols) and especially at high SNR. It is surprising that the standard deviation of the estimator presented in [Luise and Reggiannini 1995] does not reduce for increased SNR, however, the estimator is not designed to operate with the distorted received signal presented here.

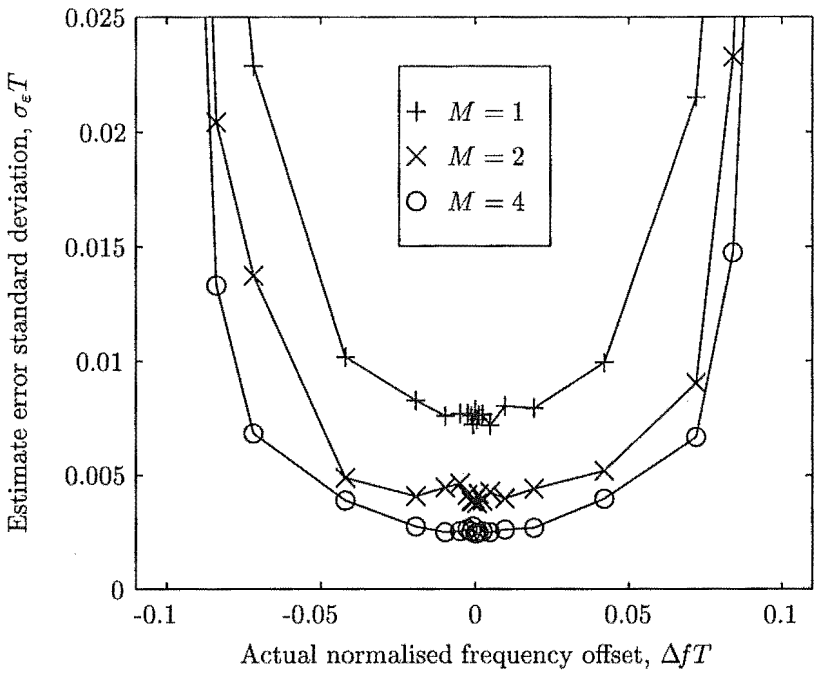

Figure 5.6 Normalised standard deviation of the carrier frequency offset estimate error. $L = 16, N_{\bar{\psi}} = 8, \text{SNR} = 10\,\text{dB}, \tau_0/T = 1$

5.5.3 The effect of delay spread on the carrier frequency offset error standard deviation

Figure 5.9 shows the effect of varying the normalised delay spread from $\tau_0/T = 0$ to $\tau_0/T = 1$, for constant SNR, observation interval length, and number of correlation terms. When $\tau_0/T = 1$, the channel introduces large amounts of ISI which is significant over several symbols. There is a large performance improvement in going from 1 branch to 2 branches, and a smaller, but still significant, improvement going from 2 branches to 4 branches. The effect is increased for lower delay spread because of the reduction in ISI that the estimator must contend with. The size of the delay spread of the channel does not have a huge effect on the performance of the estimator as observed by the gentle slope of the curves. The estimator even performs better with a large delay spread when the receiver has one branch, perhaps due to the implicit frequency diversity present in the channel [Clark 1992], also called delay diversity [Monsen 1971].

5.5.4 The effect of training sequence length on the carrier frequency offset error standard deviation

The estimator requires *hypothesized data symbols*, because the formulation of the estimator does not average over the random data symbols. This is convenient in a receiver of this type, because a *training sequence* of data symbols, known at the receiver, is used

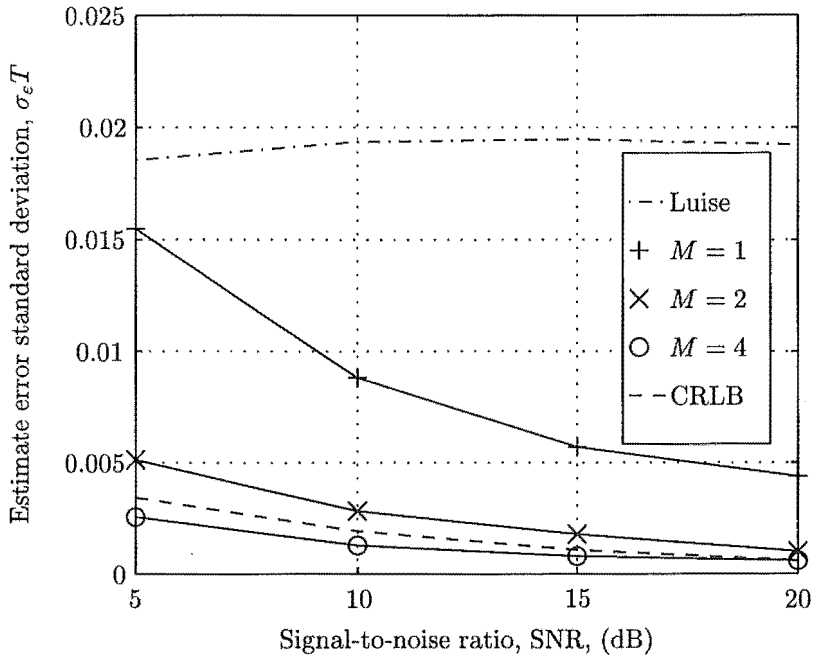

Figure 5.7 Effect of SNR on the carrier frequency offset error standard deviation. $L = 16, N_{\bar{\psi}} = 8, \Delta f = 0\,\text{Hz}, \tau_0/T = 0.1$

to train the equalisers in every timeslot, and is therefore available for use in the carrier frequency offset estimation process. It is, however, advantageous to keep the training sequence length as short as possible in order to improve bandwidth efficiency. The parameter $N_{\bar{\psi}}$ (discussed in Sec. 5.4.2) determines how much the effect of the ISI due to the channel is compensated, but increasing the parameter reduces the observation interval length for a given training sequence length, L_{TS}.

Figure 5.10 and Fig. 5.11 show the effect on the carrier frequency offset estimate error as the observation interval length is varied, whilst the training sequence length is held constant, for small and large delay spread, respectively. They show that the estimator performance improves significantly as the observation interval length is increased. However, for large delay spread, the performance is limited when $N_{\bar{\psi}}$ is reduced too much. When the normalised delay spread is $\tau_0/T = 1$, the estimate error standard deviation reduces as L is increased, but then increases again when $N_{\bar{\psi}} = L_{\text{TS}} - L + 1 = 6$. To reiterate, this parameter determines the number of terms of the channel autocorrelation function that are included in the calculation of the estimate. The result highlighted here is that $N_{\bar{\psi}}$ must be chosen to give the best results depending on the delay spread of the channel, but should be quite small as increasing the length of the observation interval improves the estimate significantly.

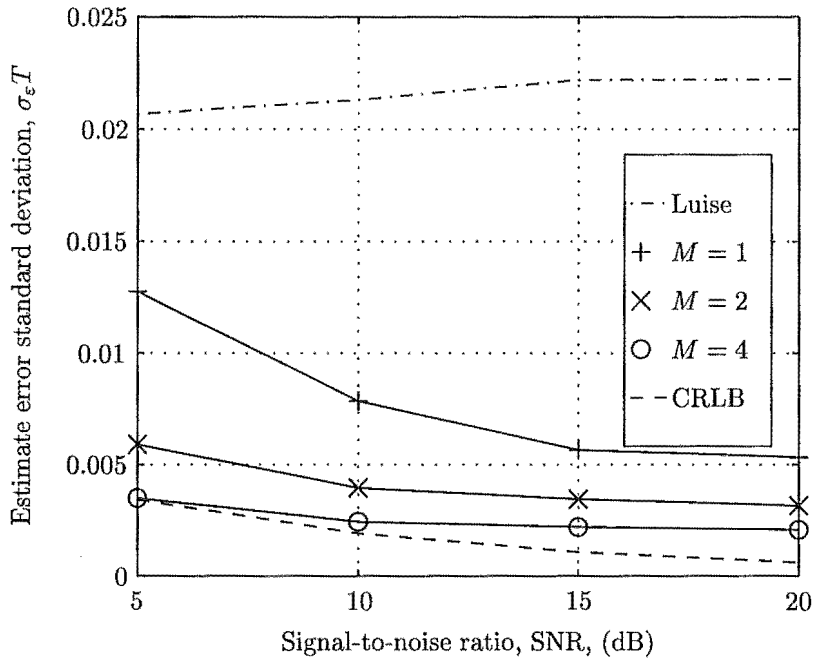

Figure 5.8 Effect of SNR on the carrier frequency offset error standard deviation. $L = 16, N_{\tilde{\psi}} = 8, \Delta f = 0\,\text{Hz}, \tau_0/T = 1$

5.5.5 The effect of symbol timing offset on the carrier frequency offset estimator

Figure 5.12 shows the effects of symbol timing offset on the normalised expected value of the estimator, and Fig. 5.13 shows the effects of symbol timing offset on the normalised standard deviation of the estimator. The x-axis is normalised to the symbol period. Results for four diversity branches are shown only. The estimator expected value for one and two diversity branches is similar to that for four branches. The estimator standard deviation for one and two diversity branches shows the same trends across the range of symbol timing offsets as that for four diversity branches, where the standard deviation for a symbol timing offset of zero is given by Fig. 5.5 and Fig. 5.6.

The estimator is remarkably insensitive to symbol timing offsets over a wide range of offsets. It remains essentially unbiased over ± 1 symbol period. For channels with large delay spread, $\tau_0/T = 1$, the estimator standard deviation increases by only about 50% over the same range. For channels with small delay spread, $\tau_0/T = 0.1$, the estimator becomes more sensitive and the standard deviation increases by approximately 2 over ± 0.5 symbol periods. The trends are applicable even for a large carrier frequency offset of $\Delta f T = 0.05$. The plots for standard deviation show a small asymmetry due to the asymmetrical channel delay-power-spectrum shape.

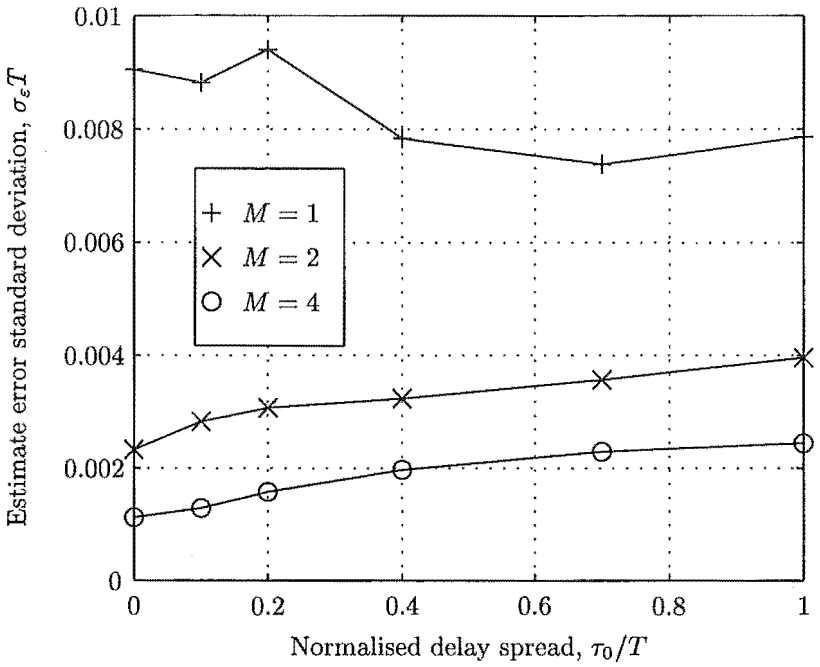

Figure 5.9 Effect of delay spread on the carrier frequency offset error standard deviation. $L = 16, N_{\tilde{p}} = 8, \Delta f = 0\,\text{Hz}, \text{SNR} = 10\,\text{dB}$

5.6 DISCUSSION OF RESULTS

The two significant considerations for the estimator are allowable frequency offset range, and the amount by which the residual frequency offset error will contribute a linear phase trend across the burst.

The range of allowable frequency offsets is large, e. g., for a symbol period of $6\,\mu$s and an observation interval length of 16 symbols, the theoretical range is $\pm 18500\,$Hz which is approximately 40 ppm of the local oscillator if the carrier frequency is 900 MHz. This is far greater than the maximum Doppler frequency of about 100 Hz observed in a car (vehicle speed of 120 kph and carrier frequency of 900 MHz). Even if the useful range is limited to half the theoretical range, the estimator still allows for relatively cheap local oscillators.

The receiver is to operate in a burst-mode manner, storing a timeslot of received samples and processing them. Each timeslot will contain a training sequence known at the receiver. The receiver will train its equalisers using the training sequence and then either hold the equaliser taps constant for the remainder of the timeslot, or dynamically update the taps using symbol estimates. The determining factor is the amount of linear phase trend experienced by the received symbols being detected at the ends of the timeslot. This phase trend is determined by the carrier frequency offset error, and the amount of Doppler spreading (which influences how fast the channel varies). For

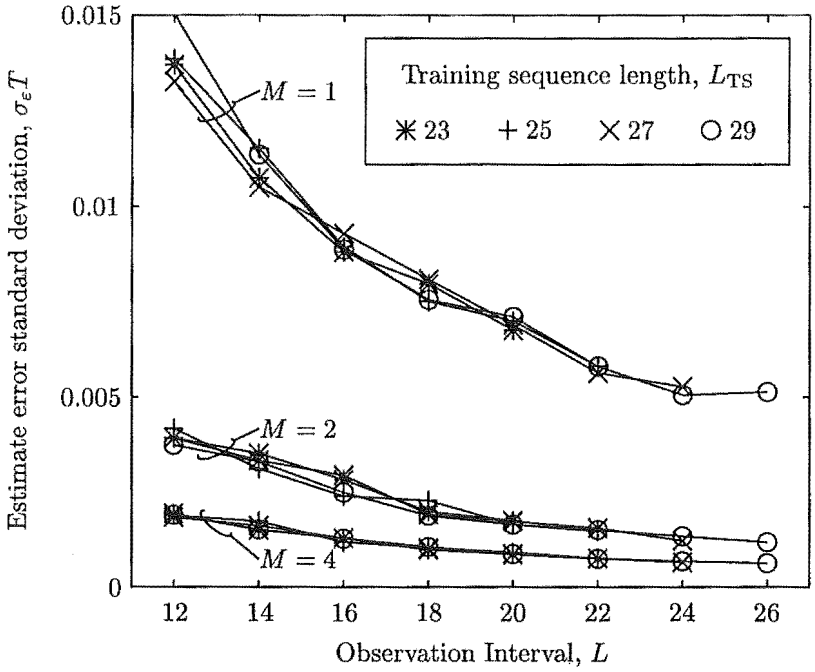

Figure 5.10 Effect of observation sequence length on the carrier frequency offset error standard deviation. $N_{\tilde{\psi}} = 8, \mathrm{SNR} = 10\,\mathrm{dB}, \Delta f = 0\,\mathrm{Hz}, \tau_0/T = 0.1$

example, for a timeslot length of .577 ms, a frequency error of 100 Hz will result in a phase trend of 0.029 cycles from the centre to the end of the timeslot. In this case, the phase trend due to the carrier frequency offset would probably not increase the bit-error-rate significantly, and therefore it would not be necessary to make the equalisers adaptively track and cancel the residual linear phase trend.

5.7 CONCLUSIONS

This chapter has presented the derivation of a carrier frequency offset estimator for a diversity receiver operating in a general time-varying frequency-selective multipath environment. The interference was assumed to be white and Gaussian in order to keep the analysis tractable, however, the estimator should still work if this is not the case. The estimator was derived using maximum likelihood techniques, but involved several approximations in order to arrive at the final expression for the estimate. The estimator is novel in that it does not require a channel estimate, but merely requires an estimate of the *channel autocorrelation function.* This is advantageous because the autocorrelation function of the channel is in general far easier to estimate in a real system than the actual channel state. Also, the estimator can work in an open-loop manner to remove any carrier frequency offset from the received signals before the distortion is removed by the equalisers in the remainder of the receiver. If this was

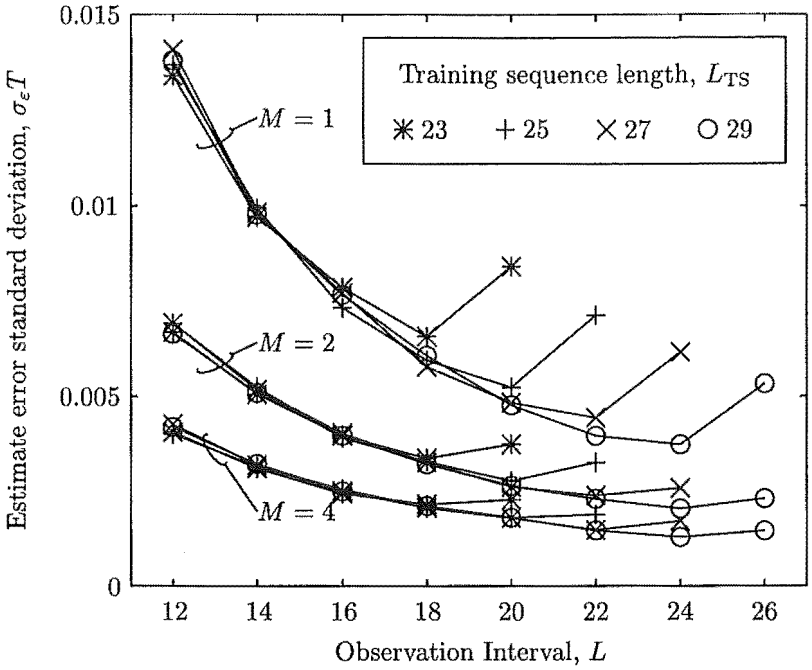

Figure 5.11 Effect of observation sequence length on the carrier frequency offset error standard deviation. $N_{\bar{\psi}} = 8, \mathrm{SNR} = 10\,\mathrm{dB}, \Delta f = 0\,\mathrm{Hz}, \tau_0/T = 1$

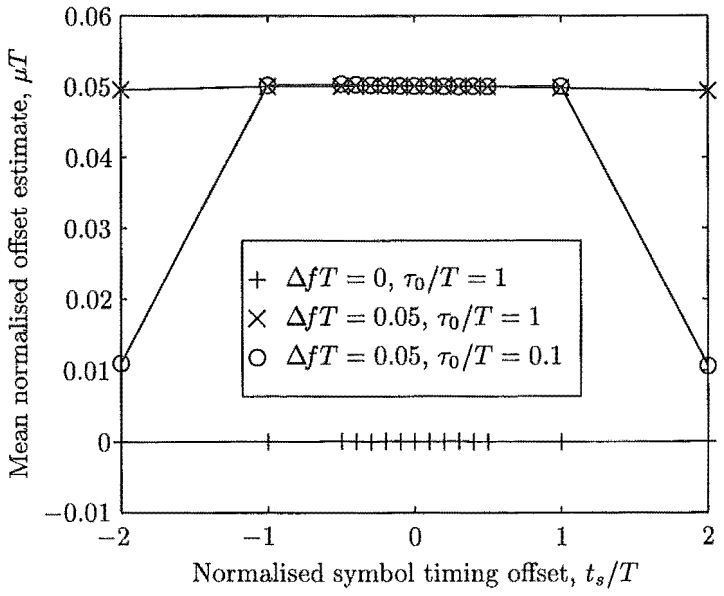

Figure 5.12 Effect of symbol timing offset on the carrier frequency offset estimate. $L = 16, N_{\bar{\psi}} = 8, \mathrm{SNR} = 10\,\mathrm{dB}, M = 4$

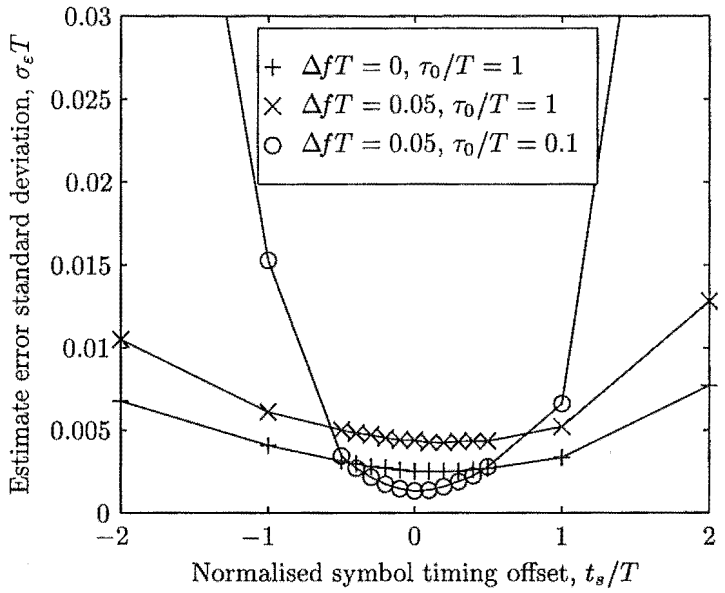

Figure 5.13 Effect of symbol timing offset on the carrier frequency offset standard deviation. $L = 16, N_{\tilde{\psi}} = 8, \text{SNR} = 10\,\text{dB}, M = 4$

not the case, and a channel estimate was required by the offset estimator, it would be difficult to estimate the channel state because the signals would contain a frequency offset.

The frequency offset estimator requires a training sequence, and is therefore well suited to a burst-mode system where a training sequence is already required by the equaliser training algorithms.

Simulation results have been presented showing that space diversity of two or four branches significantly improves the performance of a single branch receiver. It is also found that, for a given training sequence length, the observation interval should be increased until a limit is reached. This limit is determined by the number of link correlation terms included, and depends on the level of ISI, or equivalently, the delay spread of the channel.

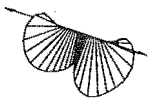

Chapter 6

CONCLUSIONS

This thesis has presented research into the performance of a digital receiver. The receiver is suited to operation in a multipath fading environment with severe intersymbol interference (ISI) and severe co-channel interference (CCI). These conditions are experienced in mobile and indoor cellular environments. The ability of the receiver to compensate for severe ISI is significant because the data rate is no longer limited by the channel dispersion and the system benefits from the intrinsic frequency selective diversity of the wideband channel. High data rates allow for a flexible system offering fast data transfer and/or many low data rate users on a TDMA protocol. The ability of the receiver to perform with severe CCI is also significant because it allows a higher density of cellular users in a given area. This is extremely desirable.

The multipath fading channel is assumed to be slowly time-varying and introduces severe distortion because of its frequency selectivity. The receiver uses space diversity and equalisation to combat the effects of distortion and fading.

Two distinct areas were focussed on: the effect of finite equaliser length on the best possible linear diversity receiver performance, assuming ideal carrier frequency recovery and ideal channel state information, and the performance of a carrier frequency offset estimator.

The main conclusions that can be drawn from the study on the effect of finite equaliser length are:

- A diversity receiver with short equalisers (e. g., 10 taps per branch) performs almost as well as the optimum linear receiver even when the significant channel dispersion is longer than the equaliser length.
- The same trends of the effect of diversity on the optimum linear receiver are exhibited by the finite-length equaliser receiver.
- The diversity receiver is less able to compensate for Gaussian noise than for non-Gaussian noise. This is because the diversity equalisers can align the contributions from the desired source, but cannot effectively cancel the contributions from the noise sources, as it can in the case of non-Gaussian noise.

- The gains obtained from diversity are significant even for short equaliser lengths, indicating that the highest possible diversity order should be used for a given total number of taps in the receiver. However, increasing the diversity order results in diminishing returns, with the largest gain obtained by increasing diversity from one to two branches, although there is still a significant gain to be made by increasing the diversity from two to four branches.

The main conclusions that can be drawn from the study of the carrier frequency offset estimator are:

- Diversity offers significant performance improvements for the carrier frequency offset estimator, roughly halving the error standard deviation for every doubling of the diversity order.

- The estimator functions linearly over a wide range of carrier frequency offsets allowing it to be used in receivers with relatively cheap local oscillators.

- The estimator is sensitive to delay spread, but not significantly. With no diversity the performance actually improves with increasing delay spread for small frequency offsets, and for large frequency offsets, the performance is approximately the same. With higher diversity, the error standard deviation is roughly doubled for small frequency offsets when the normalised delay spread is increased from 0 (flat fading) to 1 (severe distortion).

- The estimator performance improves with increasing SNR, although the performance tends to a floor indicating that the performance is limited by fading. It follows that the improvements from increased SNR are smaller when the delay spread is large.

- The performance is improved by increasing the length of the observation interval. However, since the algorithm uses a training sequence which should be made as short as possible, the length of the observation interval is limited. As the observation interval length is increased, the number of terms of the weighted received sample correlation function must be reduced for a given training sequence length, and this affects the algorithm's ability to compensate for ISI. It is found that the number of terms can be made quite small even for severe ISI distortion, because the improvements from increasing the observation interval length outweigh the degradation caused by ISI, until a limit is reached.

- The estimator is relatively insensitive to symbol timing offsets, allowing for a simple symbol timing estimator. Moreover, the receiver can acquire the carrier frequency offset before symbol timing is achieved. The standard deviation of the estimator increases by approximately 2 over ± 0.5 symbol periods from the

ideal sampling instant, when the normalised delay spread is $\tau_0/T = 0.1$. The estimator is insensitive over an even wider range of timing offsets as the delay spread is increased.

6.1 TOPICS FOR FUTURE RESEARCH

The first part of the research (i. e., the effect of finite-length equalisers on the receiver performance) obtained benchmarks for the best possible performance achievable by a linear diversity receiver for a certain set of parameters, such as channel characterisation, diversity order and equaliser length.

In a real system, the receiver would not have ideal channel-state-information, and would have to estimate the channel responses. This process of channel estimation is usually done indirectly by equaliser training algorithms. Each transmitted burst would contain message data, header information, and a *training sequence.* The receiver would know the training sequence, and can adjust the equaliser tap weights so that the distorted training sequence in the received samples is equalised to be close to the actual training sequence. Then the message symbols in the burst can be detected.

Research needs to be carried out into the degradation caused by the sub-optimal knowledge of the channel responses, and hence the sub-optimal equaliser tap weights. Many adaptive algorithms are well known, but need to be applied to this specific application.

Since the system is designed to operated in a time-division-multiple-access scheme, with adjacent bursts being transmitted to or from different mobiles (i. e., the channels in adjacent bursts are completely uncorrelated), the equalisers must be trained every burst. Therefore, the training algorithm needs to have very fast convergence. The Kalman or recursive-least-squares algorithm is a likely candidate. Unfortunately, due to the complexity of the problem, obtaining performance results is likely to be restricted to simulation techniques, which will be very computationally intensive. Attempts were made in this research to find an expression for the performance of a Kalman algorithm, training the diversity branches globally, and being averaged over the channel fading, however, the analysis became intractable.

The GSM standard specifies a 26 bit training sequence length [Steele 1992]. Presumably a similar length of training sequence would be adequate for a system such as this. The length of the training sequence is determined by the speed at which the equaliser training algorithm can converge, and is dependent on the dispersion present in the channel. The effect of training sequence length on equaliser training performance would need to be addressed in the study of equaliser training algorithms.

The second part of the research (i. e., the performance of a carrier frequency offset estimator) was an analysis of a more practical nature. The algorithm could be used in

an actual receiver. More study needs to be carried out into symbol timing estimation and burst synchronisation for this kind of system.

This thesis assumes the message data symbols to be uncorrelated, and the aim was to investigate the transmission of these message symbols using only diversity and equalisation to compensate for the distortion encountered in the fading channel. A real system would utilise some form of coding. It is better to analyse the system with coding and equalisation together rather than separately. The message symbols were assumed uncorrelated in order to derive the minimum mean-square-error equaliser responses, however, it may not be necessary to assume this when analysing the equaliser training algorithms. If this is the case, then it may be possible to investigate combined coding and equalisation, where the coding introduces redundancy, in the form of correlation, into the transmitted symbols. The performance results for the receiver with combined coding and equalisation could still be compared to the best possible linear MMSE receiver performance presented here.

One aspect of the receiver performance analysis that could be further enhanced is the performance measures used. In this thesis, the BER measure given a set of channels was defined, and by simulating many channel sets, the BER distribution could be plotted. It would be useful to develop a single parameter that would measure the effectiveness of a receiver. For instance, a receiver that performs adequately most of the time is more desirable than one that performs very well some of the time, but poorly for a significant proportion of the time. The parameter may depend on the desired characteristics, such as the useful BER threshold.

There is little point in investigating non-linear equalisation, because the optimum linear receiver performs almost as well as the maximum-likelihood receiver [Clark 1992], and the linear finite-length equaliser receiver studied in this thesis performs almost as well as the optimum linear receiver even with a small number of taps. Some small performance gains may be possible by introducing non-linear equalisation, e. g., a non-linear postcombiner filter, or even non-linear filters in each branch. However, the analysis of non-linear systems is complicated, and would be even more difficult to analyse than the linear system presented here.

Appendix A

KARHUNEN-LOÉVE ORTHOGONAL EXPANSION WITH UNCORRELATED COEFFICIENTS

This appendix summarises the Karhunen-Loéve orthogonal expansion of a non-periodic random process. It is taken from Davenport and Root [1958, pp. 96–98].

A non-periodic random process cannot be written as a trigonometric Fourier series with uncorrelated random coefficients. However, it turns out that if the term *Fourier series* is extended—as it often is—to include any series of orthogonal functions $\phi_n(f)$ with coefficients properly determined, then non-periodic processes do have a Fourier-series expansion with uncorrelated coefficients.

An expansion of a wide-sense stationary random process, with sample functions $Z(f)$, on an interval from a to b of the form

$$Z(f) = \sum_i \sqrt{\lambda_i} c_i \phi_i(f), \qquad a \leqslant f \leqslant b \tag{A.1}$$

where

$$\int_a^b \phi_{i_1}(f)\phi_{i_2}^*(f)\, df = \begin{cases} 1 & \text{if } i_1 = i_2 \\ 0 & \text{if } i_1 \neq i_2 \end{cases} \tag{A.2}$$

$$E[c_{i_1} c_{i_2}^*] = \begin{cases} 1 & \text{if } i_1 = i_2 \\ 0 & \text{if } i_1 \neq i_2 \end{cases} \tag{A.3}$$

and $\sqrt{\lambda_i}$ are real numbers, will be called an *orthogonal expansion* of the random process on the given interval.

To see how the functions $\phi_i(f)$ and the numbers λ_i are determined, suppose that (A.1), (A.2), and (A.3) are satisfied for some set of functions $\phi_i(f)$, some set of numbers

λ_i, and some set of random variables c_i. Then

$$\Xi(f_1, f_2) = E[Z(f_1)Z^*(f_2)] = E\left[\sum_i \sqrt{\lambda_i} c_i \phi_i(f_1) \sum_k \sqrt{\lambda_k} c_k^* \phi_k^*(f_2)\right]$$
$$= \sum_i \lambda_i \phi_i(f_1)\phi_i^*(f_2), \qquad a \leqslant f_1, f_2 \leqslant b \tag{A.4}$$

Using $\Xi(f_1, f_2)$, as given by (A.4), we have

$$\int_a^b \Xi(f_1, f_2)\phi_j(f_2)\, df_2 = \sum_i \lambda_i \phi_i(f_1) \int_a^b \phi_i^*(f_2)\phi_j(f_2)\, df_2 \tag{A.5}$$

or

$$\int_a^b \Xi(f_1, f_2)\phi_j(f_2)\, df_2 = \lambda_j \phi_j(f_1) \tag{A.6}$$

In the language of integral equations, the numbers λ_j must be the characteristic values and the functions $\phi_j(f_1)$ must be the characteristic functions of the integral equation

$$\int_a^b \Xi(f_1, f_2)\phi(f_2)\, df_2 = \lambda\phi(f_1), \qquad a \leqslant f_1 \leqslant b \tag{A.7}$$

See Davenport and Root [1958] for proofs of (A.1) and (A.3).

Appendix B

OPTIMISATION OF FINITE-LENGTH FSE

This appendix summarises the minimum mean-square-error (MMSE) optimisation of a finite-length fractionally-spaced equaliser (FSE) with white noise operating in a pseudo-static channel. It is taken from Qureshi [1985].

The input to the FSE is the received signal sampled at rate B/T

$$r(l\frac{1}{B}T) = \sum_k x_k q(l\frac{1}{B}T - kT) + \eta(l\frac{1}{B}T) \tag{B.1}$$

where x_k are data symbols at time $t = kT$, $q(l\frac{1}{B}T - kT)$ is the channel response, and $\eta(l\frac{1}{B}T)$ is a noise sample with power spectrum N_0.

Each symbol interval, the FSE with tap weights, v_l, produces an output according to

$$\bar{y}(kT) = \sum_{l=\lfloor\frac{J-1}{2}\rfloor}^{\lfloor\frac{-(J-1)}{2}\rfloor} v_l r(kT - l\frac{A}{B}T) \tag{B.2}$$

Denoting the complex conjugate of the J equaliser coefficients at time kT by the vector $\boldsymbol{v}_k$, and the J most recently received samples (spaced $\frac{A}{B}T$ seconds apart) by the vector $\boldsymbol{r}_k$, the equaliser output may be written as

$$\bar{y}_k = \boldsymbol{v}_k^T \boldsymbol{r}_k \tag{B.3}$$

Minimising the mean-square-error (MSE) $E[|\bar{y}_k - x_k|^2]$ leads to the set of optimum equaliser coefficients

$$\boldsymbol{v}_k = \mathbf{A}_k^{-1} \boldsymbol{\alpha}_k \tag{B.4}$$

where $\mathbf{A}$ is a $J \times J$ covariance matrix $E[r_k^* r_k^T]$, and $\boldsymbol{\alpha}$ is a J-element cross-correlation vector $E[r_k^* x_k]$.

Using the assumption that the data sequence $\{x_k\}$ is uncorrelated with unit power,

it can be shown that the elements of the matrix $\mathbf{A}$ and vector $\boldsymbol{\alpha}$ are given by

$$a_{i,j} = \sum_k q^*(kT - i\frac{A}{B}T)q(kT - j\frac{A}{B}T) + N_0\delta_{ij} \tag{B.5}$$

$$\alpha_i = q^*(-i\frac{A}{B}T) \tag{B.6}$$

REFERENCES

Amitay, N. and Greenstein, L.J. (1984), "Multipath Outage Performance of Digital Radio Receivers Using Finite-Tap Adaptive Equalizers," *IEEE Trans. Commun.*, Vol. COM-32, No. 5, May, pp. 597–608.

Aulin, T. (1979), "A Modified Model for the Fading Signal at a Mobile Radio Channel," *IEEE Trans. Veh. Tech.*, Vol. VT-28, No. 3, August, pp. 182–203.

Balaban, P. and Salz, J. (1991), "Dual Diversity Combining and Equalization in Digital Cellular Mobile Radio," *IEEE Trans. Veh. Tech.*, Vol. 40, No. 2, May, pp. 342–354.

Beck, R. and Panzer, H. (1989), "Strategies for Handover and Dynamic Channel Allocation in Micro-Cellular Mobile Radio Systems," *39th IEEE Veh. Tech. Conf.*, May, pp. 178–185.

Bello, P. (1963), "Characterization of Randomly Time-Variant Linear Channels," *IEEE Trans. Commun.*, Vol. CS-11, December, pp. 360–393.

Chuang, J.C.I. (1990), "Comparison of Coherent and Differential Detection of BPSK and QPSK in a Quasistatic Fading Channel," *IEEE Trans. Commun.*, Vol. 38, No. 5, May, pp. 565–567.

Cioffi, J.M. and Kailath, T. (1984), "An Efficient Exact-Least-Squares Fractionally Spaced Equalizer Using Intersymbol Interpolation," *IEEE J. Select. Areas Commun.*, Vol. SAC-2, No. 5, September, pp. 743–756.

Clark, M.V. (1992), *Diversity and Equalization in Digital Cellular Radio*, PhD thesis, University of Canterbury, N.Z., May.

Classen, F. and Meyr, H. (1994), "Frequency Synchronization Algorithm for OFDM System suitable for Communication over Frequency Selective Fading Channels," *IEEE Veh. Tech. Conf.*, pp. 1655–1659.

Cox, D.C. (1987), "Universal Digital Portable Radio Communications," *Proc. IEEE*, Vol. 75, April, pp. 436–477.

D'Aria, G., Muratore, F. and Palestini, V. (1992), "Simulation and Performance of the Pan-European Land Mobile Radio System," *IEEE Trans. Veh. Tech.*, Vol. 41, May, pp. 177–189.

Davenport, W.B. and Root, W.L. (1958), *An Introduction to the Theory of Random Signals and Noise*, New York: McGraw-Hill, IEEE press ed.

Falciasecca, G., Frullone, M., Riva, G. and Serra, A.M. (1989), "Comparison of Different Hand-Over Strategies for High Capacity Cellular Mobile Radio Systems," *39th IEEE Veh. Tech. Conf.*, May, pp. 122–127.

Falconer, D.D. and Ljung, L. (1978), "Application of Fast Kalman Estimation to Adaptive Equalization," *IEEE Trans. Commun.*, Vol. COM-26, No. 10, October, pp. 1439–1446.

Fechtel, S. and Meyr, H. (1993), "Combined Equalisation, Decoding and Antenna Diversity Combining for Mobile/Personal Digital Radio Transmission using Feedforward Synchronization," *IEEE Veh. Tech. Conf.*, Vol. 43, pp. 633–636.

Frech, E.A. and Mesquida, C.L. (1989), "Cellular Models and Hand-Off Criteria," *39th IEEE Veh. Tech. Conf.*, May, pp. 128–135.

Gitlin, R.D. and Weinstein, S.B. (1981), "Fractionally-Spaced Equalization: An Improved Digital Transversal Equalizer," *Bell Syst. Tech. J.*, Vol. 60, No. 2, February, pp. 275–296.

Gitlin, R.D., Hayes, J.F. and Weinstein, S.B. (1992), *Data Communications Principles*, New York: Plenum.

Glance, B. and Greenstein, L.J. (1983), "Frequency-Selective Fading Effects in Digital Mobile Radio with Diversity Combining," *IEEE Trans. Commun.*, Vol. COM-31, No. 9, September, pp. 1085–1094.

Goodman, D.J. (1991), "Trends in Cellular and Cordless Communications," *IEEE Commun. Mag.*, June, pp. 31–40.

Gradshteyn, I.S. and Ryzhik, I.M. (1980), *Table of Integrals, Series and Products*, Academic Press. Corrected and enlarged by Alan Jeffery.

Haykin, S. (1983), *Communication Systems*, New York: Wiley, 2nd ed.

Haykin, S. (1996), *Adaptive Filter Theory*, Upper Saddle River, N.J.: Prentice Hall, 3rd ed.

Hebley, M., Kennedy, W. and Taylor, D. (1994), "The Performance of a Space Diversity Receiver with Finite-Length Fractionally-Spaced Equalisers with Frequency

Selective Rayleigh Fading and Co-Channel Interference," *IEEE Global Commun. Mini-Conference*, November, pp. 90–94.

Jakes, Jr., W.C. (1974), *Microwave Mobile Communications*, New York: Wiley.

Kreyszig, E. (1988), *Advanced Engineering Mathematics*, New York: Wiley, 6th ed.

Kucar, A.D. (1991), "Mobile Radio: An Overview," *IEEE Commun. Mag.*, November, pp. 72–85.

Lee, W.C.Y. (1991), "Smaller Cells for Greater Performance," *IEEE Commun. Mag.*, November, pp. 19–23.

Lindsey, W.C. and Chie, C.M. (1981), "A Survey of Digital Phase-Locked Loops," *Proc. IEEE*, Vol. 69, No. 4, April, pp. 410–431.

Long, G., Ling, F. and Proakis, J.G. (1988), "Application of Fractionally-Spaced Decision-Feedback Equalizers to HF Fading Channels," *Military Comm. Conf.*, Vol. 1, October, pp. 103–107.

Loo, C. and Secord, N. (1991), "Computer Models for Fading Channels with Applications to Digital Transmission," *IEEE Trans. Veh. Tech.*, Vol. 40, No. 4, November, pp. 700–707.

Luise, M. and Reggiannini, R. (1995), "Carrier Frequency Recovery in All-Digital Modems for Burst-Mode Transmissions," *IEEE Trans. Commun.*, Vol. 43, No. 2/3/4, Feb/Mar/Apr, pp. 1169–1178.

Metzger, K. (1987), "On the Probability Density of Intersymbol Interference," *IEEE Trans. Commun.*, Vol. COM-35, No. 4, April, pp. 396–402.

Monsen, P. (1971), "Feedback Equalization for Fading Dispersive Channels," *IEEE Trans. on Inf. Theory*, January, pp. 56–65.

Murota, K. and Hirade, K. (1981), "GMSK Modulation for Digital Mobile Radio Telephony," *IEEE Trans. Commun.*, Vol. COM-29, No. 7, July, pp. 1044–1049.

Padgett, J.E., Günther, C.G. and Hattori, T. (1995), "Overview of Wireless Personal Communications," *IEEE Commun. Mag.*, Vol. 33, No. 1, January, pp. 28–41.

Parsons, J.D. (1992), *The Mobile Radio Propagation Channel*, London: Pentech Press.

Petersson, S. and Svensson, A. (1994), "Detectors for PDC," *IEEE Veh. Tech. Conf.*, June, pp. 992–995.

Pokrajac, D. and Nikolic, Z. (1995), "A Correction to Kurt Metzger's Algorithm in the Paper "On the Probability Density of Intersymbol Interference"," *IEEE Trans. Commun.*, Vol. 43, No. 12, December, P. 2868.

Potter, A.R. (1992), "Implementation of PCNs Using DCS1800," *IEEE Commun. Mag.*, December, pp. 32–36.

Proakis, J.G. (1989), *Digital Communications*, New York: McGraw-Hill, 2nd ed.

Qureshi, S. (1985), "Adaptive Equalisation," *Proc. IEEE*, Vol. 73, No. 9, September, pp. 1349–1387.

Rife, D.C. and Boorstyn, R.R. (1974), "Single-Tone Parameter Estimation from Discrete-Time Observations," *IEEE Trans. on Inf. Theory*, Vol. IT-20, No. 5, September, pp. 591–598.

Rummler, W.D. (1979), "A New Selective Fading Model: Application to Propagation Data," *Bell Syst. Tech. J.*, Vol. 58, May-June, pp. 1037–1071.

Rummler, W.D. (1981), "More on the Multipath Fading Channel Model," *IEEE Trans. Commun.*, Vol. COM-29, March, pp. 346–352.

Sousa, E.S., Jovanić, V.M. and Daigneault, C. (1992), "Delay Spread Measurements for the Digital Cellular Channel in Toronto," *IEEE Int. Symp. on Personal Indoor and Mobile Radio Commun.*, pp. 80–85.

Spanias, A.S. (1994), "Speech Coding: a tutorial review," *Proc. IEEE*, Vol. 82, No. 10, October, pp. 1541–1582.

Steele, R. (Ed.) (1992), *Mobile Radio Communications*, London: Pentech Press.

Tekinay, S. and Jabbari, B. (1991), "Handover and Channel Assignment in Mobile Cellular Networks," *IEEE Commun. Mag.*, November, pp. 42–46.

Tuisel, U. and Kameyer, K.D. (1992), "Carrier Recovery for Multicarrier Transmission over Mobile Radio Channels," *IEEE Int. Conf. on Acc. Speech and Signal Proc.*, pp. IV–677–IV–680.

Ungerboeck, G. (1976), "Fractional Tap-Spacing Equalizer and Consequences for Clock Recovery in Data Modems," *IEEE Trans. Commun.*, Vol. COM-24, No. 8, August, pp. 856–864.

Van Etten, W. (1976), "Maximum Likelihood Receiver for Multiple Channel Transmission Systems," *IEEE Trans. Commun.*, Vol. COM-24, February, pp. 276–283.

Weissman, D., Levesque, A.H. and Dean, R.A. (1993), "Interoperable Wireless Data," *IEEE Commun. Mag.*, February, pp. 68–77.